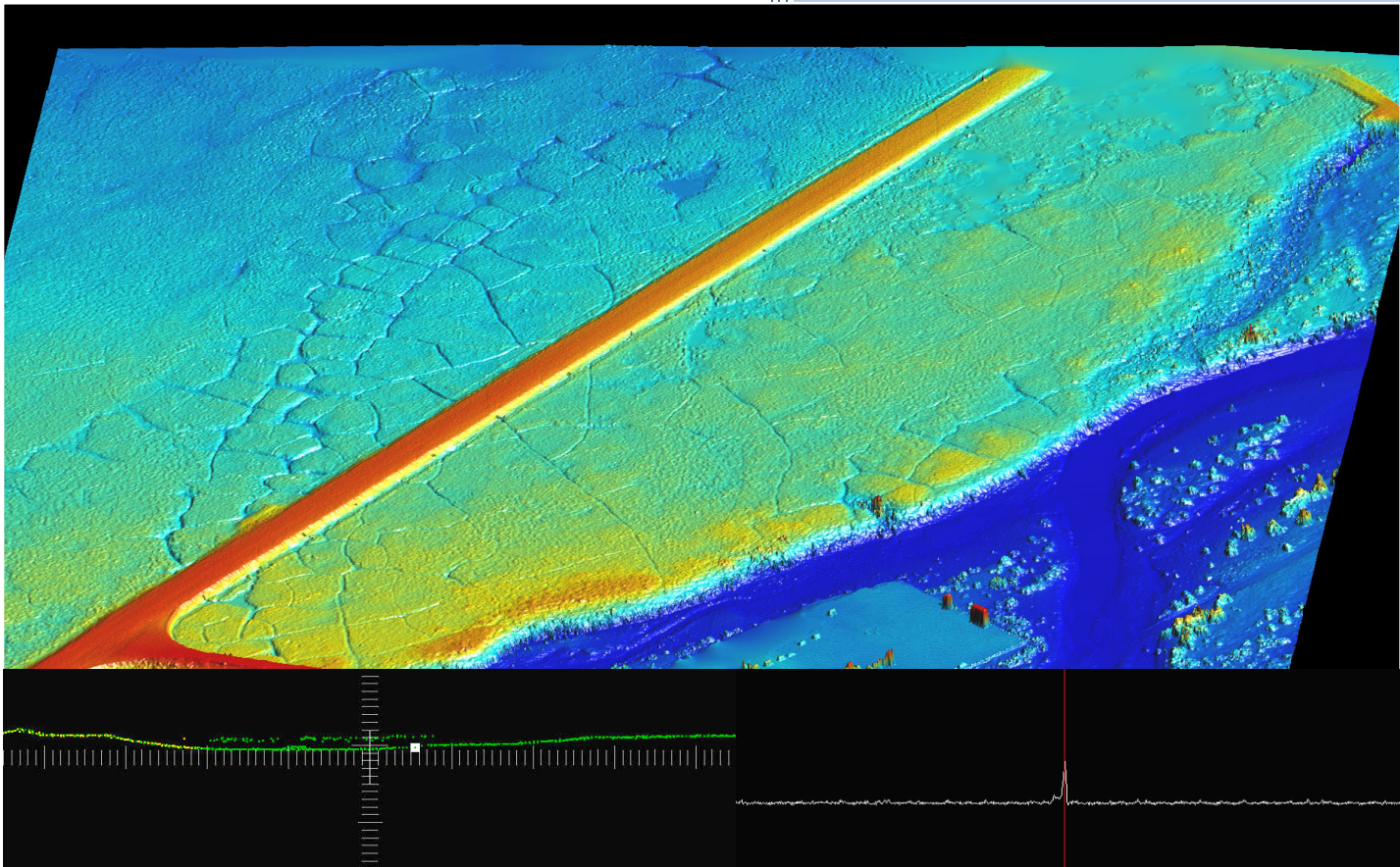




Final Technical Report

Determining Wetlands Distribution, Lake Depths, and Topography Using Airborne Lidar and Imagery on the North Slope, Deadhorse Area, Alaska



Prepared for
Great Bear Petroleum
Operating LLC
under Sponsored
Research Agreement
UTA12-0000752



October 31, 2013

Bureau of Economic Geology
Scott W. Tinker, Director
The University of Texas at Austin
Austin, Texas 78713-8924

Page intentionally blank

DETERMINING WETLANDS DISTRIBUTION, LAKE DEPTHS,
AND TOPOGRAPHY USING AIRBORNE LIDAR AND IMAGERY
ON THE NORTH SLOPE, DEADHORSE AREA, ALASKA

FINAL TECHNICAL REPORT

by

Jeffrey G. Paine¹, John Andrews¹, Kutalmis Saylam¹, Thomas Tremblay¹, Michael H. Young¹,
Chuck Abolt¹, Brian Bradford², Tiffany Caudle¹, Thoralf Meyer¹, and Amy Neuenschwander²

¹Bureau of Economic Geology
John A. and Katherine G. Jackson School of Geosciences
The University of Texas at Austin
University Station, Box X
Austin, Texas 78713

²Applied Research Laboratories
The University of Texas at Austin

Report prepared for

Great Bear Petroleum Operating LLC
Under Sponsored Research Agreement UTA12-0000752

October 31, 2013

Page intentionally blank

CONTENTS

Summary	v
Introduction	1
Methods	4
August 2012 Airborne Survey	4
Lidar Data Processing	9
Digital Terrain Model and Bare Earth Generation	9
Wetlands Delineation	10
Satellite Data Processing	11
Color-Infrared (CIR) Imagery	12
North Slope Wetlands and Uplands	15
Topographic Lidar Verification and Mapping	21
Comparison of Lidar- and GPS-derived Elevations	21
Mapping Topographic Features: Permafrost Polygons and Pingos	25
Lidar for Watershed Delineation and Topographic Wetness Index	25
Lake and Stream Bathymetry	31
Lake Water Volume	40
Lake Statistics	45
Possible Future Work	49
Hyperspectral Assessments	49
Vegetation Assessment	51
Soil Assessment and Hydrological Modeling	52
Conclusions	52
Acknowledgments	54
References	55
Appendix A: Lidar-derived Lake Areas, Depths, and Volumes (Automated Process)	57
Appendix B: Volumetric Comparison for Selected Lakes	65
Appendix C: Lidar-derived Lake Summaries (Manual Process)	67
Appendix D: Data Volume Contents	75

FIGURES

S1. Example of processed point cloud data depicting the land surface and lake bed for two lakes adjacent to the Dalton Highway.	vi
S2. Scatterplot showing fathometer- versus lidar-derived water volume	vi
1. Landsat 5 Thematic Mapper image and DEM of the Deadhorse survey area, Alaskan North Slope	2
2. Chiroptera system.	3
3. Topographic map of the lidar survey area showing approximate locations of topographic and bathymetric lidar flight lines.	5
4. Digital elevation model of the survey area showing approximate locations of infrared imagery flight lines.	7
5. Georeferenced color-infrared (CIR) mosaic of the Deadhorse survey area.	13
6. Comparison of resolution achieved with the 2012 CIR and 2009-2010 SPOT imagery along the Dalton Highway near the Merak #1 wellpad.	14
7. 2012 BEG wetland map.	16
8. Comparison of 1970s-1980s NWI map and 2012 BEG wetland map.	18
9. Habitat area comparison between NWI and BEG wetland map.	20
10. Habitat area totals from BEG and ASRC wetland maps	20
11. Digital elevation model (DEM) constructed from topographic lidar data.	22
12. Difference between GPS- and airborne lidar-derived elevation over the 2012 and 2013 seismic survey areas.	24
13. Comparison of Landsat 5 Thematic Mapper and topographic lidar DEMs on the west bank of the Sagavanirktok River	26
14. Perspective view of the Merak #1 well pad.	27
15. Topographic models, elevation profiles, perspective views, and RGB imagery of a large pingo	28
16. Local watersheds identified using a quarter-meter resolution DEM.	30
17. Topographic Wetness Index within the same study area.	30
18. Bathymetric lidar data acquired across a water body in the Deadhorse survey area.	32
19. DEM of the water surface constructed from topographic and bathymetric lidar data points	33

20. DEM of the water bottom constructed from bathymetric lidar data points	34
21. DEM constructed from full-resolution bathymetric lidar returns, North Slope survey area and tile F3	35
22. Map of water depth in shallow North Slope lakes calculated by subtracting water-surface elevations from water-bottom elevations	37
23. Water-surface and water-bottom DEMs constructed from full-resolution bathymetric lidar data for a shallow lake west of the Dalton Highway	38
24. Comparison of fathometer-derived water depths acquired during boat-based surveys with bathymetric lidar-derived water depths	39
25. Gridded topographic and bathymetric lidar data from along the Dalton Highway before noise removal	41
26. Bathymetric lidar point cloud consisting of returns classified as ground, water bottom, and shallow-water bottom before and after removal of noisy data	42
27. Water-surface elevation determined from topographic lidar data and water depth determined by subtracting water-bottom surface from water surface elevation	44
28. Location of Deadhorse survey area lakes for which surface area, depth, and water volume have been calculated from lidar data	46
29. Scatterplot showing fathometer- versus lidar-derived water volume	47
30. Lidar-surveyed lakes that may have underestimated water volumes.	48
C1. Overview of survey area tiles showing 137 lakes analyzed manually.	68
C2. North Slope airborne survey tiles showing individual lake locations	69-73

TABLES

1. Data acquisition flights, 2012 airborne lidar and imaging survey, Deadhorse area, Alaska.	8
2. Habitat area totals for BEG map.	17
3. Percentage of water regime modifiers for wetland habitats. Saturated is least wet, semipermanently flooded is most wet.	17
4. Habitat area totals for NWI and BEG maps.	17
5. Comparison of GPS-derived seismic source and receiver elevations with airborne lidar-derived elevations	24

Page intentionally blank

SUMMARY

On the Alaskan North Slope, a permafrost-dominated coastal plain above the Arctic Circle, the ability of lakes to support a fish population is a function of water depth and wetlands classification is highly dependent on soil saturation (and thus microtopography). Using a new airborne lidar instrument that combines laser ranging at near-infrared wavelengths for topography and green wavelengths for bathymetry, we flew a pilot study over a 490-km² area south of Prudhoe Bay in August 2012 to measure surface topography at a density of about 20 points/m² and water-body depths at a density of about 2 points/m². High-resolution digital elevation models, having vertical accuracies of a few centimeters, have been generated from the topographic laser data that was acquired at a 400 kHz pulse rate. These models and associated point clouds can be used along with high-resolution color-infrared imagery to map permafrost landscape features such as soil/ice polygons and pingos and identify microtopographic features that influence soil moisture and consequently wetlands distribution. Bathymetric lidar data, acquired at a pulse rate of 36 kHz, can be used to produce elevation models for the water surface and the water bottom, allowing water depths to be determined for shallow, fresh-water lakes and anastomosing stream channels. Water penetration to depths greater than 6 m has been achieved in lakes with reported turbidities ranging from 0.7 to 4.3 nephelometric turbidity units (NTU). Topographic and bathymetric lidar data were used to establish the boundaries, measure water depths, and estimate total and incremental water volumes for 283 shallow lakes in the survey area having surface areas greater than about 0.8 ha. These lakes together are estimated to contain 20,343,051 m³ (5,374,064,326 gal) of water, of which 724,813 m³ (191,475,524 gal) is found in 83 lakes with depths greater than 1.5 m (5 ft) and 116,753 m³ (30,842,854 gal) is found in 38 lakes with depths greater than 2.1 m (7 ft). A semi-automated process was developed to produce point clouds and digital elevation models from which water-volume estimates have been made (fig. S1). Point clouds and DEMs clearly show irregular lake beds and a relatively flat topographic expression for the land area. Comparisons of lidar-derived lake volumes with volumes determined in 2011 using fathometer-based surveys show excellent agreement between the two approaches (fig. S2).

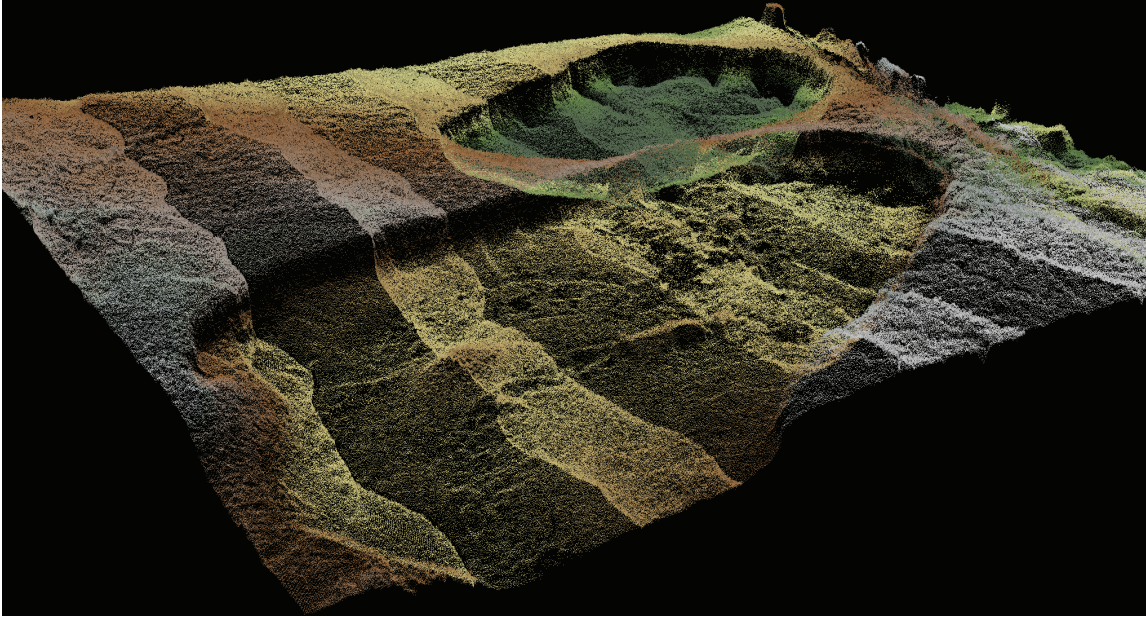


Figure S1. Example of processed point cloud data depicting the land surface and lake bed for two lakes adjacent to the Dalton Highway.

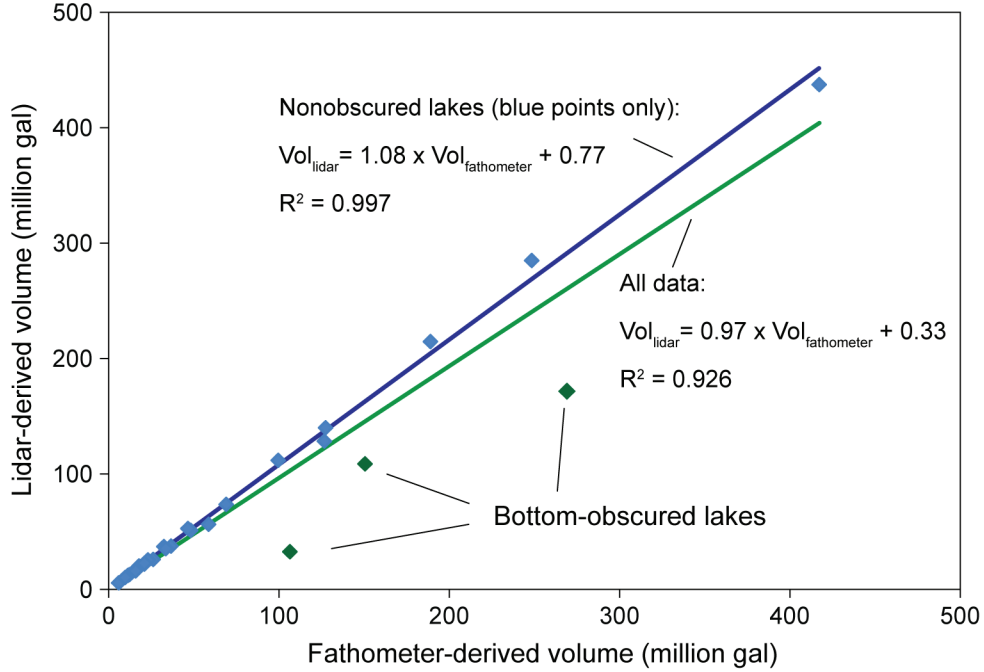


Figure S2. Scatterplot showing fathometer- versus lidar-derived water volume for 26 lakes that were surveyed by ASRC in 2011 (blue points and best-fit line) and three additional lakes surveyed by ASRC in 2013 (green points and best-fit line for all 29 lakes).

Additional fathometer surveying done by ASRC during 2013 identified three lakes within the survey area for which the volume determined by bathymetric lidar significantly underestimated the lake volume. Imagery of these lakes, located in the northern part of the airborne survey area, acquired during the airborne lidar survey indicates that the laser's view of the lake bottom was obscured over part of the lake surface by either floating matter, water turbidity, or a dark lake bottom that resulted in a lack of an identifiable water-bottom return and consequently an underestimation of water volume. Subsequent analysis of aerial photography indicates that partial bottom obscuration, and possible underestimation of lake volume, affects less than 10 percent (21 of 283) surveyed North Slope lakes. The overall relationship between fathometer- and lidar-derived lake volumes remains strong despite inclusion of the three partly obscured lakes (fig. S2).

Land-surface elevation data acquired by Great Bear's contractor CGG during 2012 and 2013 seismic surveys provided more than 31,000 GPS-derived data points to evaluate the accuracy of lidar-derived topography. On average, GPS-derived elevations acquired for the seismic surveys were about 0.5 m higher than those determined during the airborne lidar survey. This difference is largely attributable to differing surface conditions during the wintertime seismic surveys (frozen ground and accumulation of snow and ice) and the summertime lidar survey (thawed ground and no surface snow or ice).

The wetland system on this part of the North Slope is dominated by the mixed unit of emergent/scrub-shrub covering 15,547 ha. The next most common habitat with a total area of 8,164 ha is freshwater emergent. In the study area, lake area totals 2,304 ha. The mixed unit scrub-shrub/emergent covers 1,405 ha. In this area of the coastal plain, scrub-shrub are assigned the least wet water regime and cover 286 ha. Most wetland habitats, other than scrub-shrub, are assigned a mid-level moisture regime. Wetland water regimes in this part of the North Slope tend toward the less wet water regimes, as compared to the least common and wettest regime. Relatively speaking, wetlands in the study area are of medium to lower ground moisture regimes. Compared to the NWI, we mapped fewer emergent wetlands and more emergent/scrub-shrub, indicating a shift

toward ground moisture conditions that favor scrub-shrub habitat. This trend is also reflected in our increased mapping of scrub-shrub. Combined scrub-shrub/emergent and scrub-shrub totals for both time periods are similar, though we mapped more scrub-shrub. This suggests that changes in environmental conditions that favor a spread of scrub-shrub are subtle.

Advantages of the airborne approach compared to conventional wetlands and water-body depth surveys include the ability to (1) cover large areas rapidly, (2) produce more accurate water-volume estimates in reasonably clear water, and (3) guide ground-based, labor-intensive wetland surveys to areas where soil is most (or least) likely to be saturated.

INTRODUCTION

In August 2012, staff from the Bureau of Economic Geology (Bureau or BEG), Airborne Hydrography AB (AHAB), and Aspen Helicopters (Aspen) conducted an airborne lidar and imaging survey on behalf of Great Bear Petroleum Operating, LLC (Great Bear) in the Deadhorse area on the Alaskan North Slope (fig. 1). The purpose of the survey, conducted as a proof-of-concept study using a new airborne lidar and imaging system (Chiroptera) recently acquired by the Bureau, is to develop, demonstrate, and evaluate the unique environmental mapping capabilities of the system to rapidly, accurately, and cost-effectively determine key physical parameters relevant to environmental assessment on the North Slope. The system was used to determine microtopography (using the topographic laser) that controls vegetation distribution and drainage patterns; discriminate wetlands and uplands (using bathymetric and topographic lasers and imagery); map wetland type and distribution (using both lasers and imagery); and determine depths and volumes of shallow, clear lakes common in the survey area (using the bathymetric laser).

The Chiroptera system (fig. 2), as delivered by AHAB in late July 2012 as part of the survey mobilization to Alaska, consists of separate topographic and bathymetric laser systems and a high-resolution, 50 MP digital camera that can acquire RGB and infrared images.

The topographic lidar scanner operates at a near-infrared wavelength of 1 μm , a pulse rate as high as 400 kHz, and an incident angle (from vertical) of 14 to 20 degrees. It can operate to a maximum height of about 1500 m, allowing the system to rapidly scan large areas with a range accuracy of about 2 cm over a flat target. The bathymetric lidar scanner operates at a shorter green wavelength (0.515 μm) and a lower pulse rate (36 kHz). The shorter wavelength allows the laser to penetrate water of reasonable clarity. After the laser reflects off the bottom surface of the lake and back to the source, the transit-time delay between water-surface and water-bottom reflections can be used to determine water depths to a flat-bottom accuracy of about 15 cm. We can estimate lake volume by differencing the upper and lower surfaces of the lake. Also mounted in the Chiroptera chassis is a Hasselblad DigiCAM 50 megapixel natural color or color infrared

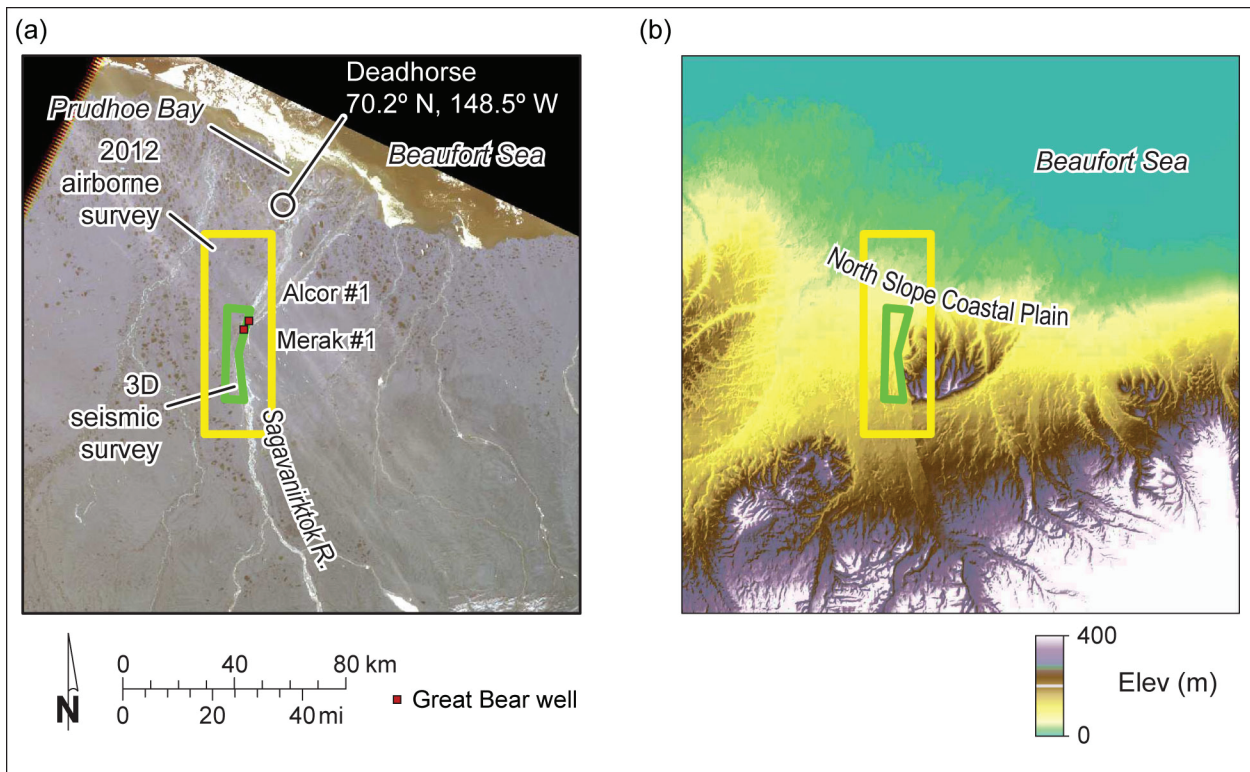


Figure 1. (a) Landsat 5 Thematic Mapper (TM) image of the Deadhorse survey area, Alaskan North Slope, along the Beaufort Sea showing the 2012 airborne lidar and imagery survey area, the 2012 3D seismic survey area, and the Great Bear Alcor #1 and Merak #1 well locations. (b) Digital elevation model (30-m cell size) of the Deadhorse area constructed from TM data. Landsat 5 image and topographic data acquired in June 2009. Landsat data from the U. S. Geological Survey.

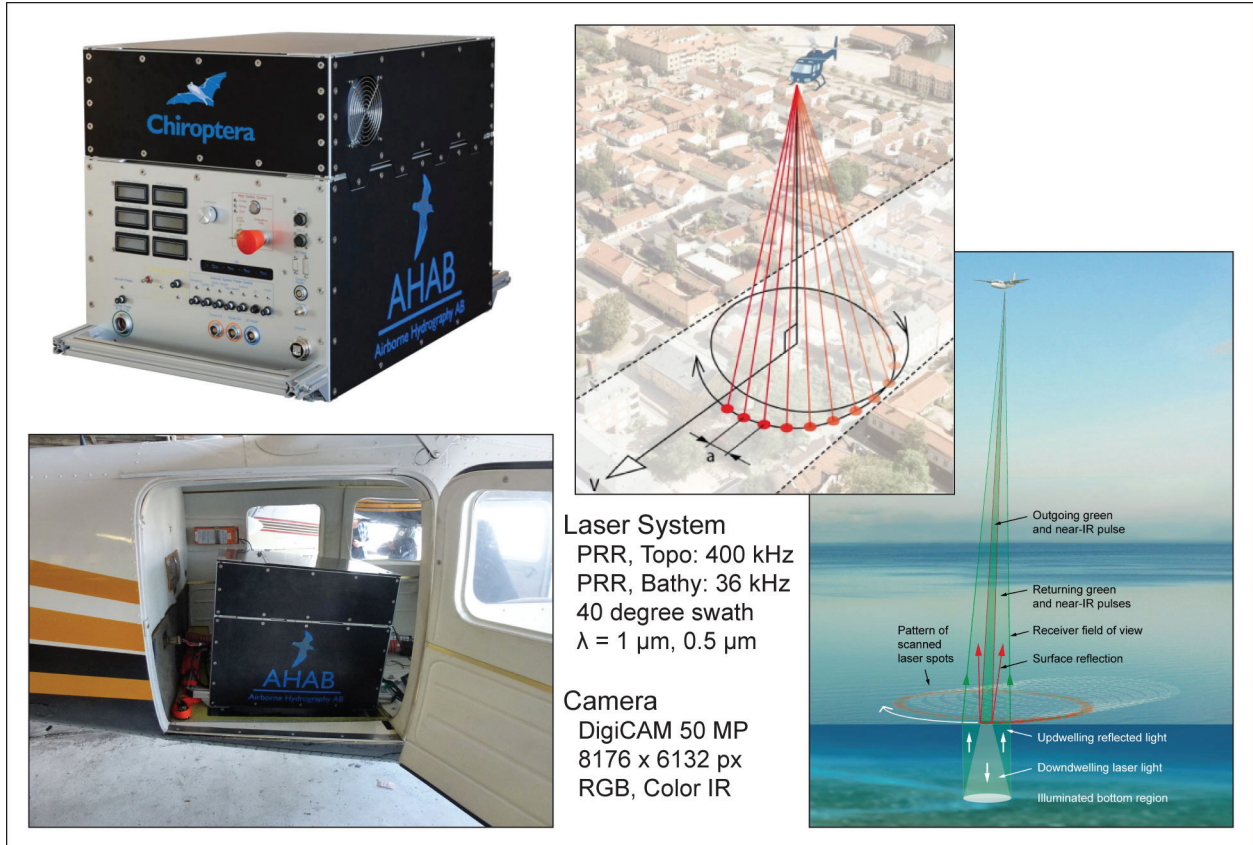


Figure 2. (left) The Chiroptera system and the system mounted in a twin-engine Partenavia P68 aircraft for the North Slope survey. Instruments include topographic and bathymetric lidar and a high-resolution camera. (right) Elliptical (Palmer) scanning pattern employed by the Chiroptera topographic and bathymetric lasers and generalized illustration of water-surface and water-bottom returns.

camera that acquires images at a resolution of 8,176 by 6,132 pixels. The Chiroptera can acquire simultaneous high-resolution imagery and topographic and bathymetric lidar data.

This report summarizes processing, analysis, and interpretation of lidar data and imagery acquired during the August 2012 airborne survey and wetlands mapping completed using airborne data and other data sources that apply to shallow-lake bathymetry and wetlands mapping. Ground-truthing information provided by Great Bear contractors ASRC Energy Services (wetlands maps and bathymetry for selected lakes) and CGG (GPS-derived source and receiver locations and elevations acquired during seismic surveys completed in 2012 and 2013) has been incorporated into the study to help evaluate the accuracy and understand the advantages and disadvantages of airborne lidar surveying for topographic and bathymetric applications on the Alaskan North Slope.

METHODS

August 2012 Airborne Survey

In preparation for the Alaska survey, AHAB, Aspen, and Bureau staff installed and tested the Chiroptera system at the Aspen facility in Oxnard, California. An Aspen pilot and mechanic flew the instrument to Deadhorse, Alaska from Oxnard, where they joined Bureau and AHAB staff to conduct the airborne survey.

Ground-based global-positioning system (GPS) reference stations were established in the survey area using Trimble Net R9 GPS receivers capable of acquiring satellite navigation data from U. S. (GPS) and Russian (GLONASS) satellites. Using both constellations ensured that adequate satellite geometries were available at all flight times. These stations were set up at benchmarks at the Deadhorse Airport (benchmark SCCB, fig. 3) and in the eastern part of the survey area (benchmark L146). Both stations were operating during each flight and calibration test. GPS data, acquired at 1-s intervals, were used along with aircraft GPS and attitude data to determine precise flight trajectories and camera and laser pointing directions during data processing.

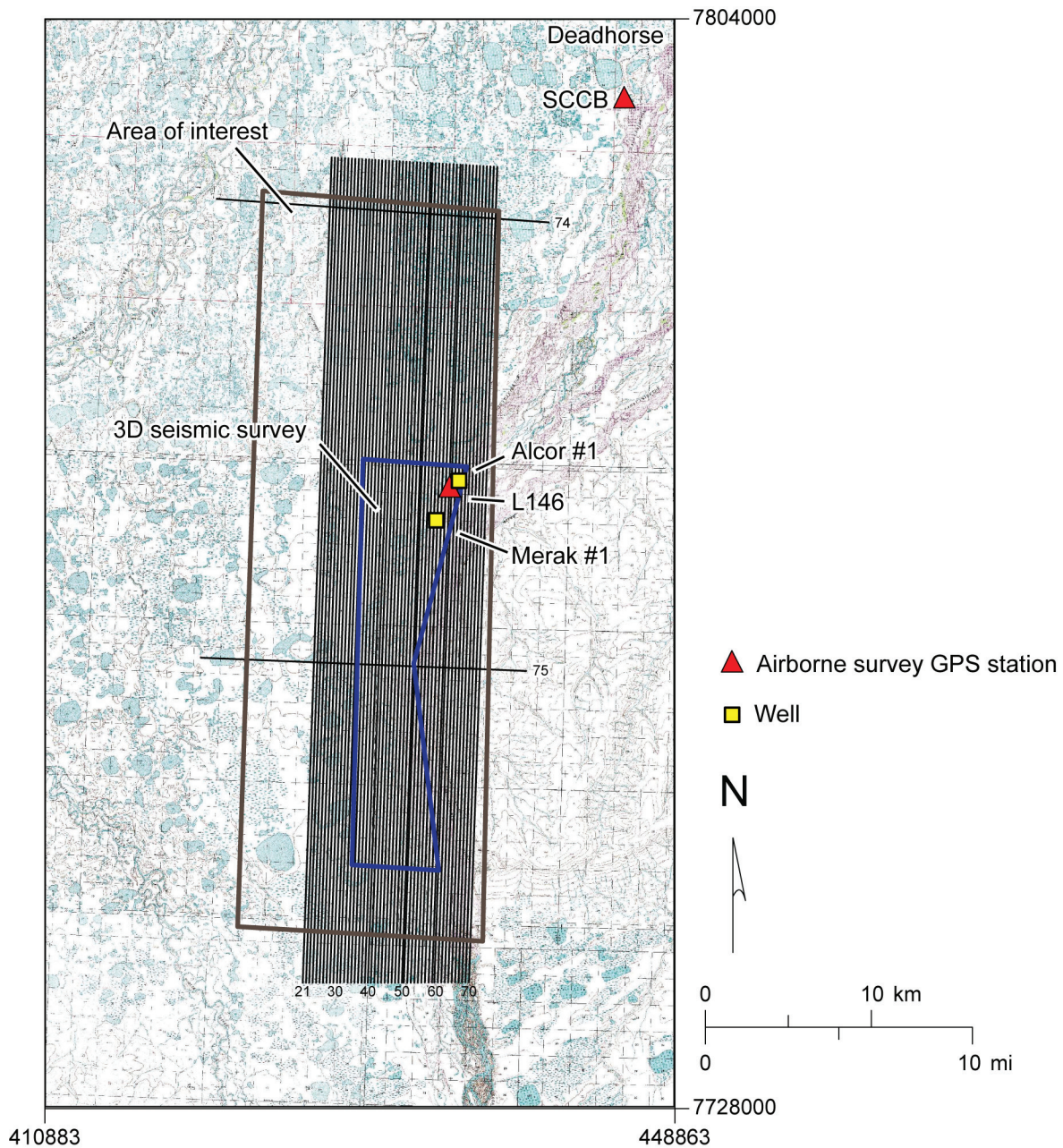


Figure 3. Topographic map of the lidar survey area showing approximate locations of topographic and bathymetric lidar flight lines (north–south main lines and east–west tie lines), the area of interest, and the 2012 3D seismic survey area. Also shown are the Alcor #1 and Merak #1 well locations and benchmarks used as GPS base stations (SCCB and L146) for the airborne survey. Topographic map from the U.S. Geological Survey. Area corner coordinates are in meters, UTM zone 6 north, 1983 North American Datum.

At Great Bear's request, primary objectives for the Deadhorse airborne survey included the entire 3D seismic survey area and as much of the surrounding area of interest (fig. 3) as possible during the surveying time available. Two airborne surveys were completed: a low-altitude topographic and bathymetric lidar survey covering approximately 490 km² (10 km east–west by 49 km north–south, fig. 3), and a higher-altitude infrared imagery survey (fig. 4). Airborne data were acquired during eight flights from the Deadhorse Airport between August 5 and August 9, 2012, with two flights each on August 5, 7, 8, and 9 (table 1). Weather (rain or low cloud ceiling) precluded flights on August 6, 10, and 11.

Flight altitudes for the Deadhorse lidar survey were constrained by the bathymetric laser scanner, which has a maximum flight height of about 400 m above the water surface. To ensure complete coverage and adequate swath overlap, flight-line spacing for the lidar survey was 180 to 200 m. Lidar data were acquired along 57 north-south lines, each approximately 49 km long, and two east-west tie lines about 20 km long (fig. 3). Calibration data were acquired at the beginning and end of flights by acquiring lidar data over ground-surveyed areas on the airport taxiway. At the end of each flight, topographic and bathymetric lidar data were downloaded to field computers and backed up on storage drives. Preliminary field processing included determining initial flight trajectories from aircraft and ground station GPS data, verifying data quality and ground coverage, and decimating the data to produce sample maps and cross sections in key areas.

Color infrared imagery was acquired during a single flight on August 9, 2012. Flight elevation was increased to 915 m to increase the swath width and maximize the survey area while retaining adequate pixel size (table 1). Infrared imagery was acquired along 13 north-south flight lines spaced about 660 m apart (fig. 4). Total area flown during this survey was about 420 km² (8.6 km east–west by 49 km north–south). Images were downloaded to field computers and backed up on external storage drives for post-survey processing.

Total survey flight distance for the 2012 Deadhorse survey included more than 2800 km for lidar data acquisition and more than 630 km for infrared imagery. The bathymetric lidar survey, using

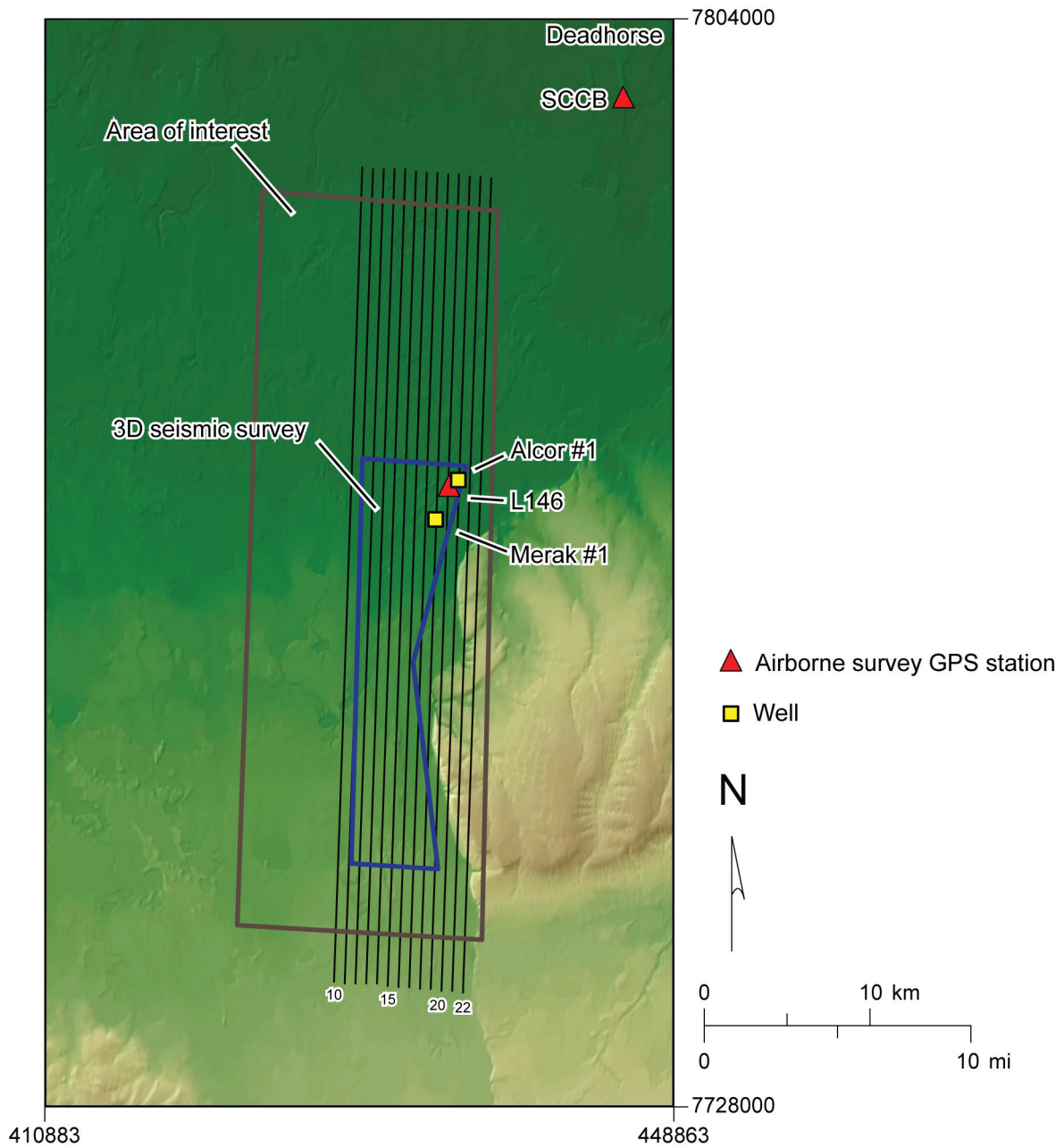


Figure 4. Digital elevation model of the survey area showing approximate locations of infrared imagery flight lines, the area of interest, and the 3-D seismic survey area. Area corner coordinates are in meters, UTM zone 6 north, 1983 North American Datum.

Table 1. Data acquisition flights, 2012 airborne lidar and imaging survey, Deadhorse area, Alaska.

Date	Flight	Elev. (m)	Instruments	Lines	Notes
7/30/2012	20120730a	n/a	Topo, bathy	n/a	Installation test flight, Oxnard, CA
8/5/2012	20120805a	400	Topo, bathy, RGB	32-40, 69	Lidar and RGB imagery
8/5/2012	20120805b	400	Topo, bathy, RGB	41-50	Lidar and RGB imagery
8/7/2012	20120807a	n/a	Topo, bathy, RGB	n/a	Low clouds; calibration only
8/7/2012	20120807b	400	Topo, bathy, RGB	31, 51-59	
8/8/2012	20120808a	400	Topo, bathy, RGB	60-68, 70	
8/8/2012	20120808b	400	Topo, bathy, infra-red	23-30, 74, 75	
8/9/2012	20120809a	915	Infrared	10-22	
8/9/2012	20120809b	400	Topo, bathy, infra-red	21, 22, 42, 44, 55, 62, 69	Reflights
8/11/2012	20120811a	n/a	n/a		Navigation calibration, Deadhorse airport

a laser that fires at 36 kHz, yielded more than 1 billion laser pulses and recorded waveforms. The topographic lidar survey, using a laser that fires more than 10 times faster, yielded more than 13 billion laser pulses and recorded surface returns. Total amount of data acquired exceeded 3 terabytes, including 2.2 terabytes of lidar data and 1 terabyte of high-resolution imagery.

Lidar Data Processing

Basic lidar data processing steps included (1) precisely determining the airborne instrument trajectory by combining ground GPS base station data with aircraft position and attitude information acquired during each flight; (2) processing the topographic and bathymetric lidar data at full resolution to determine the absolute, three-dimensional position of individual topographic lidar returns from plants and ground surfaces and bathymetric lidar waveforms; (3) combining topographic lidar returns from all flights to produce “point clouds” (collections of individual lidar returns) as well as digital elevation models (surfaces fit to point clouds at one or more spatial resolutions; 1-m lateral resolution models have been constructed from the Alaska data set); (4) analyzing bathymetric lidar waveforms to classify laser returns as water surface or water bottom and create associated point clouds for those surfaces; and (5) combining bathymetric lidar point clouds from the entire survey area to produce digital elevation models (DEMs) of key surfaces, such as the water surface and water bottom. These surfaces are generally shown at lower resolution in this report and at higher resolution on the accompanying maps and data volume.

Digital Terrain Model and Bare Earth Generation

The topographic lidar processing described above produces DEMs that may include the tops of vegetation, buildings, roads, and other structures. Raw topographic lidar returns over the survey area were further processed at full resolution using the AHAB LSS processing software in an attempt to remove these features. To create a Digital Terrain Model (DTM), or a Bare Earth Surface, the lidar point cloud data are used in a series of processing steps to first generate a rasterized surface model, then a filtered and interpolated ground model. A DTM contains all ground

points captured in the lidar data and removes all vegetation and man-made structures. Given that the Alaska data were virtually free of buildings and vegetation, the DTM closely resembles the point cloud returns.

Because the entire data set is so large, the data were tiled for processing. Using software written at Applied Research Laboratories at The University of Texas at Austin, a Digital Surface Model (DSM) was created for each tile by gridding the point cloud data at 1-m resolution. A DSM is a raster product containing one elevation value per x-y grid cell. This surface model is the starting point for generating a DTM. Using several algorithms, the ground return points in the surface model are identified and separated from the non-ground return points. Following this classification, non-ground regions (for example, those containing vegetation and buildings) are interpolated over from the ground regions using bilinear interpolation. This creates a continuous surface model that represents the ground surface. Finally, the DTM tiles are combined to form larger tiles spanning the entire data set. The entire Alaska data set formed five 10 km x 13 km DTM tiles, each approximately 500 MB in size in GeoTIFF format. The files are geographic information system (GIS) compatible and are included on the accompanying data volume (Appendix D).

The 1-m resolution of the DTM surface provides detail of both large- and small-scale features. These include a series of connected shallow lakes, the highly variable terrain on the eastern bank of the Sagavanirktok River, permafrost structure especially in the southern part of the data set, the Dalton Highway adjacent to the Sagavanirktok River, and the subtle flow patterns visible in the river basin.

Wetlands Delineation

Wetlands were previously mapped by the U.S. Fish and Wildlife Service (USFWS) in the late 1970s and early 1980s as part of the National Wetlands Inventory (NWI). The NWI was mapped from aerial photography at a scale of 1:24,000. The high-resolution color-infrared (CIR) aerial imagery acquired in August 2012 (table 1 and fig. 4) served as the base for our wetland mapping

at a scale of 1:10,000. Wetland boundaries were interpreted from multiple sources in addition to the CIR imagery. The primary source for wetland interpretation was classified SPOT imagery acquired in 2009. Other ancillary data sets include a classified Landsat scene, a National Land Cover Database 2001 map, and the 1970s–1980s NWI map.

The CIR imagery acquired during the airborne survey was processed and brought into the GIS environment. The imagery served as the spatial reference for positioning wetland boundaries and, in some instances, provided the spectral signature for wetland interpretation. An unsupervised SPOT image classification was the primary source for wetland interpretation and in many instances served as the source for wetland boundary locations. The unsupervised Landsat classification was also frequently consulted for visual interpretation of wetland habitat type.

Habitat classification relied heavily upon previous NWI mapping. While boundaries were mapped from the 2012 CIR imagery, the 1970s–1980s NWI map served as a proxy for the recent map. Both maps employed the Cowardin and others (1979) classification system.

Satellite Data Processing

Satellite data provided the larger context for the high-resolution airborne survey data and were useful in establishing the geomorphic setting and in supporting wetlands mapping. The principal satellite data used in this study was a Landsat 5 TM image acquired on July 5, 2009. The thermal band was resampled to 30 m resolution to be used in the image classification with the six other bands. All bands were stacked and the image was then subset to the area of interest. A raster DEM was extracted from the image using ERDAS Imagine software. A NDVI (Normalized Difference Vegetation Index) image was calculated as well using the standard formula of $NDVI = (NIR - red) / (NIR + red)$, where NIR (near infrared) is Landsat TM band 4 and red is Landsat TM band 3. Next, two classifications were run using the ISODATA (iterative self-organizing data analysis technique) unsupervised classification as follows: (1) Landsat TM bands plus NDVI and (2) Landsat TM bands plus both NDVI and the raster DEM. Parameters for both classifica-

tions were 30 iterations, 0.98 convergence threshold, and 30 output classes. In each case, the 30 spectral clusters were identified and reclassified to the final 10 classes based upon divergence statistics and visual discrimination. Additionally, a SPOT 5 mosaic of the entire area was analyzed using the same parameters indicated above.

Features were more clearly identifiable after the inclusion of the DEM band. Differences in NDVI across the area were minimal. The largest differences were observed among water bodies, the riverbed, and the surrounding vegetated wetland area. In comparison to the NWI, there were significant differences in water bodies. The NDVI classification identified areas that the NWI classified as open water bodies as having vegetation present. If the wetland inventory is accurate, this could be caused by aquatic vegetation or algae that are photosynthetically active. The classification was successful with regards to the identification of ten spectrally and topographically distinguishable landforms and habitats. Topography in particular appears to be a major factor in these differences. Further assessments using high spatial and spectral resolution techniques are necessary to distinguish among different types of wetlands as well as permanently dry areas.

COLOR-INFRARED (CIR) IMAGERY

Mosaics created from high-resolution CIR imagery acquired in August 2012 (fig. 5) cover approximately the same area that the airborne lidar data covered (figs. 2 and 3). Georeferenced and color-adjusted mosaics were used to identify soil and ice polygon features and determine land and water boundaries and subtle vegetation assemblage differences across the survey area. These features are much more distinct on individual images with an original pixel size smaller than 10 cm than they are on higher-altitude and satellite imagery such as the 2009-2010 SPOT imagery available for the area (fig. 6). Interpretability of topographic lidar data is enhanced by draping high-resolution CIR images on DEMs and point clouds.

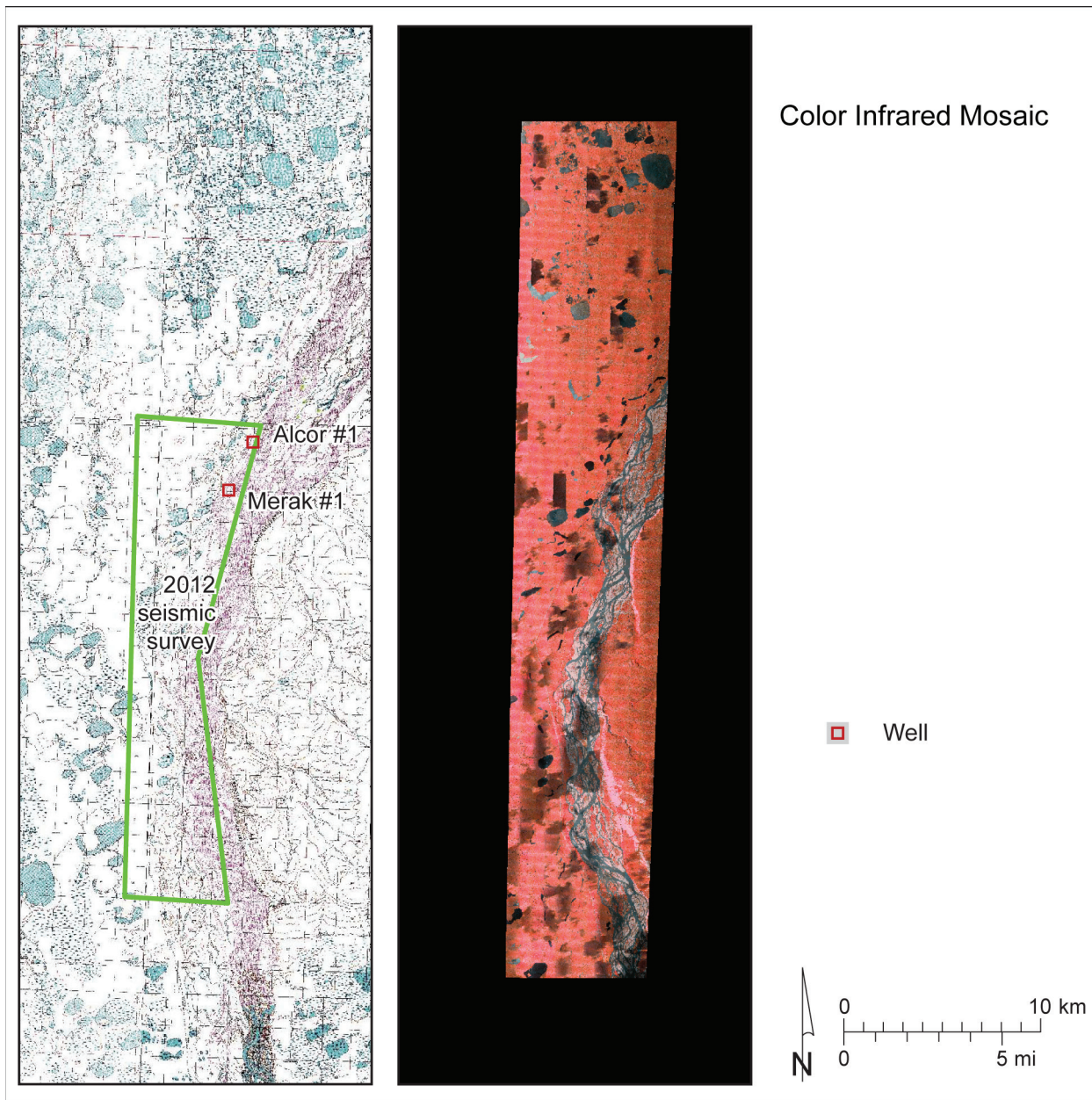


Figure 5. Georeferenced color-infrared (CIR) mosaic of the Deadhorse survey area acquired in August 2012. Full-resolution images have an individual pixel dimension smaller than 10 cm.

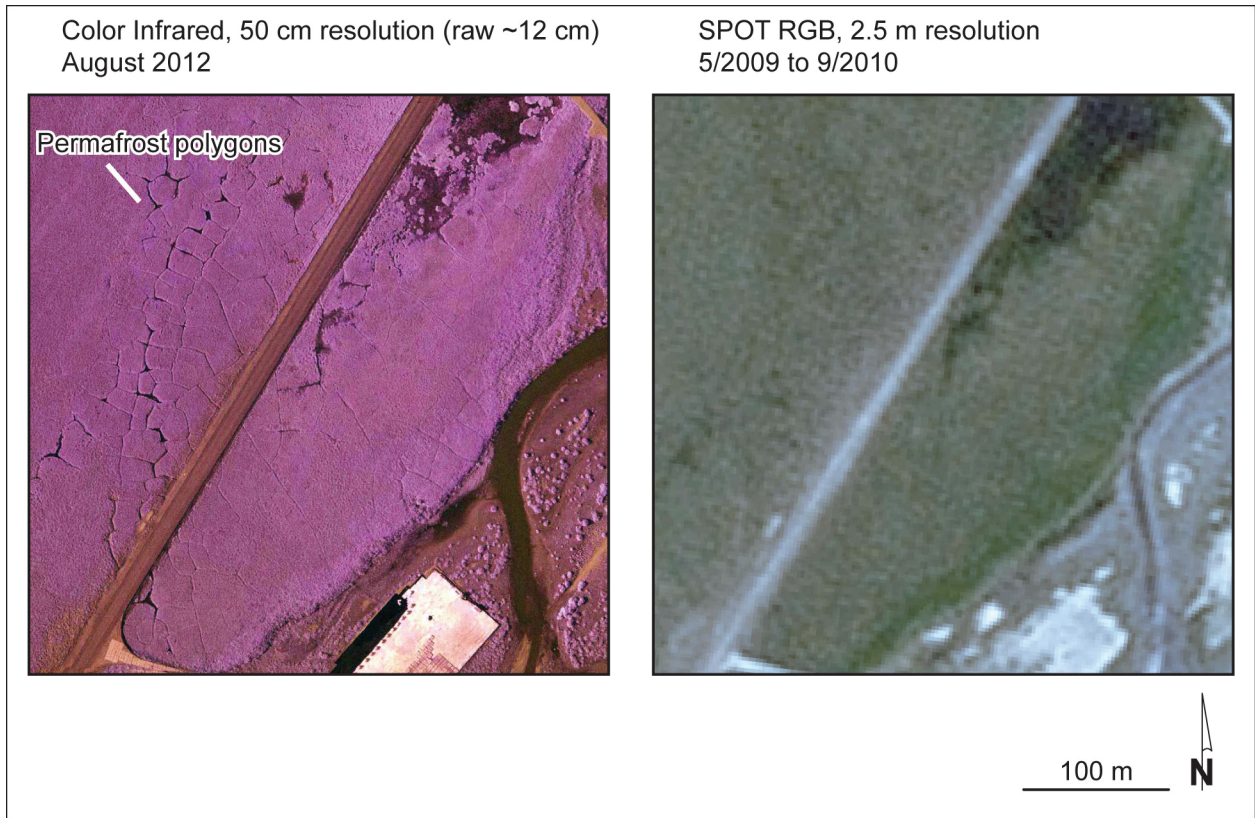


Figure 6. Comparison of resolution achieved with the (left) 2012 CIR and (right) 2009-2010 SPOT imagery along the Dalton Highway near the Merak #1 wellpad. Permafrost polygons are clearly visible in the CIR imagery.

NORTH SLOPE WETLANDS AND UPLANDS

Wetland habitats delineated from remotely-sensed imagery were captured in the GIS environment where acreage calculations were made. Water bodies over 8.33 ha (20.6 acres) were coded as lakes, smaller water bodies as ponds. Water bodies are found throughout the study area, but larger lakes are concentrated in the north (fig. 7). The combined total for all water bodies (exclusive of the river) was 2,304 ha (5,693 acres) (table 2). All emergent wetlands in the study area are freshwater emergent and cover a total area of 8,164 ha (20,174 acres). When emergent wetlands are found in conjunction with scrub-shrub, with at least 30 percent of each habitat occurring in the same general area, the habitat is identified as a mixed unit. The mixed unit of emergent/scrub-shrub covers 15,547 ha (38,418 acres). In this area of the coastal plain, scrub-shrub (primarily composed of dwarf willow species) are saturated with water and cover 286 ha (707 acres). The mixed unit scrub-shrub/emergent covers 1,405 ha (3,472 acres). The Dalton Highway comprises much of the upland category in the study area with 148 ha (365 acres) mapped.

Following the Cowardin (1979) classification system, water regime designations are assigned to the habitat class providing soil moisture information. The majority of all wetland habitats, other than scrub-shrub, are assigned a seasonally flooded/saturated water regime (table 3). This is the mid-level moisture regime found in this wetland system. Scrub-shrub habitat in the region is assigned a saturated moisture level, the least wet water regime. The second-most common water regime assigned to wetland habitats is saturated. Wetland water regimes in this part of the North Slope tend toward the less wet saturated and seasonally flooded/saturated water regimes, as compared to the least common and wettest semipermanently flooded regime. Relatively speaking, wetlands in the study area are of medium to lower ground moisture regimes.

Overall acreage of wetland habitats in the Bureau (BEG) map and NWI map is similar. However, the locations of habitats differ between the two maps (fig. 8). Wetland habitats may be shifting through time due to climatic conditions that affect ground moisture conditions. As with all

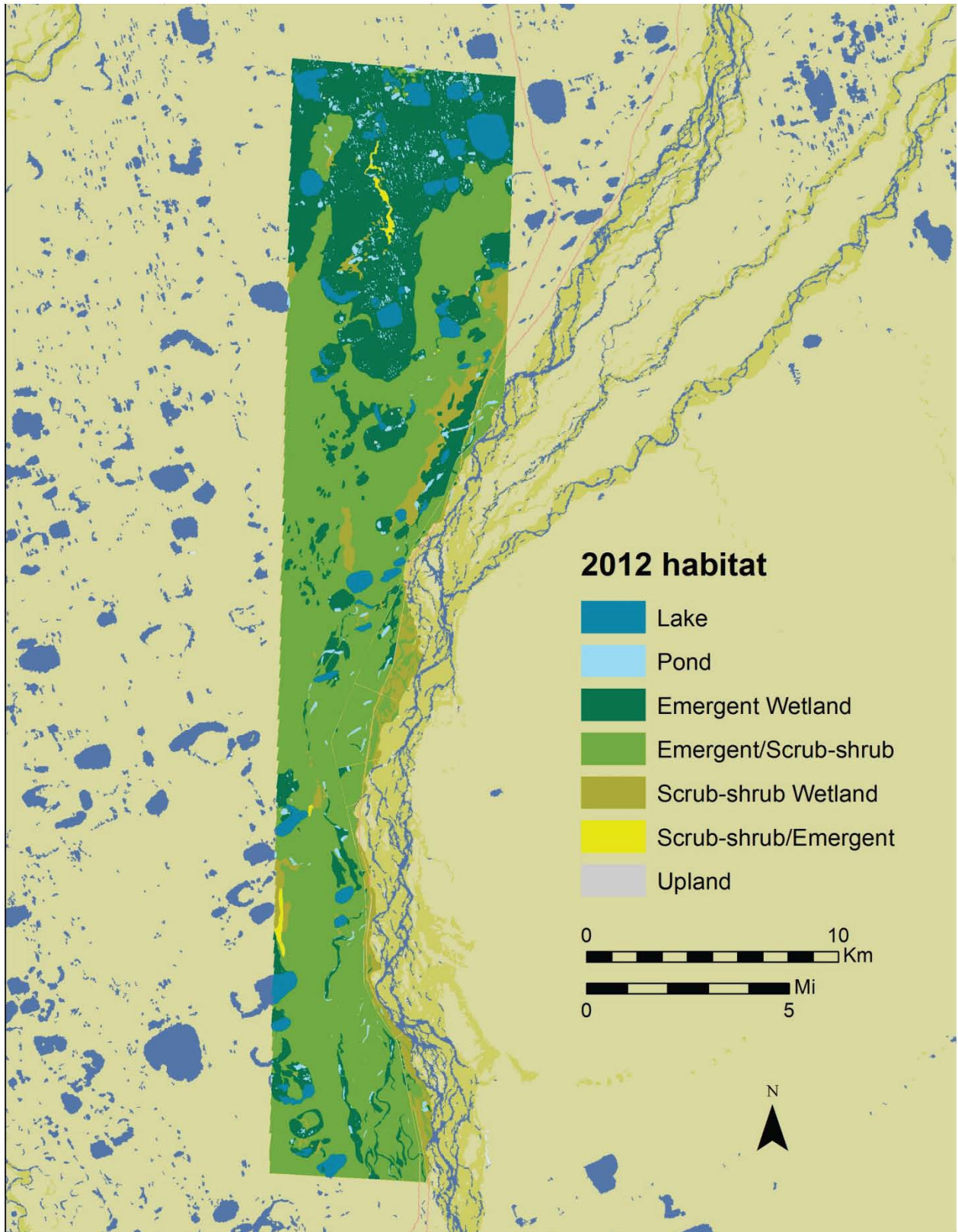


Figure 7. 2012 BEG wetland map.

Table 2. Habitat area totals for BEG map.

Habitat	Area (ha)	Area (acres)
Lake	2,304	5,693
Emergent wetland	8,164	20,174
Emergent/Scrub-shrub	15,547	38,418
Scrub-shrub	286	707
Scrub-shrub/Emergent	1,405	3,472
Upland	148	365

Table 3. Percentage of water regime modifiers for wetland habitats. Saturated is least wet, semi-permanently flooded is most wet.

Habitat	Saturated	Seasonally flooded/ saturated	Semipermanently flooded
Emergent wetland	16	58	26
Emergent/Scrub-shrub	46	52	1
Scrub-shrub	100		
Scrub-shrub/Emergent	40	51	9

Table 4. Habitat area totals for NWI and BEG maps.

Habitat	NWI (ha)	NWI (acres)	BEG (ha)	BEG (acres)
Lake	2,210	5,461	2,304	5,693
Emergent wetland	10,647	26,310	8,164	20,174
Emergent/Scrub-shrub	12,967	32,042	15,547	38,418
Scrub-shrub	97	240	286	707
Scrub-shrub/Emergent	1,522	3,761	1,405	3,472
Upland	45	112	148	365

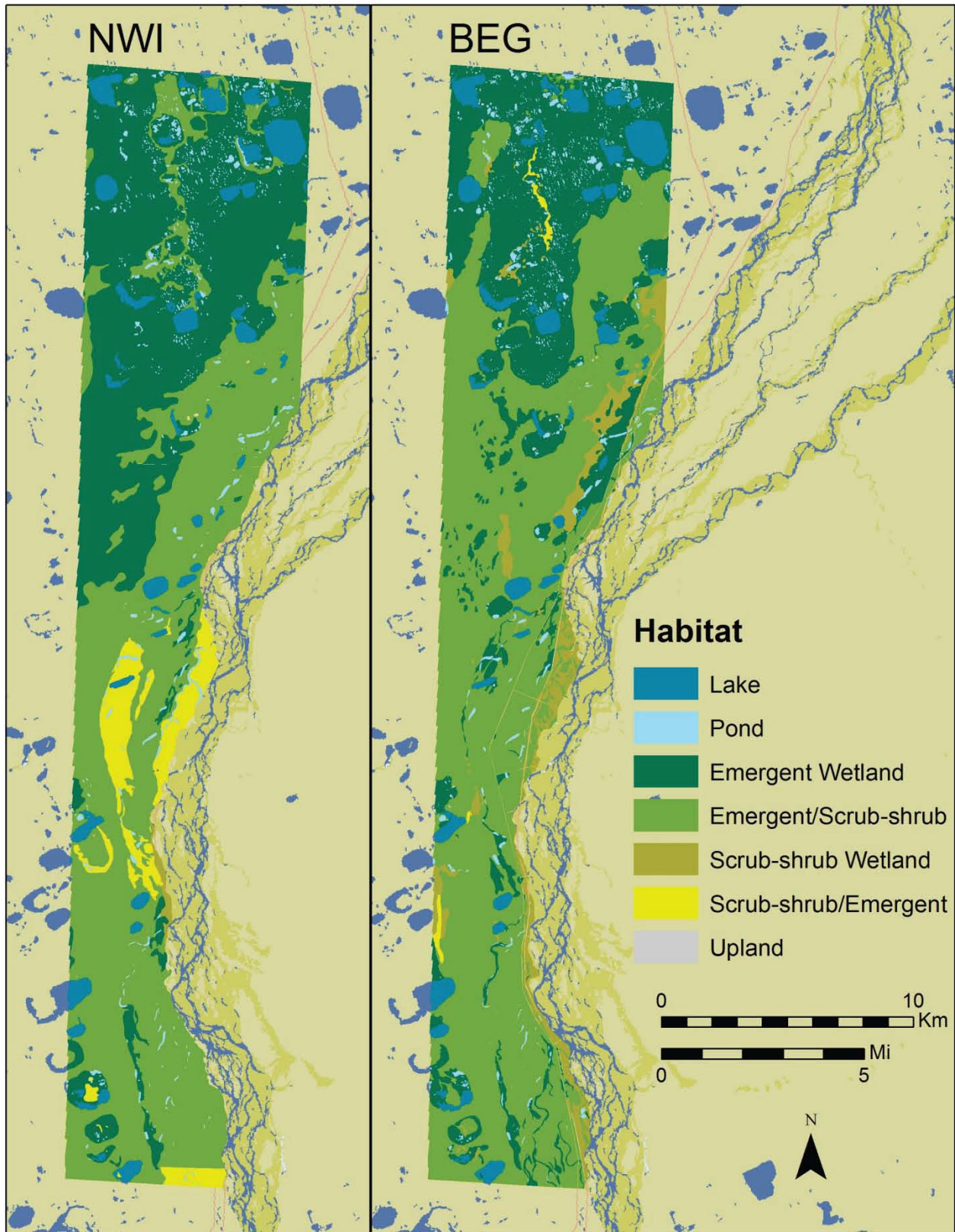


Figure 8. Comparison between 1970s-1980s NWI map and 2012 BEG wetland map.

mapping, interpretational differences are reflected in the final map products. In 2012, we mapped fewer emergent wetlands and more emergent/scrub-shrub, indicating a shift towards ground moisture conditions that favor scrub-shrub habitat. This trend is also reflected in the increased area of scrub-shrub mapped in the study area in 2012. When scrub-shrub/emergent and scrub-shrub numbers area combined, the totals for each time period are very similar. This suggests that changes in environmental conditions that favor a spread of scrub-shrub are subtle.

Combined scrub-shrub emergent and scrub-shrub totals were nearly the same (fig. 9 and table 4), though we mapped much more scrub-shrub, mostly between the Dalton Highway and the Sagavanirktok River. We mapped significantly less emergent wetland and more emergent/scrub-shrub. Lake and pond area were very similar, with a 4 percent increase between the 1970s-80s and 2012 area totals. Much of this is likely due to more precise mapping of water bodies in 2012. There appears to be some alteration of the wetland habitat due to the Dalton Highway. The highway forms a hydrologic impediment between the Sagavanirktok River and the adjacent floodplain and wetlands. In the northern half of the study area, emergents and patches of scrub-shrub are mapped to the west of the highway. Toward the middle of the study area, the buried pipeline forms a levee along the river where water ponds on either side. Scrub-shrub wetlands are common in the depressions flanking the pipeline embankment.

In 2013, ASRC provided BEG with a high-resolution wetlands map for comparison and review purposes. The most significant differences between the BEG and ASRC wetland maps are the delineations between emergent marsh/scrub-shrub mixed units and fully emergent marsh (fig. 10). The BEG map includes nearly double the amount of emergent/scrub-shrub as was mapped by ASRC (4,030 ha vs. 2,044 ha). Both groups mapped the majority of emergent/scrub-shrub with the saturated (B) water regime. The difference between the two wetland interpretations is accounted for in the mapping of emergent marsh. ASRC mapped significantly more emergent marsh than BEG (2,719 ha vs. 472 ha). Roughly half of the emergent marsh mapped by ASRC was assigned the same water regime (B) that the BEG assigned to the emergent/scrub-shrub

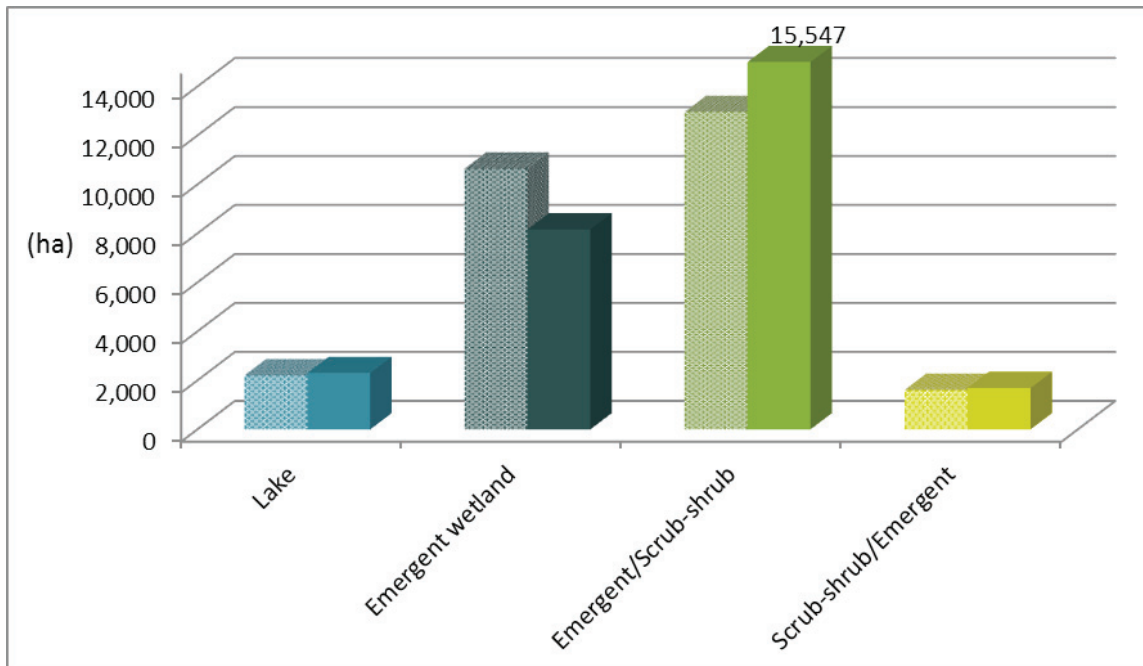


Figure 9. Habitat area comparison between NWI (hatched) and BEG wetland map (solid).

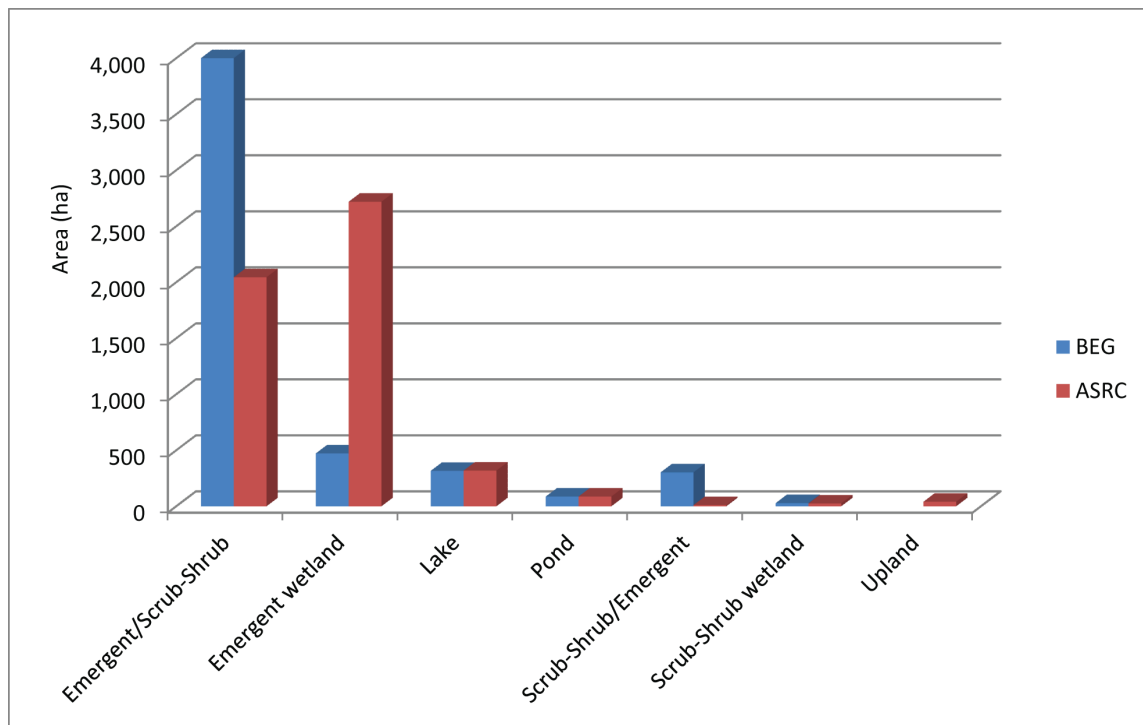


Figure 10. Habitat area totals (hectares) from BEG and ASRC wetland maps.

wetlands. When dominantly emergent marsh habitat are combined, emergent + emergent/scrub-shrub, ASRC mapped more emergent wetland in the map area than BEG (4,763 ha vs. 4,502 ha). BEG mapped more scrub-shrub dominated habitat.

TOPOGRAPHIC LIDAR VERIFICATION AND MAPPING

Airborne and ground-based laser systems have been used for many years to produce high-resolution DEMs. The Alaskan North Slope is an area of generally low relief (fig. 1), having important periglacial and permafrost features such as soil and ice polygons and pingos (hydrolaccoliths, or roughly conical ice-heave structures mantled with soil that can be tens of meters high). Standard topographic data over this region within the Arctic Circle consists of small-scale (1:63,360) U. S. Geological Survey topographic maps contoured at 25-ft (~8 m) intervals (fig. 11) and DEMs created from satellite data at 30-m spatial resolution. These maps have insufficient lateral and vertical resolution to effectively map critical permafrost features or the elevation-influenced distribution of wetlands. High-frequency topographic lidar systems such as Chiroptera can produce high-resolution elevation models at single-pass point densities greater than 10 points/m² (fig. 11). At the survey-area scale, these lidar-derived maps of the North Slope depict the general elevation decrease on the coastal plain from the foothills of the Brooks Range on the south to the Saganavirktok River delta and associated deposits adjacent to the Beaufort Sea on the north. Lack of backscattered near-infrared laser reflection from specular surfaces such as lakes and rivers leaves holes in the lidar data where water stands at the surface. These holes can be used to delineate water-body boundaries.

Comparison of Lidar- and GPS-derived Elevations

Three-dimensional seismic data were acquired in parts of the airborne lidar survey area for Great Bear in 2012 and 2013. CGG, the seismic survey contractor, provided kinematic GPS locations and elevations for the two surveys to allow comparisons of GPS- and topographic lidar-derived elevations. The GPS elevations, acquired using fixed base stations and roving receivers, should

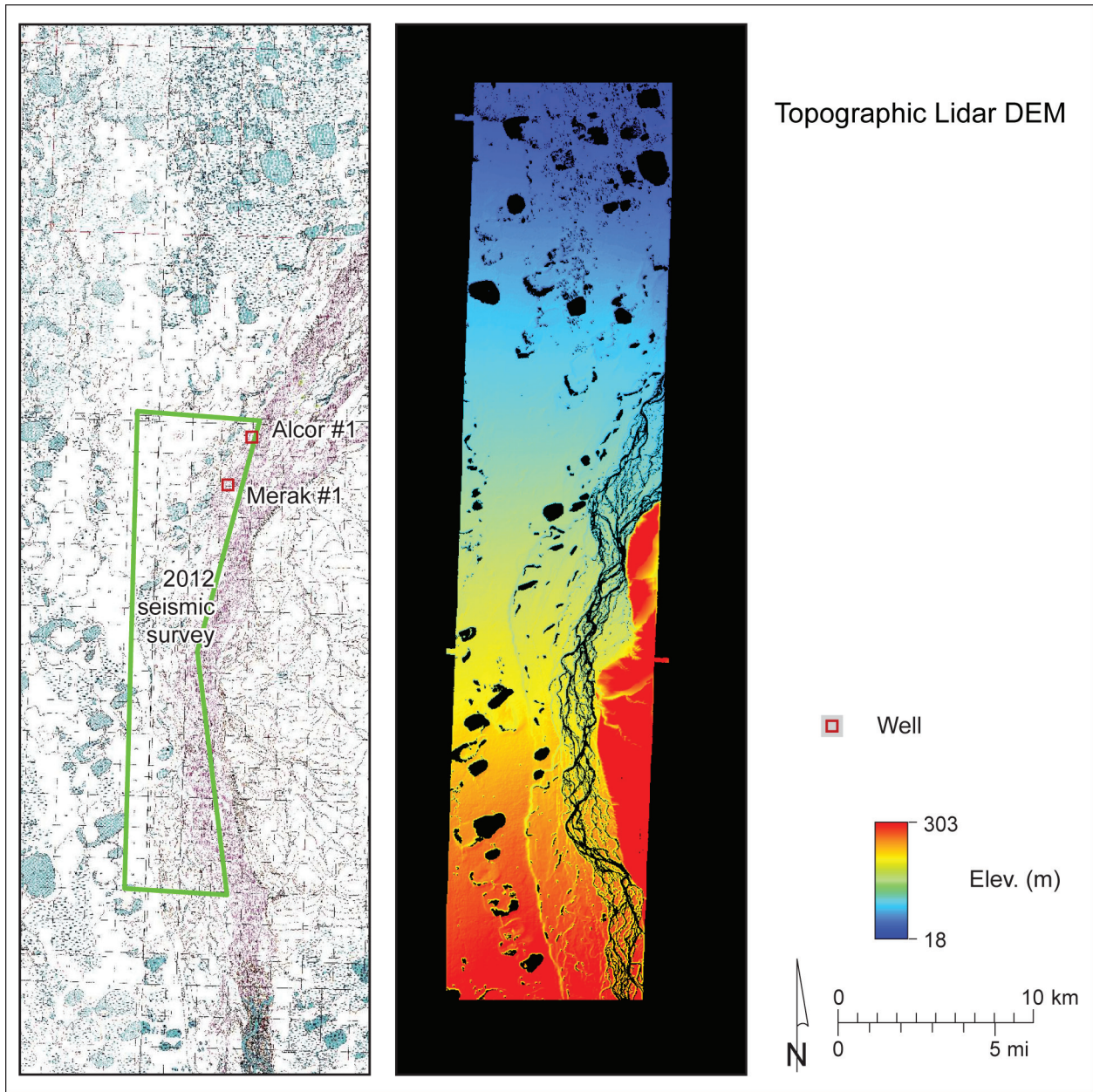


Figure 11. Comparison of (left) U. S. Geological Survey topographic map (1:63,360 scale) and (right) digital elevation model (DEM) constructed from nearly 13 billion topographic lidar data points over the North Slope survey area. Point density at full resolution is about 15 to 20 points/m². Dark areas on the DEM are lake and river surfaces with no near-infrared laser return.

provide locations and elevations accurate to a few centimeters, but were acquired during winter when ground was frozen and snow and ice were present in the survey area. The airborne lidar survey was acquired in the summer of 2012, when the land surface was partly thawed and free of snow and ice. CGG provided locations for seismic source, receiver, and common depth point (CDP) surface locations. Only source and receiver locations were used for lidar comparisons because CDP locations are calculated from primary source and receiver locations rather than measured directly.

For the 2012 seismic survey, we compared 23,438 source or receiver locations with topographic lidar-derived elevations extracted from the 1-m resolution DEM at the source or receiver location. The lidar-derived elevations were adjusted to match the vertical datum (NAVD88, Geoid99) used by CGG. On average, the GPS-derived elevations are 0.45 m higher than lidar-derived elevations (table 5). The standard deviation of the elevation difference is 0.3 m. There were 7817 source or receiver locations available for comparison from the 2013 seismic survey. For these points, GPS-derived elevations were an average of 0.69 m higher than lidar-derived elevations (table 5). Standard deviation for this set of points was 0.2 m. Combining the data from the two seismic surveys yields 31,255 points for comparison. On average, GPS-derived elevations are 0.51 m higher than lidar-derived elevations, with a standard deviation of 0.3 m (table 5).

Maps depicting the difference in elevation between the lidar- and GPS-derived elevations (fig. 12) show that GPS-derived elevations are higher over most of the survey area. East-west banding is evident in both seismic surveys that is strongly correlated with the orientation of seismic source and receiver lines. The banding pattern is attributable to elevation differences in adjacent seismic source and receiver lines, not the lidar-derived elevation data. The average vertical offset between GPS- and lidar-derived elevations of 0.45 to 0.69 m is likely attributable to true elevation differences between winter conditions (presence of frozen ground, ice, and snow) during the 2012 and 2013 seismic surveys and partly thawed ground with no ice or snow during the 2012 airborne lidar survey.

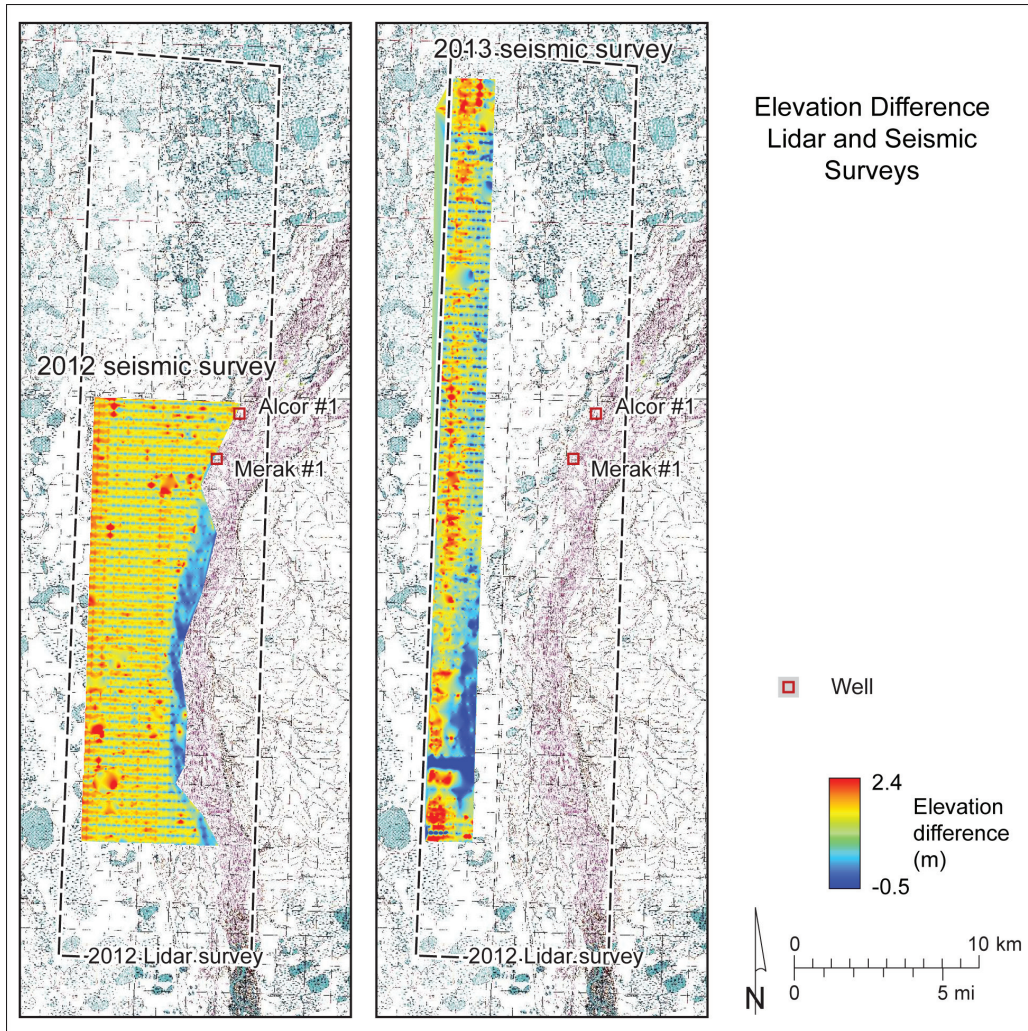


Figure 12. Difference between GPS- and airborne lidar-derived elevation over the 2012 and 2013 seismic survey areas. Positive values denote GPS-derived elevations higher than lidar-derived elevations. GPS-derived elevations are those of source and receiver locations provided by CGG.

Table 5. Comparison of GPS-derived seismic source and receiver elevations with airborne lidar-derived elevations. GPS-derived elevations were provided by CGG for seismic surveys completed in winter 2012 and winter 2013. Positive differences indicate GPS-derived elevations that are higher than lidar-derived elevations.

	2012 Seismic Survey	2013 Seismic Survey	Combined Surveys
Number of points	23,438	7,817	31,255
Average difference (m)	0.45	0.69	0.51
Standard deviation (m)	0.30	0.20	0.30

Mapping Topographic Features: Permafrost Polygons and Pingos

Full-resolution (400 kHz), near-infrared laser returns reveal topographic detail that cannot be achieved with available satellite, aerial imagery, and ground-based surveying methods. We constructed a detailed DEM (25-cm resolution) from full-resolution lidar data at the Merak well pad between the Sagavanirktok River and the Dalton Highway and compared that to the 30-m resolution DEM constructed from Landsat 5 Thematic Mapper data (fig. 13). Critical permafrost-related features such as soil and ice polygons that are a few to a few tens of meters across are not detectable using lower-resolution data, but are well captured and readily mappable at topographic lidar resolution. DEMs such as these allow discrimination of individual soil polygons and the lower-elevation areas between them. Elevation profiles across individual polygons can be used to classify them as low- or high-centered. This information can then be used to better predict water movement and soil moisture patterns in wetland and upland environments. Lidar data are also routinely converted to three-dimensional surfaces (fig. 14) that can be viewed to highlight critical surface features and aid analysis and interpretation of permafrost terrain.

Pingos are distinctive periglacial features found on the Alaskan North Slope and in other Arctic and subarctic regions. These soil-mantled, ice-heave structures thrust upward from the coastal plain, forming roughly conical shapes that can dominate the low-relief landscape. Topographic lidar data and high-resolution imagery greatly assist in characterizing and monitoring the growth or decay of these features over time. Lidar data (DEMs and profiles) acquired across a pingo in the northern part of the survey area (fig. 15) show that it is a 17-m high and 160-m wide conical structure that occupies a basin that is about 3 m below the surrounding coastal-plain surface. High-resolution (5-cm pixel size) imagery overlain on the DEM (1-m cell size) enhance the appearance of the summit crater, the central ice core, mantling soil, and flank crevices.

LIDAR FOR WATERSHED DELINEATION AND TOPOGRAPHIC WETNESS INDEX

To illustrate uses of high-resolution topographic lidar in understanding subtle topographic variations and their possible influence on soil moisture and wetlands distribution, a quarter-meter

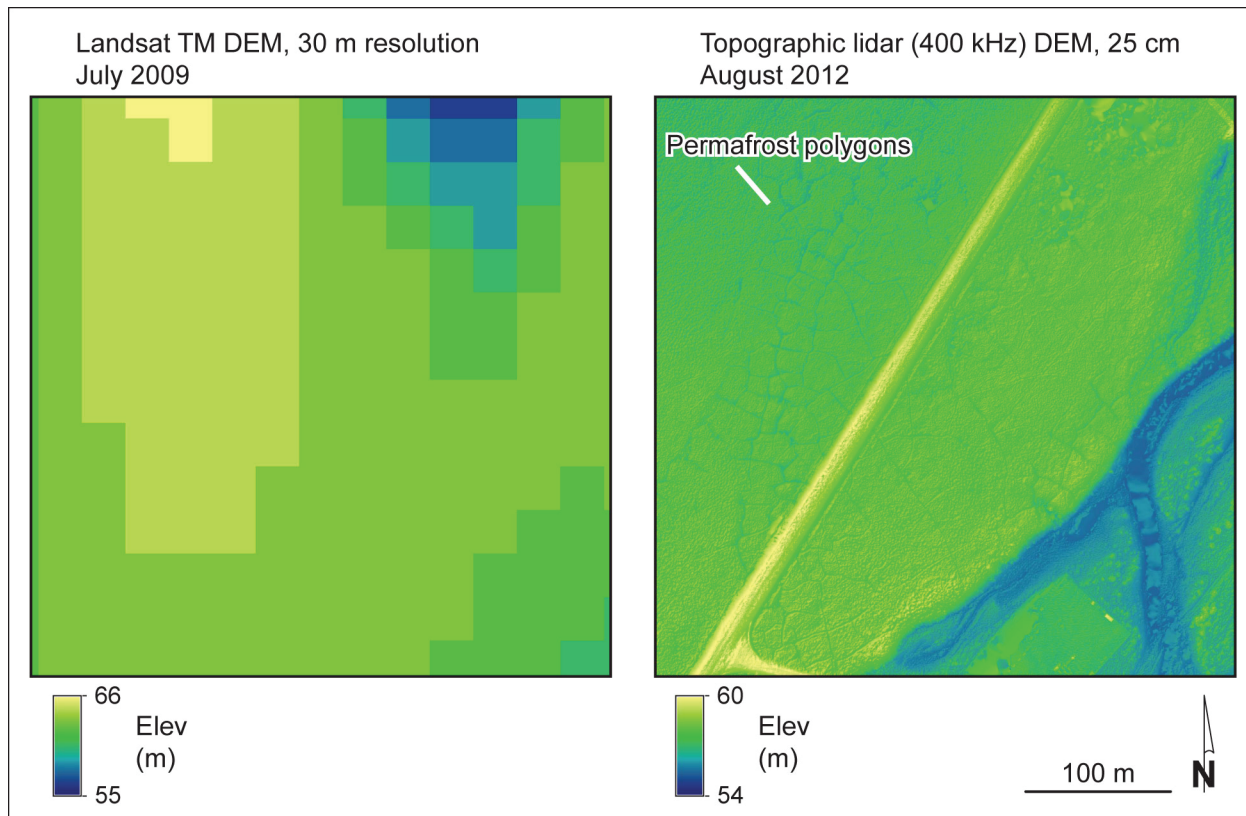
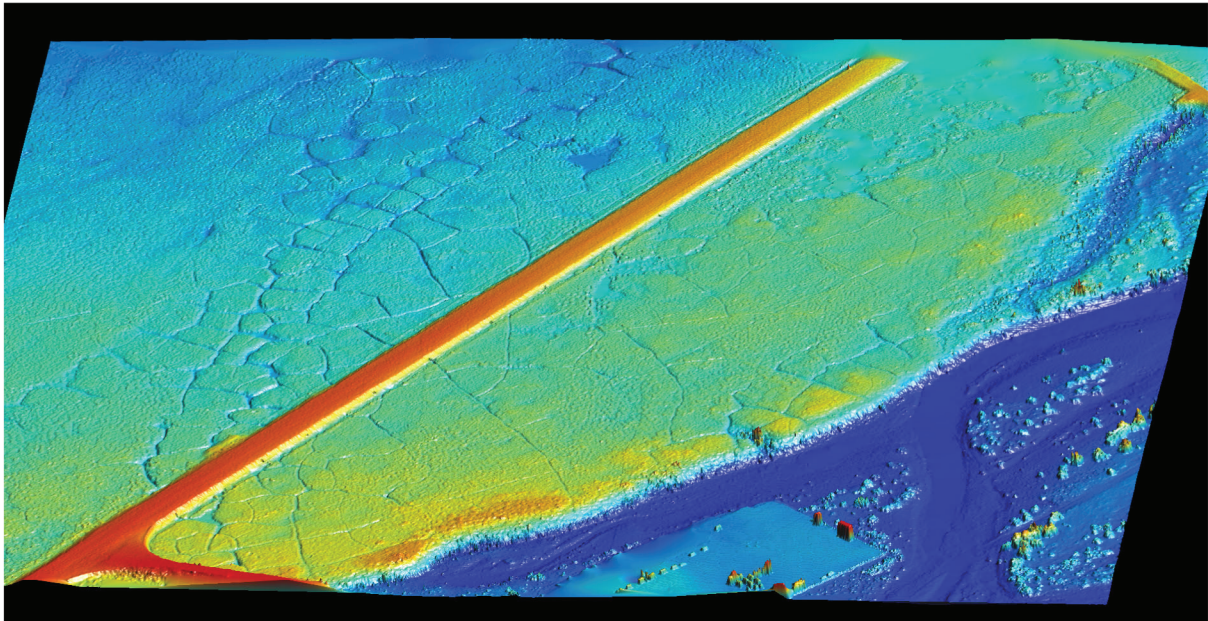


Figure 13. Comparison of typical resolution achieved in DEMs created using (left) Landsat 5 Thematic Mapper data acquired in July 2009 (30-m cell size) and (right) full-resolution topographic lidar data (0.25-m cell size) over a 400×400 m area on the west bank of the Sagavanirktok River. Visible features on the lidar DEM include soil/ice polygons, the Dalton Highway, channels of the Sagavanirktok River, and part of the Merak #1 well pad in the southern part of the image. Landsat 5 data from U. S. Geological Survey.

DEM (25 cm cell) from 400 kHz data, Merak area



Perspective view to northwest

Figure 14. Perspective view toward the northwest of the Merak #1 well pad (foreground), the Dalton Highway, and permafrost-related soil and ice polygons in the North Slope survey area. Image constructed from full-resolution topographic lidar data before vegetation and feature removal.

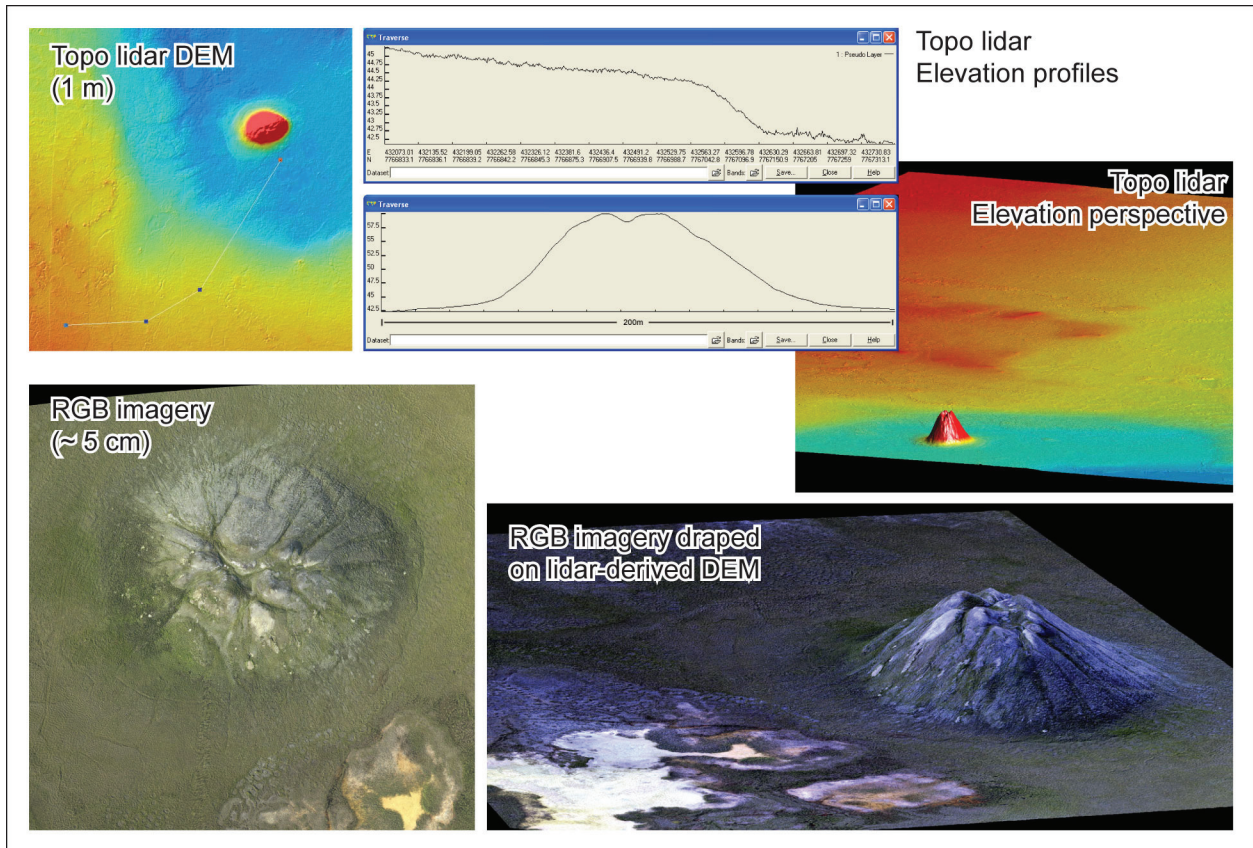


Figure 15. Topographic models, elevation profiles, perspective views, and RGB imagery of a large pingo (17-m high and 160-m wide) in the northern part of the North Slope survey area.

resolution DEM was generated from the lidar point cloud for an area of roughly 30 km² near Milepost 401 of the Dalton Highway. The DEM was analyzed to infer microtopographic controls on soil hydrology and investigate the suitability of lidar for hydrologic analysis within extremely flat terrain, demonstrating its potential for both flow-path modeling and wetland delineation.

Three watersheds contained completely within a subset of the DEM area were identified using ArcMap's Hydrology toolset (fig. 16). All watersheds flow from south to north, and a single watershed may include low-centered polygons, high-centered polygons, and non-polygonated soils. The steepest topographic gradients are located near the edges of thaw lakes, and thus a watershed may exist within meters of a body of open water without flowing into it. The primary microtopographic features within a watershed are associated with the rims of polygons, and water flow is believed to be greatest in the interpolygon troughs. Due to low topographic variation, watershed boundaries are not relevant for roughly ten days during the spring thaw when the region experiences its greatest surface water flow; however, they may characterize both water and solute transport for the area throughout the remainder of the spring and summer.

Secondly, a topographic wetness index (TWI) was created for the DEM area using ArcMap's Spatial Analyst toolbox and Raster Calculator (fig. 17). The TWI is commonly used to predict areas of soil moisture accumulation, and it is defined at any point as the natural logarithm of the upslope contributing area divided by the local slope gradient. Therefore, it is greatest in flat areas with significant flow accumulations. As has been shown, the lidar DEM possesses sufficient resolution to predict microtopographic variation in soil moisture, with the greatest TWI values in the interpolygon spaces and in the low centers of individual polygons. On a larger scale, TWI may hold power to predict the spatial extent of wetlands within the Great Bear lease area, serving as a tool to guide ground delineation efforts in accordance with U. S. Army Corps of Engineers standards.

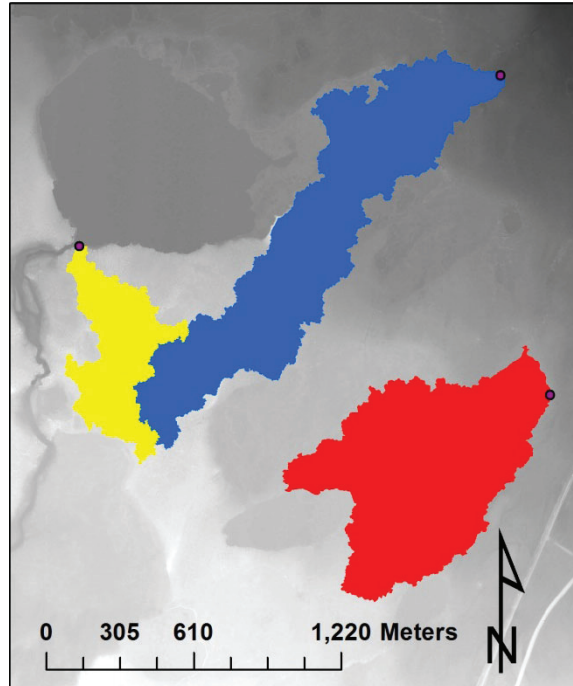


Figure 16. Local watersheds identified using a quarter-meter resolution DEM.

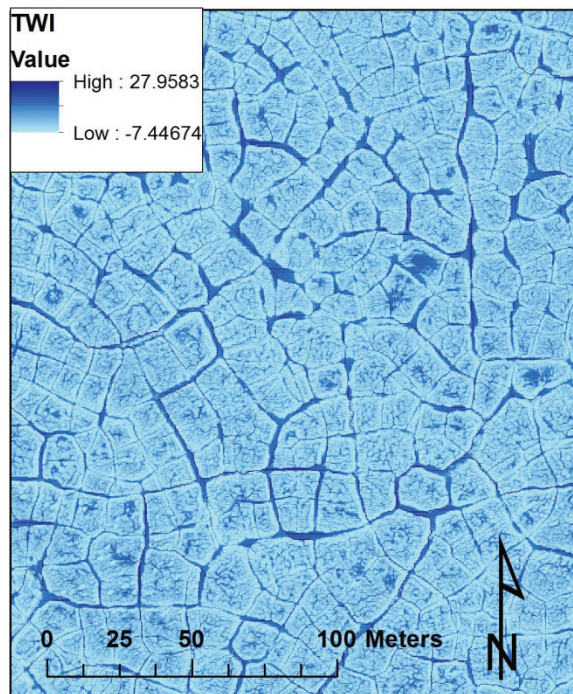


Figure 17. Topographic Wetness Index within the same study area, enlarged to show variation on the scale of individual polygons.

LAKE AND STREAM BATHYMETRY

The numerous fresh-water lakes on the Alaskan North Slope are relatively clear, shallow, and can be important habitat for overwintering fish populations if the water depths are greater than about 2.1 m (ASRC, 2012). These lakes are also potential water sources for ice-road construction and hydrocarbon-development activities. In 2011, ASRC staff conducted fathometer and fish population studies in 26 lakes along the Dalton Highway using helicopters to transport field crews and small boats. The lakes surveyed by boat in 2011 had surface areas between 4 and 191 ha, measured depths as deep as 3.5 m, and water clarity (a key factor controlling bathymetric laser penetration depths) ranging from 0.7 to 4.6 nephelometric turbidity units (NTU) (ASRC, 2012). The 2012 airborne lidar survey covered an area that included nearly all the lakes surveyed by boat in 2011, providing an opportunity to compare results from the different surveying methods and analyze airborne bathymetric lidar data from the hundreds of lakes within the area of interest. ASRC returned to the field area in 2013, surveying three additional lakes within the airborne survey area.

Amplitudes of returns from the bathymetric laser are recorded as a waveform (fig. 18) from which interpreted features such as the water surface and water bottom can be interpreted and extracted. DEMs can be created from each return type. Survey area-wide DEMs constructed from bathymetric lidar returns classified as the upper surface of the water (fig. 19) and the water bottom (fig. 20) define the location and extent of water bodies as well as the elevation of the water bottom, depicting generally decreasing water-surface elevations southward on the coastal plain. A larger-scale view of tile F3, a 4×4 km area along the Sagavanirktok River and Dalton Highway that includes the Alcor and Merak well pads, clearly shows water-bottom elevation variations within several lakes west of the river and the intricate anastomosing pattern within the numerous individual stream channels that together form the Sagavanirktok River (fig. 21). Information on water depths in channels such as these would be difficult to obtain using traditional marine or ground-based surveying methods. Stream cross sections produced from data such as

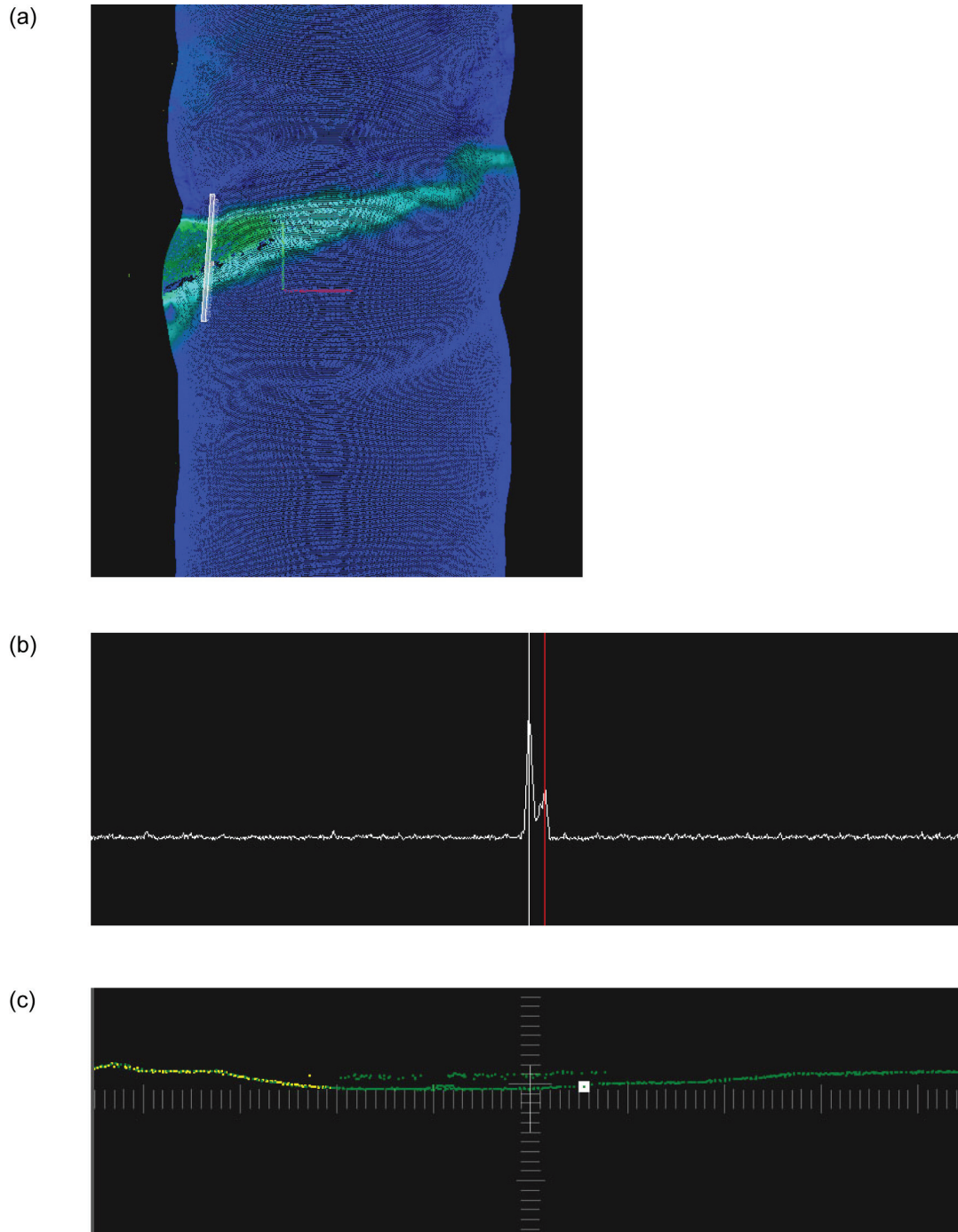


Figure 18. Bathymetric lidar data acquired across a water body in the Deadhorse survey area, August 5, 2012. (a) Map view showing bathymetric lidar returns along a single flight-line segment across a shallow water body. (b) Bathymetric lidar waveform showing large-amplitude return (marked by a white line) at the water surface and smaller-amplitude return (marked by red line) from the water bottom. (c) Cross section showing bathymetric lidar returns from land surface, water surface, and water bottom across a shallow water body located at the white line on (a). The white square in (c) marks the location of the waveform displayed in (b).

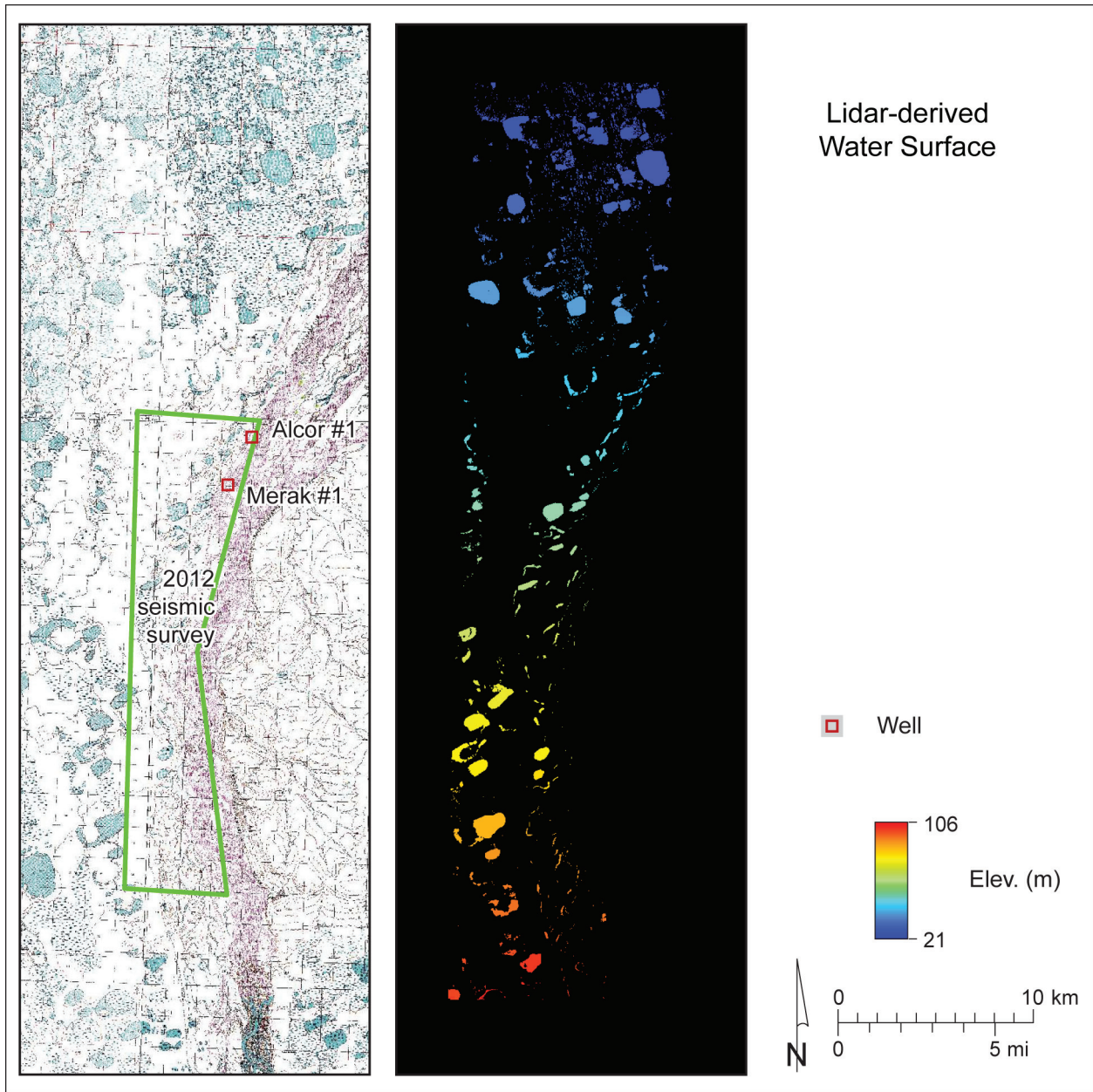


Figure 19. (right) Digital elevation model (DEM) of the water surface constructed from topographic and bathymetric lidar data points over the North Slope survey area. Point density at full resolution is 1 to 2 points/m². (left) U. S. Geological Survey topographic map.

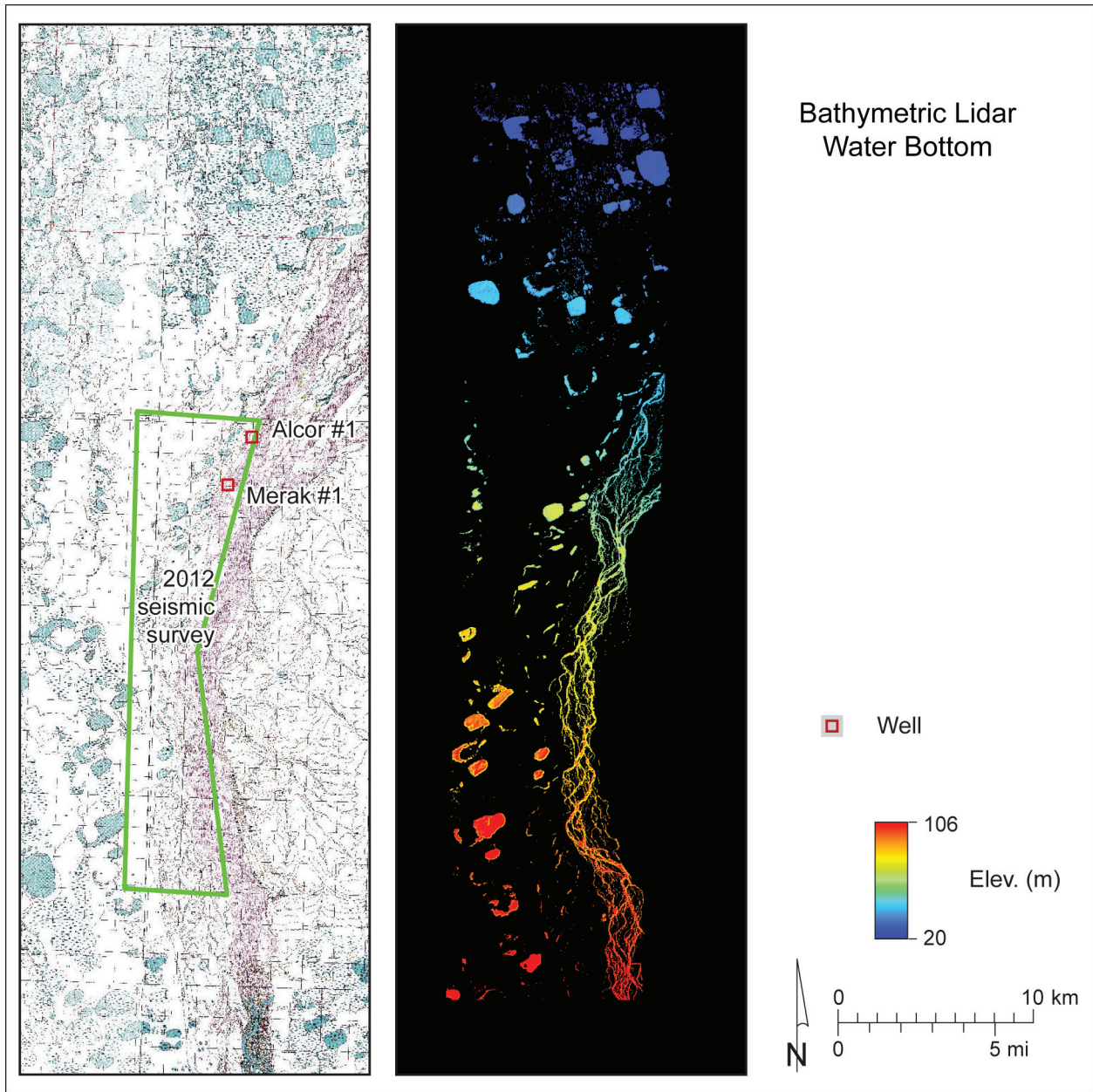


Figure 20. (right) Digital elevation model (DEM) of the water bottom constructed from more than 500 million bathymetric lidar data points over the North Slope survey area. Point density at full resolution is 1 to 2 points/m². (left) U. S. Geological Survey topographic map.

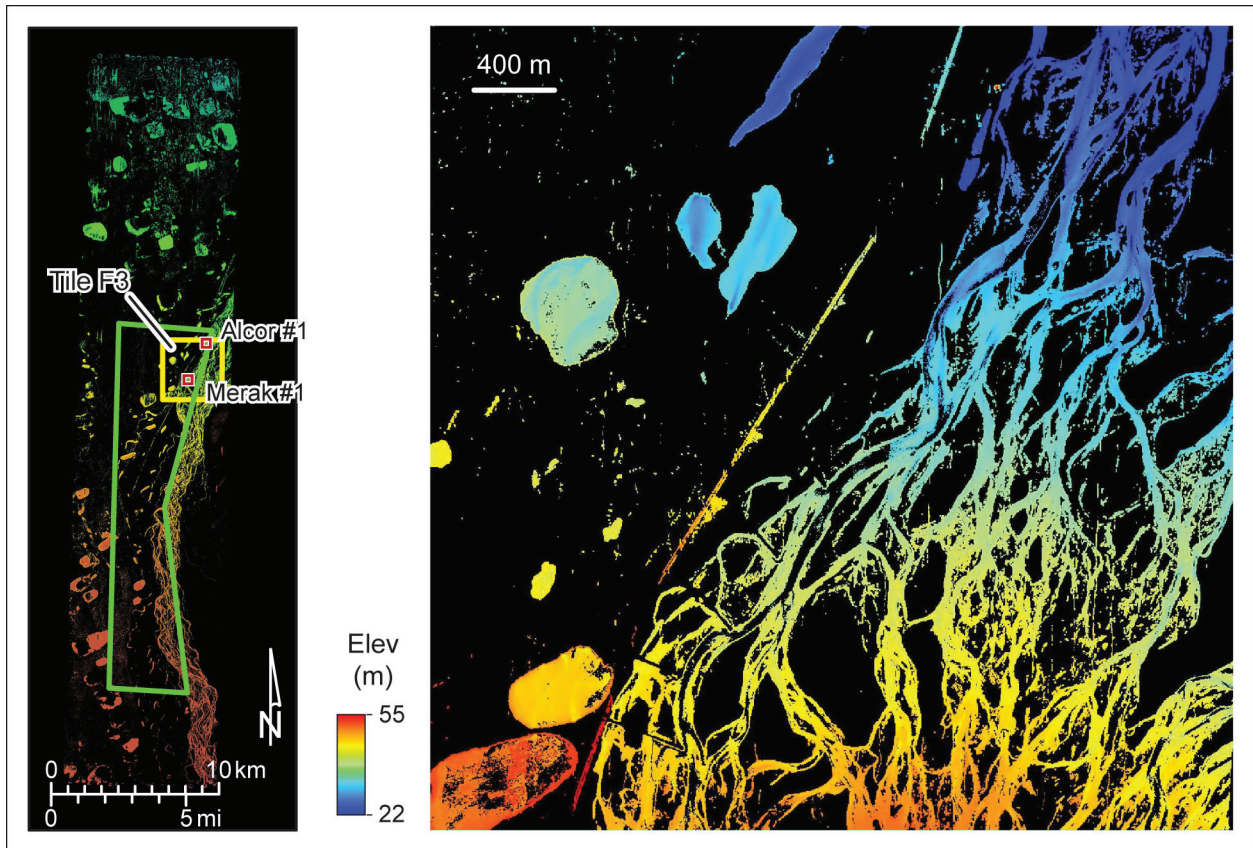


Figure 21. DEM constructed from full-resolution bathymetric lidar returns classified as water bottom (lake or river floor) for the (left) North Slope survey area and (right) tile F3, a 4×4 km area along the Sagavanirktok River near the Alcor #1 and Merak #1 well pads.

these, when combined with measured stream velocities, could provide highly accurate flow-rate measurements in braided streams where water clarity is sufficient to allow laser penetration to the water bottom.

Surfaces that define the water surface and water bottom can be combined to determine water depths and total or incremental water volumes below threshold depths (fig. 22). North Slope survey examples of these surfaces include one from a shallow lake (ASRC lake 9; BEG lake L169, Appendices A and B) in the F3 area that measures about 500 m across (fig. 23). The water surface has a lidar-determined elevation of about 48.6 m. Total apparent relief on the water surface, which could be caused by wind setup, waves, or possibly by density contrasts associated with depth changes, is about 7 cm (fig. 23a). Water-bottom returns extend over the entire lake, reaching a maximum depth of about 2.2 m. The lake-bottom surface (fig. 23b) clearly shows the location of deeper channels and between-channel bars related to deposition from local streams such as the one that flows into the southern part of the lake. Boat-based surveys of this lake acquired in 2011 indicate a turbidity of 2.0 NTU and a maximum measured depth of 2.5 m (ASRC, 2012).

A second example from another North Slope lake (ASRC lake 18, BEG lake L208) surveyed by boat in 2011 shows excellent agreement between fathometer- and lidar-derived lake depths (fig. 24). ASRC Lake 18, an elongate water body that has a surface area of about 5.3 ha and a maximum depth of 3.6 m, is the deepest lake surveyed by boat (ASRC, 2012). Measured water clarity in 2011 was 2.3 NTU, slightly more turbid than the first example. Despite the greater depth and higher turbidity, lake-bottom laser returns were identified across the entire lake (fig. 24). Comparisons of fathometer- and lidar-derived depths show good general agreement in overall shape of, and depth to, the lake bottom. Point-by-point depths at selected locations compare reasonably well: 3.6 m by fathometer and 3.8 m by lidar in the southern deep pool, 2.6 m by fathometer and 2.6 m by lidar on a shallow shelf in the middle of the lake, and 3.6 m by fathometer and 3.7 m by lidar in the northern deep pool (fig. 24). Maximum measured depths are only slightly different: 3.6 m by fathometer, 3.8 m by lidar. Density of coverage obtained by lidar

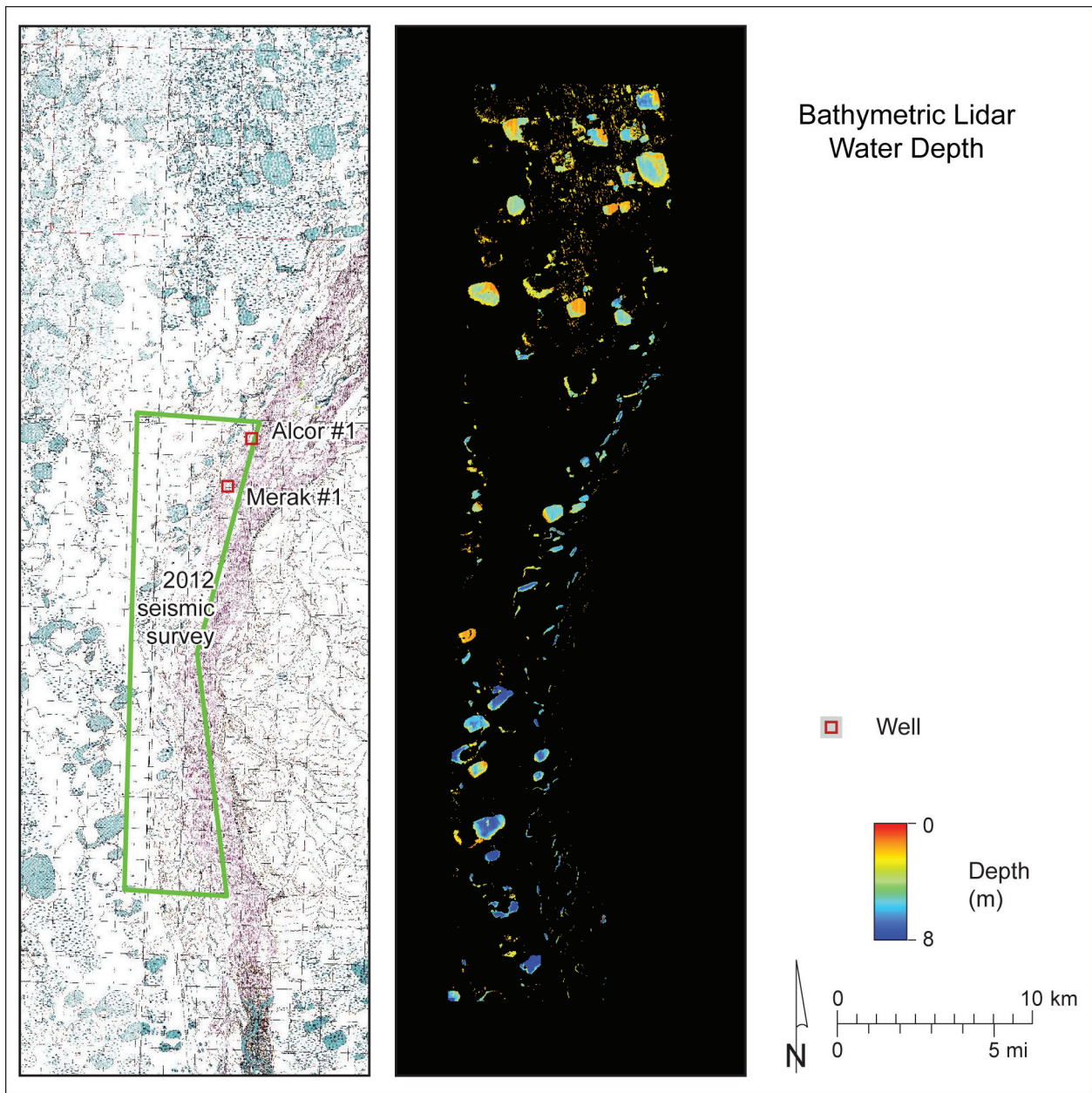


Figure 22. (right) Map of water depth in shallow North Slope lakes calculated by subtracting water-surface elevations (fig. 19) from water-bottom elevations (fig. 20). (left) U. S. Geological Survey topographic map.

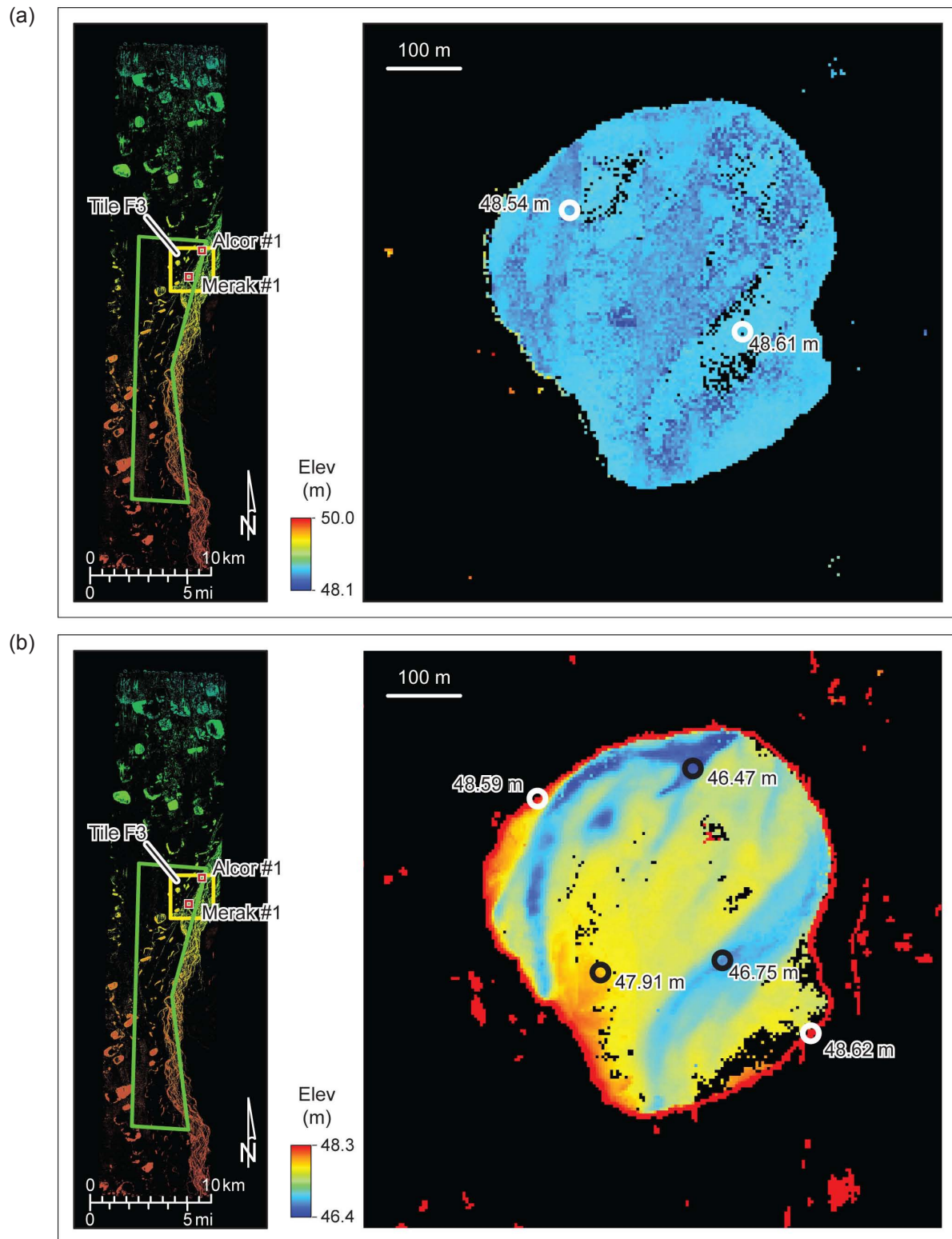


Figure 23. (a) Water-surface and (b) water-bottom DEMs constructed from full-resolution bathymetric lidar data for a shallow lake (ASRC lake 9, BEG lake L169, Appendices A and B) west of the Dalton Highway. Total apparent relief on the water surface is about 7 cm. Water-bottom returns were recorded to the maximum depth of the lake at about 2.2 m.

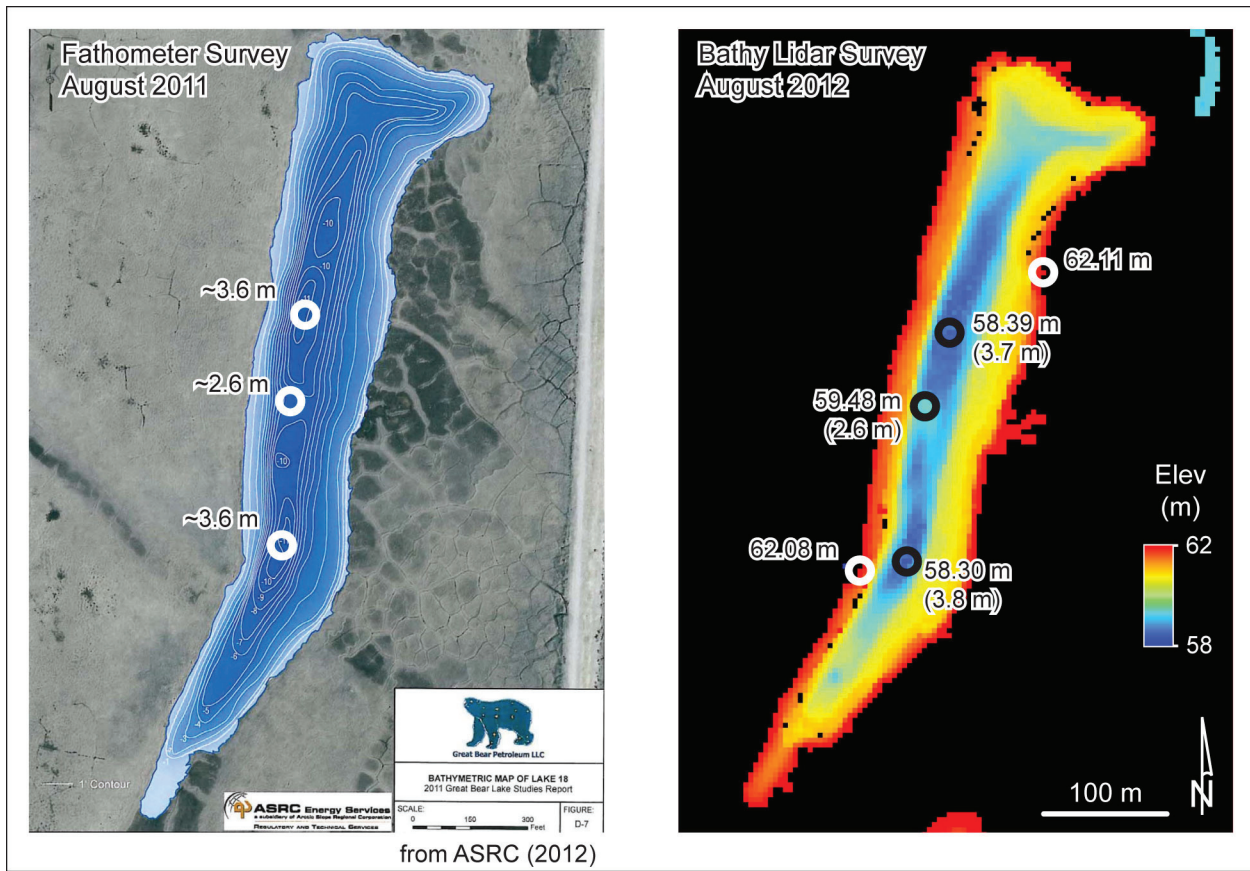


Figure 24. Comparison of (left) fathometer-derived water depths acquired during boat-based surveys of ASRC lake 18 (BEG lake L208) in August 2011 with (right) bathymetric lidar-derived water depths acquired during the August 2012 airborne survey on the North Slope. Water depths in comparable lake positions are similar. Fathometer data from ASRC (2012).

averaged about 1 point/m² over the entire lake, providing greater coverage than is practical with a boat-based survey.

LAKE WATER VOLUME

Bathymetric lidar has been shown to penetrate to the water bottom over most of the Deadhorse area lakes and streams. By establishing the water surface (fig. 19) and water bottom (fig. 20), those surfaces can be combined to determine water depths (fig. 22) and water volumes (both total volume and incremental volumes between arbitrary depth ranges). We employed two approaches to determine water depths and water volumes for comparison purposes: an interactive approach using commercial software tools on a lake-by-lake basis (Appendix C), and a semi-automated, custom-software-based procedure that combines information derived from survey-wide topographic and bathymetric lidar data to produce cleaned water surface, water bottom, and water depth layers that can be manipulated to generate total and incremental water-volume estimates for arbitrary lake area thresholds and depth ranges (appendices A and B). The data presented in this section were generated from the semi-automated approach. The interactive approach was used to verify and improve the semi-automated approach.

Both volumetric estimation processes begin with classified lidar data exported from AHAB's lidar processing software. These data are then merged into individual flight lines, tiled into convenient geographic extents (593 tiles measuring 1000 x 1000 m in this case), and then gridded to produce digital elevation models of ground topography, water surface, and water bottom (fig. 25). To produce volumetric estimates, we have concentrated on extracting water-surface and water-bottom returns.

Water-bottom surfaces for the survey area were produced by combining bathymetric lidar returns classified as ground, water bottom, and shallow-water bottom (fig. 26a), removing noise (fig. 26b), and then gridding the merged and cleaned returns. This process produced a 1-m resolution DEM that included areas within and outside the lakes. The extent of the lakes, which

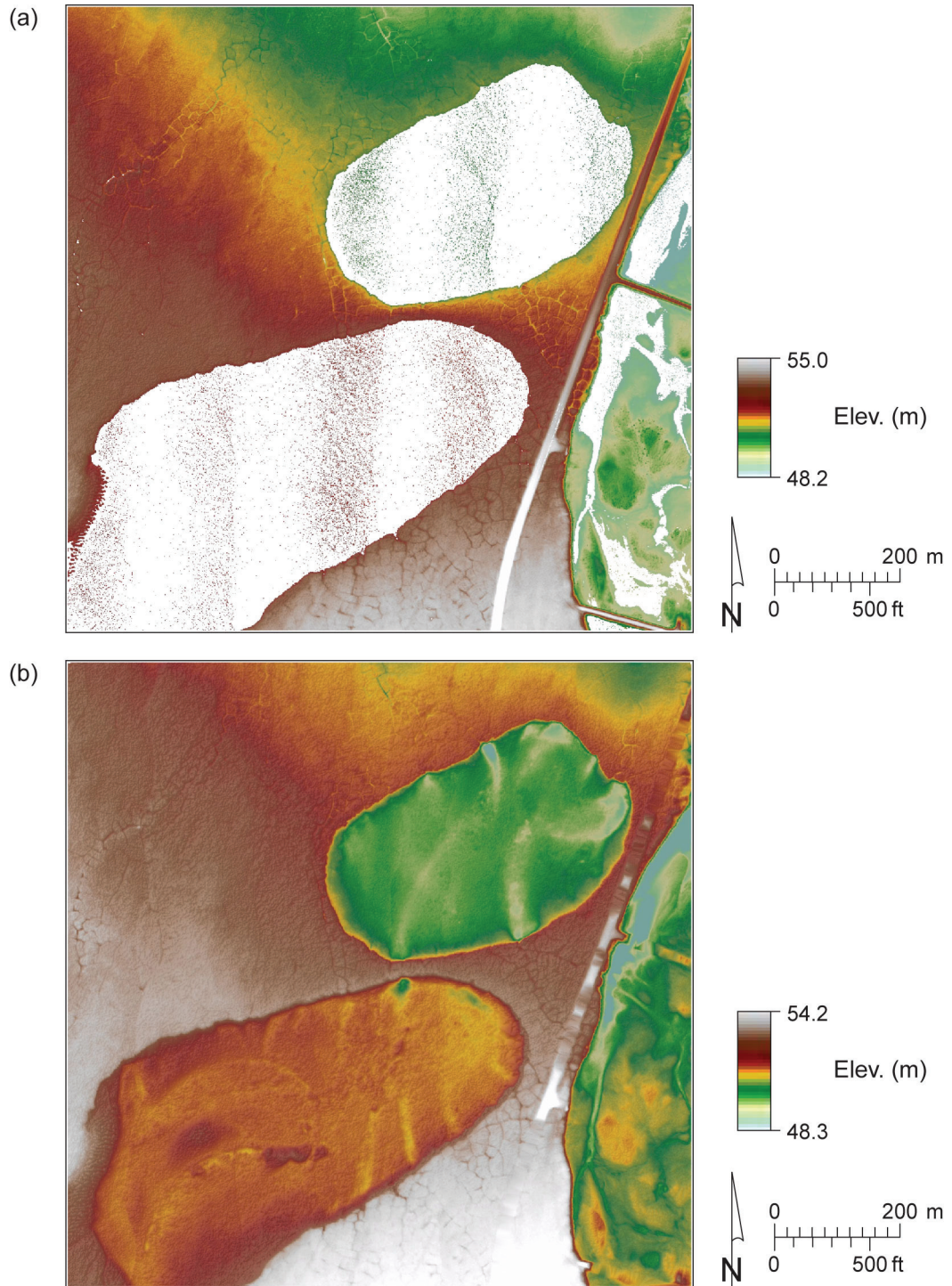


Figure 25. Gridded (a) topographic and (b) bathymetric lidar data from a 1 x 1 km tile along the Dalton Highway before noise removal. For the bathymetric data (b), the image includes returns classified as land, bottom, and shallow bottom.

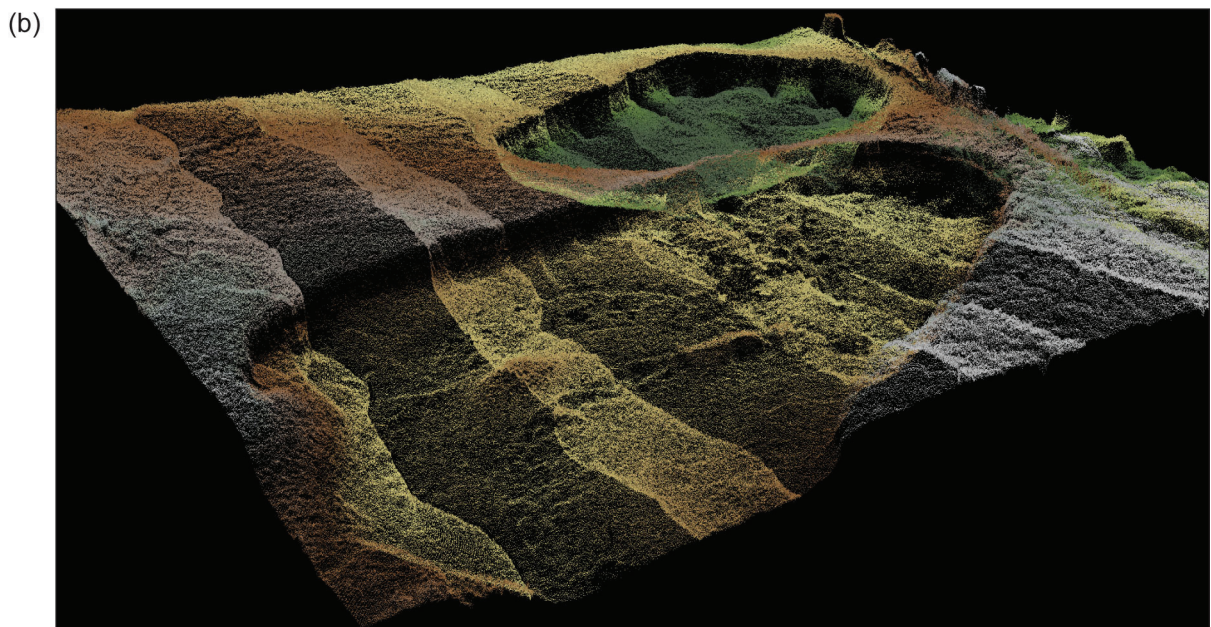
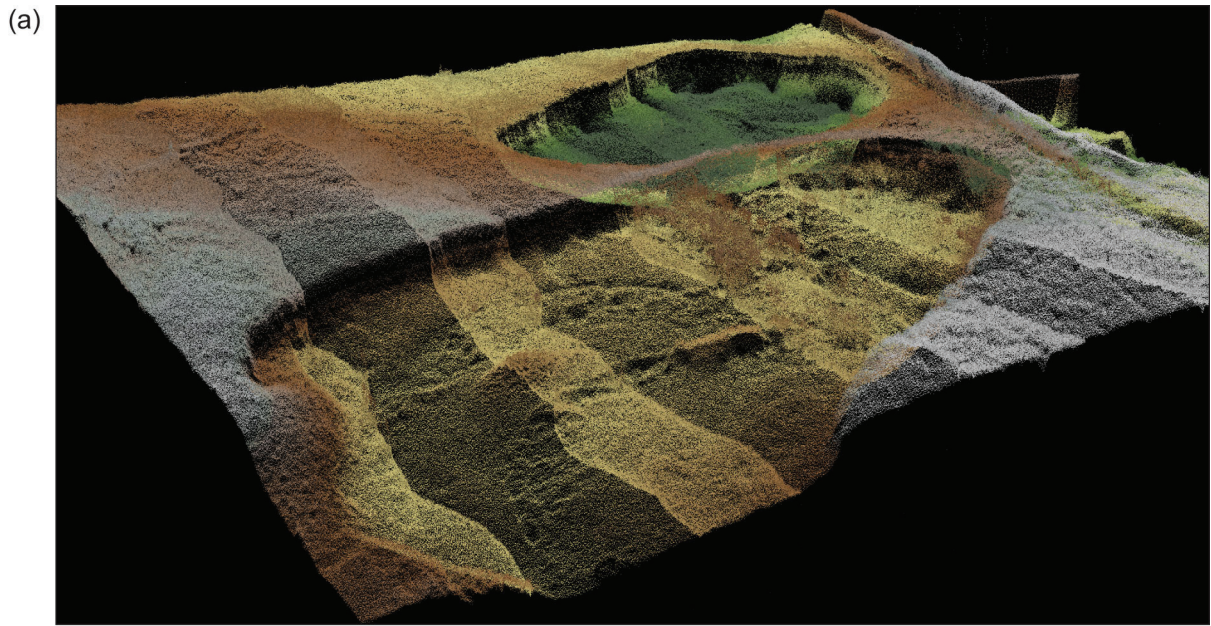


Figure 26. Bathymetric lidar point cloud consisting of returns classified as ground, water bottom, and shallow-water bottom (a) before and (b) after removal of noisy data. Returns within water bodies constitute the water bottom surface. Vertical exaggeration 30x.

can then be used to clip out the parts of the DEM that represent lakes or streams, was determined separately from topographic lidar data (fig. 25a).

Water surface elevations can be determined in several ways: (1) extracting the lowest elevations from the topographic lidar data acquired at the edge of the water bodies; (2) extracting the highest elevations from the bathymetric lidar returns classified as water bottom at the margins of the water body; (3) determining the elevations of the few topographic lidar returns that are recorded from the water surface (fig. 25a, for example) and extrapolating them over the water surface; and (4) determining the elevations of bathymetric lidar returns classified during processing as water surface. In the approach used for the calculations presented in this report, the lake boundary and surface elevation were determined for each lake from the topographic lidar data (fig. 27a).

The topographic lidar data were filtered to remove extraneous returns from water surfaces and produce clean DEMs that clearly indicate water surfaces and allow extraction of water-body boundaries (fig. 27a). Comparisons of minimum topographic lidar elevations at the boundaries of these water bodies with bathymetric lidar returns classified as water surface indicate that the topographic boundary elevations are about 20 cm higher than water-surface elevations determined from bathymetric lidar data. Water-surface elevations could be established directly from the bathymetric lidar data, but those return classifications remain very noisy. Water-surface elevations used for water-depth calculations were obtained from topographic lidar data around the margins of the lake, but were shifted 20 cm lower to offset the elevation discrepancy.

Water-bottom elevations were then subtracted from lake surface elevations (fig. 27a) to produce a water-depth surface that excluded areas where topographic lidar data indicated there was no surface water (fig. 27b). The water-depth information was then used to estimate total water volume for survey-area lakes as well as incremental volumes at 0.3-m (1-ft) depth intervals to a maximum depth of 2.1 m (7 ft).

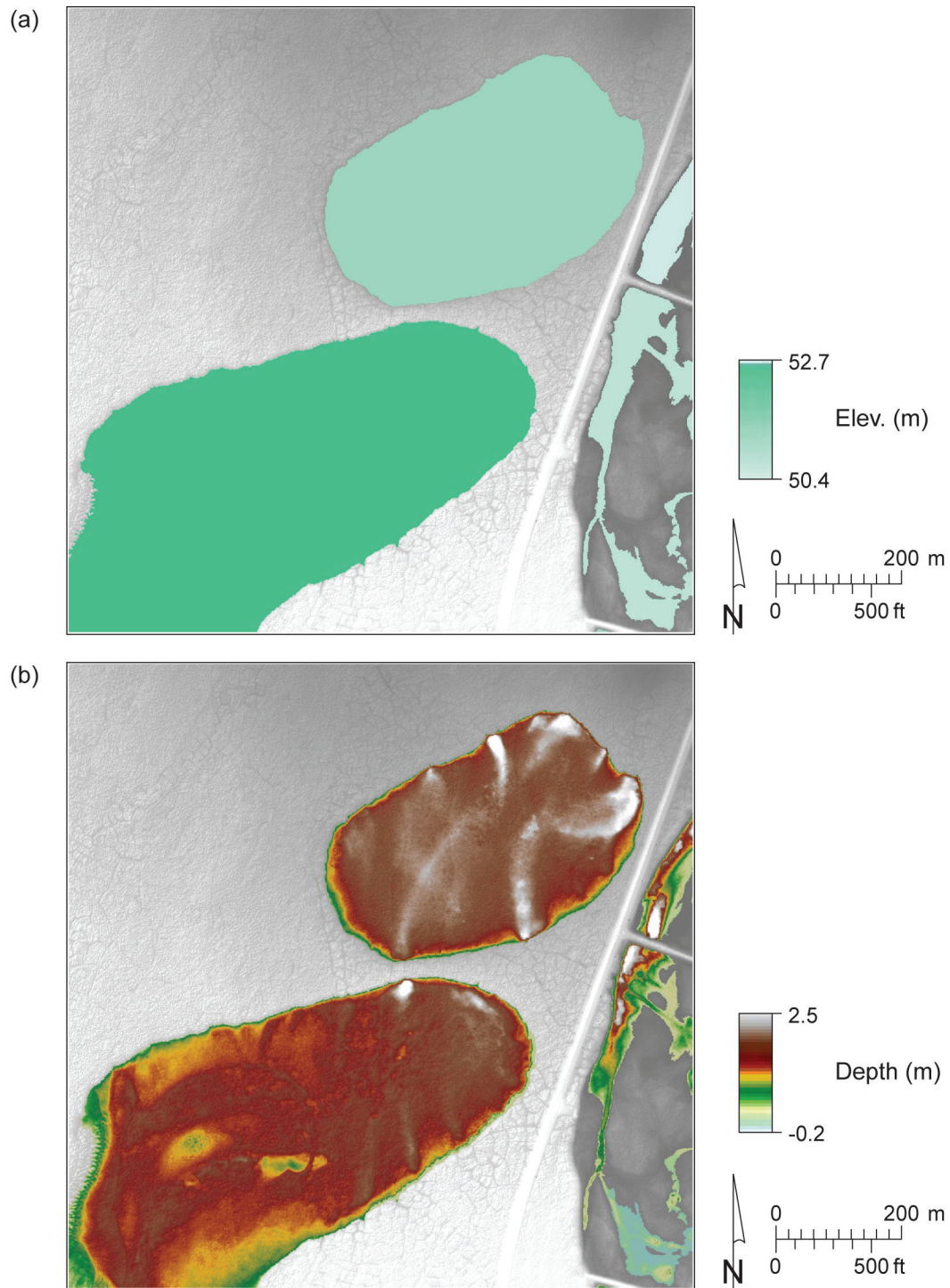


Figure 27. (a) Water-surface elevation determined from topographic lidar data at water-body boundaries and (b) water depth determined by subtracting water-bottom surface from water surface elevation. Topography outside the lake boundary is included for reference.

Lake Statistics

Analysis of airborne lidar data indicates that there are 283 lakes within the survey area that have a surface area larger than 0.8 ha (about 2 acres) (fig. 28, Appendix A). The largest (L067, Appendix A) has a surface area of 234 ha (578 acres). The “average” lake has a surface area of 10.5 ha (25.9 acres). In all lakes combined, the total volume of water is calculated to be 20,343,051 m³ (5,374,064,326 gal), although the estimated volume of individual lakes varies greatly from less than about 100 m³ (26,400 gal) to as much as 1,657,598 m³ (437,891,243 gal). Average lake volume for lakes with surface area greater than 0.8 ha is 72,138 m³ (19,056,965 gal).

Most of the lake volume occupies shallow water. Of the 283 lakes analyzed, only 84 (30 percent) are deeper than 1.5 m (5 ft) and only 39 (14 percent) are deeper than 2.1 m (7 ft). Just over 35 percent of the total lake water volume (13,200,306 m³, or 3,487,153,500 gal) is found in water depths of 0.3 m or less. Almost four percent (724,813 m³, or 191,475,524 gal) of the total lake water volume is at depths greater than 1.5 m (5 ft) in 84 of the lakes, and less than one percent (116,753 m³, or 30,842,854 gal) of the total water volume is at depths greater than 2.1 m (7 ft).

Comparisons of water volumes calculated using August 2012 lidar data with volumes calculated using boat-based fathometer data acquired in August 2011 (ASRC, 2012) and 2013 by ASRC show that, for unobscured lakes, the lidar-calculated total volumes are greater by an average of about 9 percent (Appendix B). The statistical relationship between lidar-calculated volumes and fathometer-based volumes is excellent for the 26 lakes surveyed by fathometer in 2011 (fig. 29). Three additional lakes (17B, 25B, and 28B in the northern part of the survey area, fig. 28) surveyed by ASRC in 2013 contain significantly greater water volume than those determined by airborne lidar for the same lakes. Aerial photographs taken during the lidar survey suggest that, over parts of these lakes, lidar penetration to the lake bottom is obscured by the presence of floating matter or suspended sediment, or is absorbed by a dark lake bottom. Analysis of photographs over the entire survey area indicates that bottom obscuration (and thus underestimated total volume determined from lidar data) may be present in as many as 21 lakes (fig. 30, left), less

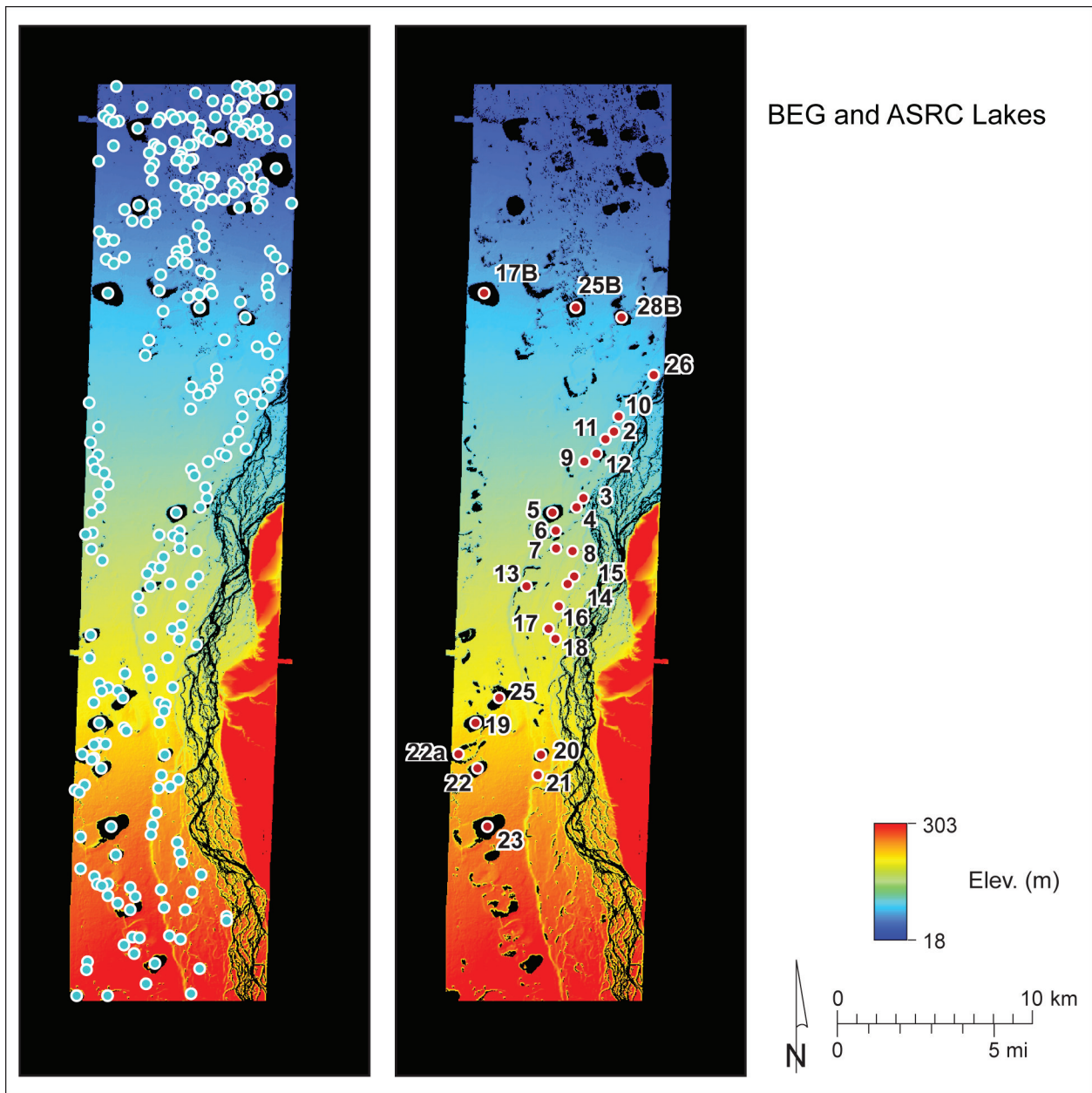


Figure 28. Location of Deadhorse survey area lakes for which surface area, depth, and water volume have been calculated from lidar data. Shown at left are the 283 lakes identified in the 2012 airborne lidar survey with surface areas greater than 0.8 ha (Appendix A). Shown at right are the locations and names of the 28 lakes surveyed by ASRC in 2011 and 2013 (Appendix B). Lakes with a "B" suffix were surveyed by ASRC in 2013. Names for the lakes identified in the airborne lidar survey are listed in Appendix A and are shown on an accompanying map.

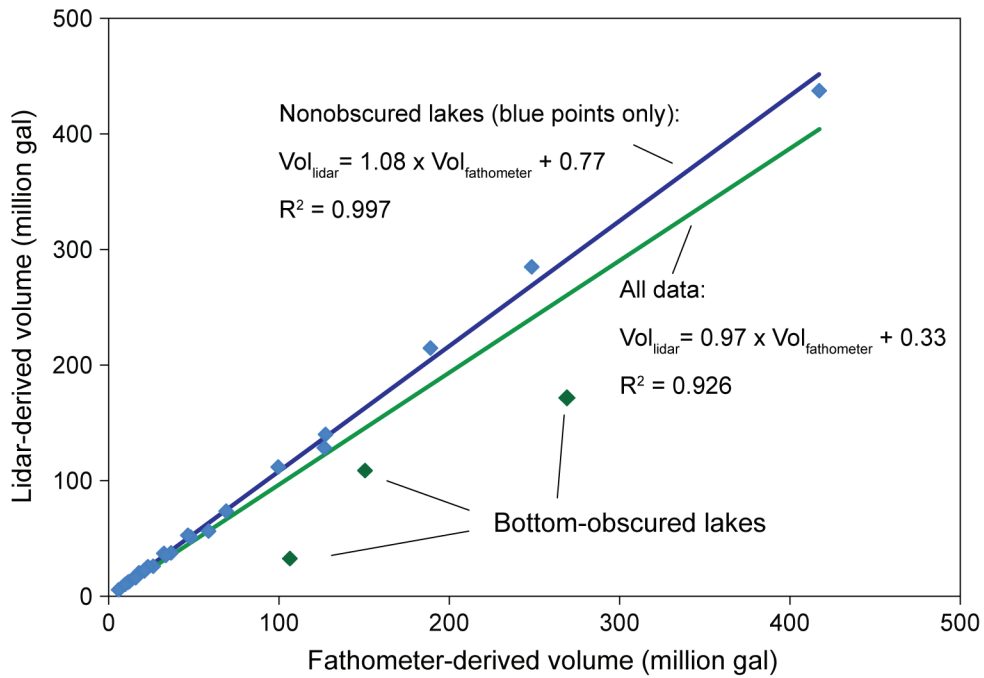


Figure 29. Scatterplot showing fathometer- versus lidar-derived water volume for 26 lakes that were surveyed by ASRC in 2011 (blue points and best-fit line) and three additional lakes surveyed by ASRC in 2013 (green points and best-fit line for all 29 lakes).

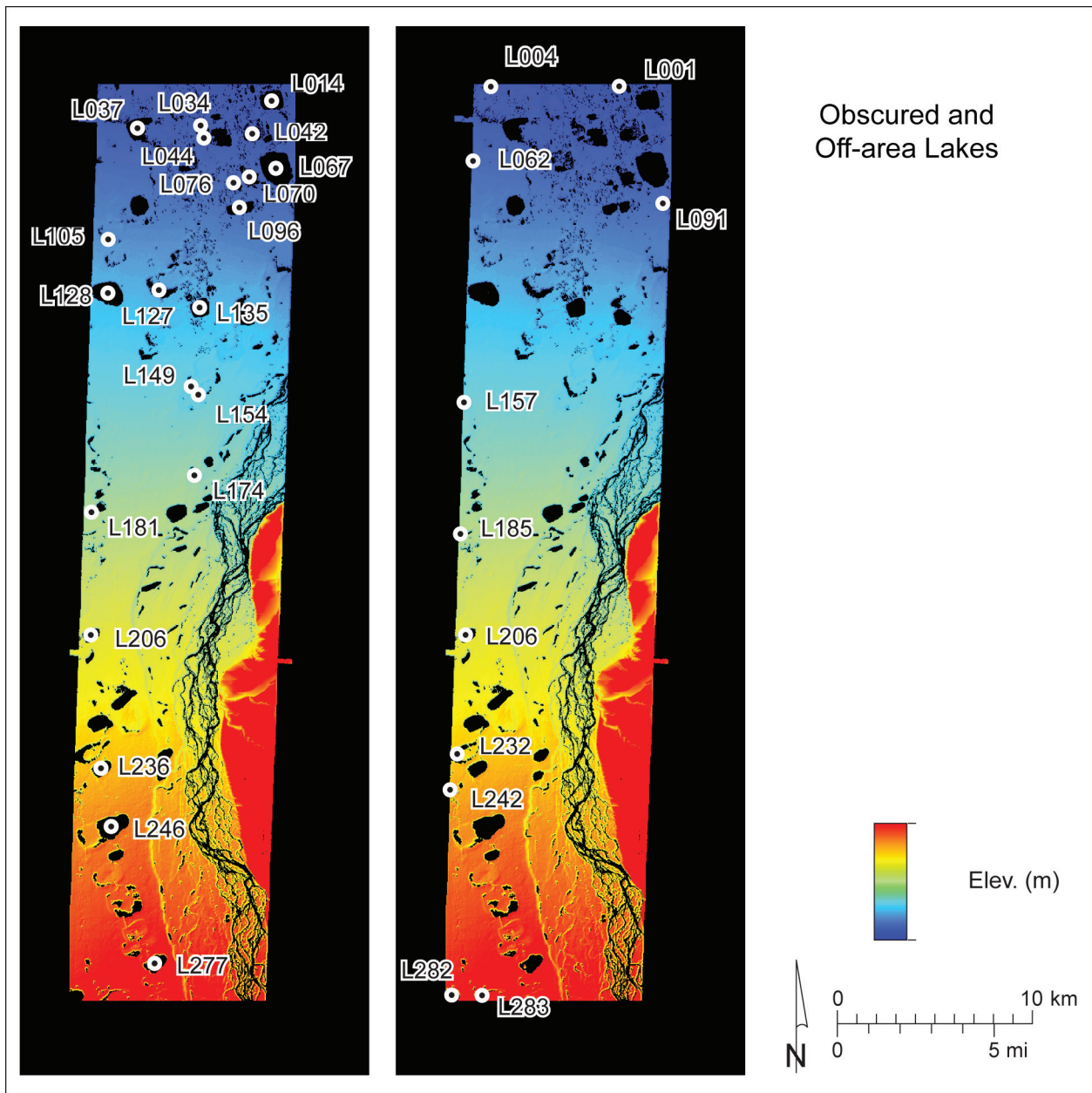


Figure 30. Lidar-surveyed lakes that may have underestimated water volumes because (left) the water bottom is partly obscured by floating matter, suspended sediment, or a nonreflective bottom, or (right) the lake extends outside the lidar survey area. Lake names are listed in Appendix A and are shown on an accompanying map.

than 10 percent of the total number of lakes surveyed. An additional 11 lakes may have underestimated volumes because the lake extends beyond the lidar survey area (fig. 30, right). Aside from the potentially large differences arising from lake-bottom obscuration in a small number of lakes, nonobscured lakes have minor differences in volumes determined using the two methods. These smaller differences in calculated volumes from lidar and fathometer approaches could represent real volumetric differences resulting from water-level differences between the two survey dates, or they could be artifacts of one or both methods. For example, lidar sampling of the water bottom is more complete than fathometer data would be, particularly in very shallow water not accessible by boat. Alternatively, misclassification of water-bottom returns in lidar data could lead to erroneous water-depth calculations that would cause errors in volumetric calculations, as would errors in water-surface elevations.

POSSIBLE FUTURE WORK

This study focused on applying and verifying airborne topographic and bathymetric lidar and color-infrared imagery for microtopography, lake depth and volume, and wetlands discrimination in the Great Bear lease area near Deadhorse, Alaska. Similar surveys employing these tools could be undertaken over larger areas of the North Slope where similar issues of permafrost characterization and monitoring, wetlands distribution, and lake depths and volumes are important environmental and energy development issues. Other instruments, including high-resolution airborne hyperspectral systems, are available that may facilitate discrimination of subtle differences in vegetation assemblages that can improve speed and accuracy of wetlands mapping.

Hyperspectral Assessments

Hyperspectral imaging is an effective and efficient approach to determine or monitor a variety of environmental parameters across large distances with high spectral and spatial resolution. The technology is based on the detection of unique spectral signatures of objects, whether solid materials, fluids, or gases. This approach leverages differences in reflective, transmission, and

absorption properties caused by differences in the physical and chemical characteristics of the target. Most objects show unique patterns when illuminated with energy across a range of specific wavelengths. What sets hyperspectral data apart from multispectral data is the number, placement, and width of bands in which the sensor detects energy returns. While multispectral data tend to have up to about 15 rather wide bands of observation, hyperspectral data tend to have more than 100 narrow bands of observation. Because these narrow bands necessarily are sensitive to much smaller portions of the electromagnetic spectrum, the overall energy response is lower. Therefore, hyperspectral systems are usually airborne rather than satellite-borne in order to achieve adequate responses and signal-to-noise ratios. The lower platform altitude also thus offers increased spatial resolution and reduced atmospheric effects on the data compared to that of satellite-borne sensors.

The technology has been used to monitor the status of vegetation and soils, detect gas leaks, quantify gas concentrations, conduct hydrological monitoring and modeling, and for many other purposes. Data collection across the full spectrum provides useful baseline data sets with regards to vegetation composition, health and vegetative stress factors, soil humidity (particularly important for North Slope wetlands delineation), and thermal assessment of the permafrost soils. This information provides valuable baseline data to monitor and manage the environmental conditions and evaluate the environmental risk associated with current or planned operations. Hyperspectral data have also been noted as an improvement over multispectral data when finer-scaled spectra are needed for object identification, such as with crop health monitoring, woody species identification, and soil discrimination.

The Bureau's hyperspectral imaging system operates across a wide range of the electromagnetic spectrum, starting at the visible and near-infrared section (VNIR), followed by the short wave (SWIR), mid wave (MWIR), and long wave infrared (LWIR) or thermal sections of the spectrum. The spectral range and resolution enables assessments of both vegetation and soils utilizing the VNIR to thermal section of the spectrum, with VNIR spectra (notably NIR and red) espe-

cially helpful for vegetation discrimination and MWIR spectra especially useful for water stress in vegetation as well as soil discrimination (particularly in conjunction with red spectra).

Vegetation Assessment

Due to permafrost soil conditions, vegetation in arctic environments is limited to mosses, herbaceous, and small shrub vegetation. The species composition is characterized by the occurrence of typical, mainly annual pioneer species. These species react quickly to changes in environmental conditions such as changes in hydrological conditions, temperature, carbon dioxide concentrations, nutrients, and absence or presence of phytotoxic materials. Therefore, vegetation is an excellent indicator of the overall ecological conditions of ecosystems and changes in ecosystem function.

Due to the high spectral and spatial resolution of hyperspectral imaging applications, the technology provides the unique opportunity to collect information on species composition (assemblages), the general health of vegetation, and stress factors caused by changes in environmental conditions. The overall goal of the assessment is to produce a highly detailed habitat map based on the occurrence of different plant communities. Currently, the existing habitat classification is rather coarse and should be conducted at a higher spatial resolution to extract more detailed information with regards to species composition.

A combination of field-derived spectra, airborne data collection, and hyperspectral satellite imagery would allow assessing environmental change in the past as well as the future. Upscaling processes can be used to relate in situ spectra measurements to data derived from an airborne mission. This data set can form the base to assess changes in environmental conditions. By considering differences in scale, in situ measurements and airborne hyperspectral data can be leveraged against satellite-based hyperspectral or multispectral sensors such as AVIRIS, Hyperion, Spot, MODIS, or others to determine intra- and inter-annual change. This approach provides an excellent tool to monitor vegetation and wetlands in particular.

Soil Assessment and Hydrological Modeling

Soils of the areas are characterized as permafrost, sometimes resulting in topographical features such as soil and ice polygons and pingos. The thawing of permafrost soil has been identified as a major issue of climate change, with current research and various climate change models predicting an overall decrease in permafrost soils and a migration northward. Associated with these processes are an increase in carbon dioxide flux (thus creating a positive feedback), loss of coastline, subsidence of land (thaw settlement), sedimentation of rivers, and many others. However, anthropogenic or natural differences and changes in microclimatic conditions and inter-annual differences also cause severe problems with regards to the physical properties of permafrost soils.

Monitoring soil conditions along industrial developments should therefore become a main concern in the area since especially volumetric changes in soils caused by thawing and freezing of soil water can cause severe damage to buildings, pipelines, and other infrastructure. Permafrost conditions do not have to disappear completely, as the effects can be observed at even small changes in soil temperature. An increase in the mobility of water observed during the thawing process can lead to renewed heaving.

Another future survey objective to consider would be to determine the permafrost conditions along the pipeline and drilling well facilities to establish a baseline data set by leveraging the VNIR, MIR, and thermal range of the airborne hyperspectral system. Data analysis will reveal areas showing anomalies in the vicinity of infrastructure with regards to soil temperatures and soil water content. This survey, in combination with the extraction of permafrost features from the lidar data set, would highlight current potential impact areas as well as provide an excellent baseline data set to monitor change over time in this frontier area.

CONCLUSIONS

Airborne topographic and bathymetric lidar systems permit rapid surveying of upland, wetland, lacustrine, and riverine environments in critical periglacial and permafrost terrain such as that

found on the Alaskan North Slope. Unprecedented topographic detail achieved using a near-infrared laser operating at 400 kHz allows mapping of small geomorphic features such as soil and ice polygons, better defining their role in wetland distribution, and monitoring possible change over time at a vertical scale of a few centimeters. High-resolution DEMs of the land surface in remote regions such as the North Slope, where detailed topographic information has not been available, allow better delineation of drainage basins and prediction of soil moisture that are critical to wetland classification. Bathymetric lidar has been shown to penetrate reasonably clear North Slope lakes and streams to depths greater than 6 m (20 ft) at single-pass densities of about 1 point/m², allowing estimates of total and incremental water volumes that are important parameters for determining which lakes are likely to support overwinter fish populations and serve as potential industrial water sources. Detailed maps of lake-bottom morphology provide a unique and comprehensive data set to support studies of the formation, sedimentation, evolution, and future change of these common Arctic landscape features.

A combination of bathymetric and topographic lidar data was used to delineate 283 shallow lakes in the survey area that have surface areas greater than 0.8 ha (about 2 acres). Using a semi-automated volume calculation process, these lakes are estimated to contain 20,343,051 m³ (5,374,064,326 gal) of water, of which 724,813 m³ (191,475,524 gal) is found in 83 lakes with depths greater than 1.5 m (5 ft) and 116,753 m³ (30,842,854 gal) is found in 38 lakes with depths greater than 2.1 m (7 ft). For lakes where both lidar and boat-based fathometer data have been collected, (a) lidar-based volumetric estimates are an average of 9 percent higher, and (b) there is an excellent statistical correlation between lidar-derived and fathometer-derived total lake volumes for the majority of lakes having little or no surface obscuration. Lidar water-bottom returns for a minority of North Slope lakes were partly obscured by vegetation, suspended sediment, or nonreflective bottoms, resulting in underestimated water volumes for the obscured parts of those lakes. For the non-obscured lakes, minor volumetric differences between the fathometer and airborne lidar approaches may be real or be an artifact of one or both methods.

The wetland system on this part of the North Slope is dominated by the mixed unit of emergent/scrub-shrub covering 15,547 ha. The next most common habitat with a total area of 8,164 ha is freshwater emergent. In the study area, lake area totals 2,304 ha. The mixed unit scrub-shrub/emergent covers 1,405 ha. In this area of the coastal plain, scrub-shrub are assigned the least wet water regime and cover 286 ha. Most wetland habitats, other than scrub-shrub, are assigned a mid-level moisture regime. Wetland water regimes in this part of the North Slope tend toward the less wet water regimes, as compared to the least common and wettest regime. Relatively speaking, wetlands in the study area are of medium to lower ground moisture regimes. Compared to the NWI, we mapped fewer emergent wetlands and more emergent/scrub-shrub, indicating a shift toward ground moisture conditions that favor scrub-shrub habitat. This trend is also reflected in our increased mapping of scrub-shrub. Combined scrub-shrub/emergent and scrub-shrub totals for both time periods are similar, though we mapped more scrub-shrub. This suggests that changes in environmental conditions that favor a spread of scrub-shrub are subtle.

ACKNOWLEDGMENTS

This project was conducted under Sponsored Research Agreement No. UTA12-0000752 between Great Bear Petroleum Operating LLC (Great Bear) and The University of Texas at Austin. Jeffrey G. Paine and Michael H. Young, Bureau of Economic Geology (Bureau), served as Principal Investigators. Field survey participants included Bureau researchers John Andrews, Aaron Averett, Jeffrey Paine, and Thomas Tremblay; Airborne Hydrography AB representatives Petter Kullenberg, Daniel Andersson, and Daniel Gustafsson; and Aspen Helicopters staff Bradley Busch (pilot) and Marcos Rico (mechanic). Torbjorn Karlsson, Airborne Hydrography AB, developed processing algorithms to extract water-surface and water-bottom returns from bathymetric lidar data. Ed Duncan and Karen Duncan, Great Bear, facilitated field logistics for the airborne survey in the Deadhorse area. Joe Christopher of ASRC Energy Services, Inc. provided fathometer-based bathymetric data from select North Slope lakes, field guidance on wetland mapping, and

ASRC's wetland maps for review and comparison purposes. CGG provided location and elevation data acquired during seismic surveys conducted for Great Bear in 2012 and 2013.

REFERENCES

- ASRC Energy Services, 2012, 2011 Great Bear lake studies report, North Slope, Alaska: ASRC Energy Services, Anchorage, Alaska, 16 p.
- Cowardin, L.M., Carter, V., Golet, F.C., and LaRoe, E.T, 1979, Classification of Wetlands and Deepwater Habitats of the United States: U.S. Department of the Interior, Fish and Wildlife Service, Washington, DC. FWS/OBS-79/31.
- Homer, C., Huang, C., Yang, L., Wylie, B., and Coan, M. 2004, Development of a 2001 National Landcover Database for the United States: Photogrammetric Engineering and Remote Sensing, v. 70, no. 7, July 2004, pp. 829-840.

Page intentionally blank

APPENDIX A: LIDAR-DERIVED LAKE AREAS, DEPTHS, AND VOLUMES

Map label, name, center location, surface area, average depth, total volume, and incremental volume of lakes in the 2012 airborne survey area. Lakes are ordered by northerly coordinate, from northernmost to southernmost. Lakes are identified by map label on the bathymetric map that accompanies this report. Complete incremental volumes at 1-ft intervals can be found in a spreadsheet in the lake volumes directory of the data volume. One asterisk following the map label name indicates a lake that extended beyond the survey boundary and was not completely surveyed. Two asterisks following the map label name indicates a lake for which lidar-derived water volumes are likely to be underestimated because of a lack of an identifiable water-bottom return over part of the lake caused by turbidity, vegetation, or a nonreflective bottom surface.

Map label	Name	x utm83 (m)	y utm83 (m)	Area (acre)	Avg. depth (ft)	Volume (gal)	Volume > 5 ft (gal)	Volume > 7 ft (gal)
L001**	435719_7783893	435719	7783893	2.5	0.10	77,930	0	0
L002	435221_7783892	435221	7783892	2.7	0.82	718,812	0	0
L003	436856_7783892	436856	7783892	2.6	0.67	561,629	0	0
L004**	428995_7783883	428995	7783883	13.3	2.99	12,888,687	85,327	0
L005	436777_7783847	436777	7783847	3.1	1.73	1,767,310	0	0
L006	436560_7783821	436560	7783821	5.3	1.70	2,904,835	0	0
L007	435940_7783771	435940	7783771	18.8	1.33	8,136,497	0	0
L008	435618_7783645	435618	7783645	4.9	0.43	698,734	0	0
L009	433068_7783551	433068	7783551	4.8	0.93	1,456,908	0	0
L010	437707_7783471	437707	7783471	4.7	0.50	756,324	0	0
L011	436118_7783305	436118	7783305	6.4	0.35	725,944	0	0
L012	434765_7783162	434765	7783162	6.9	1.92	4,330,043	0	0
L013	433953_7783153	433953	7783153	2.5	0.49	393,352	0	0
L014*	436999_7783146	436999	7783146	285.8	2.37	220,383,641	9,774	0
L015	435588_7782859	435588	7782859	2.6	0.41	345,801	0	0
L016	430319_7782820	430319	7782820	2.5	0.31	254,397	0	0
L017	434686_7782762	434686	7782762	2.8	0.14	124,689	0	0
L018	435482_7782738	435482	7782738	2.7	0.40	359,273	0	0
L019	428652_7782673	428652	7782673	2.3	0.29	216,092	0	0
L020	431826_7782440	431826	7782440	9.6	0.85	2,651,230	0	0
L021	428356_7782371	428356	7782371	4.7	0.35	532,834	0	0
L022	432310_7782325	432310	7782325	7.2	1.09	2,553,750	0	0
L023	434090_7782309	434090	7782309	38.4	2.14	26,811,608	0	0
L024	432908_7782292	432908	7782292	2.9	0.76	729,643	0	0
L025	431239_7782259	431239	7782259	4.6	0.83	1,228,928	0	0
L026	435159_7782247	435159	7782247	7.6	0.60	1,481,212	0	0
L027	432014_7782205	432014	7782205	6.1	0.65	1,294,442	0	0
L028	428599_7782183	428599	7782183	15.0	0.88	4,316,306	0	0
L029	436275_7782155	436275	7782155	4.1	0.65	869,654	0	0
L030	429115_7782104	429115	7782104	8.1	0.33	874,937	0	0

Map label	Name	x utm83 (m)	y utm83 (m)	Area (acre)	Avg. depth (ft)	Volume (gal)	Volume > 5 ft (gal)	Volume > 7 ft (gal)
L031	431131_7782061	431131	7782061	3.5	0.66	748,927	0	0
L032	428844_7782059	428844	7782059	2.6	0.17	145,030	0	0
L033	435742_7781965	435742	7781965	11.0	0.78	2,782,523	0	0
L034	433335_7781877	433335	7781877	55.7	1.21	21,907,255	0	0
L035	435090_7781801	435090	7781801	2.9	0.02	15,057	0	0
L036	436753_7781752	436753	7781752	13.0	1.86	7,879,194	20,077	0
L037*	430086_7781734	430086	7781734	278.2	1.26	113,969,612	0	0
L038	435571_7781704	435571	7781704	3.2	0.70	729,643	0	0
L039	435408_7781565	435408	7781565	2.2	0.03	19,812	0	0
L040	436312_7781551	436312	7781551	5.0	1.17	1,916,039	0	0
L041	433232_7781501	433232	7781501	13.5	0.40	1,751,460	0	0
L042*	435994_7781443	435994	7781443	139.5	1.91	86,848,394	0	0
L043	434377_7781304	434377	7781304	195.7	1.74	111,096,742	528	0
L044	433502_7781227	433502	7781227	16.1	1.43	7,479,501	0	0
L045	436758_7781204	436758	7781204	37.3	2.24	27,159,787	0	0
L046	437680_7781087	437680	7781087	2.5	0.28	228,508	0	0
L047	433755_7781071	433755	7781071	9.3	0.72	2,167,795	0	0
L048	431991_7781051	431991	7781051	5.3	0.76	1,317,425	0	0
L049	430937_7780913	430937	7780913	6.6	0.71	1,533,782	0	0
L050	432949_7780890	432949	7780890	3.9	0.80	1,010,457	0	0
L051	432735_7780878	432735	7780878	2.2	0.08	59,967	0	0
L052	428842_7780836	428842	7780836	4.1	0.16	218,470	0	0
L053	431089_7780762	431089	7780762	7.9	0.80	2,076,391	0	0
L054	431243_7780694	431243	7780694	3.0	0.60	592,009	0	0
L055	432353_7780479	432353	7780479	20.7	0.55	3,712,937	0	0
L056	430694_7780476	430694	7780476	2.5	1.36	1,091,822	0	0
L057	432272_7780278	432272	7780278	3.8	0.29	360,066	0	0
L058	432932_7780147	432932	7780147	43.2	1.09	15,401,491	0	0
L059	432423_7780143	432423	7780143	2.6	0.04	34,870	0	0
L060	432087_7780102	432087	7780102	14.5	0.99	4,671,089	0	0
L061	432769_7780099	432769	7780099	3.9	1.37	1,722,401	0	0
L062**	428072_7780053	428072	7780053	14.7	1.54	7,368,549	528	0
L063	430911_7779934	430911	7779934	5.7	1.16	2,142,699	0	0
L064	436159_7779893	436159	7779893	2.3	1.01	770,325	0	0
L065	432527_7779688	432527	7779688	45.0	1.54	22,614,179	0	0
L066	430733_7779672	430733	7779672	3.6	0.80	942,301	0	0
L067*	437215_7779669	437215	7779669	577.7	1.83	343,981,531	0	0
L068	435845_7779629	435845	7779629	2.8	0.12	107,782	0	0
L069	435588_7779589	435588	7779589	2.1	0.14	93,781	0	0
L070*	435835_7779235	435835	7779235	133.4	1.97	85,498,475	0	0

Map label	Name	x utm83 (m)	y utm83 (m)	Area (acre)	Avg. depth (ft)	Volume (gal)	Volume > 5 ft (gal)	Volume > 7 ft (gal)
L071	433501_7779195	433501	7779195	6.3	0.83	1,699,946	0	0
L072	433997_7779167	433997	7779167	4.1	0.61	807,573	0	0
L073	433891_7779147	433891	7779147	2.4	0.56	443,544	0	0
L074	430847_7779060	430847	7779060	14.1	0.95	4,376,009	0	0
L075	436552_7778933	436552	7778933	8.5	0.87	2,428,004	0	0
L076*	435029_7778929	435029	7778929	19.2	0.54	3,370,306	0	0
L077	433798_7778867	433798	7778867	2.5	0.03	21,662	0	0
L078	432056_7778791	432056	7778791	5.6	0.78	1,428,906	0	0
L079	436070_7778738	436070	7778738	5.8	0.63	1,178,207	0	0
L080	435295_7778693	435295	7778693	16.3	2.58	13,671,429	0	0
L081	432546_7778607	432546	7778607	2.9	0.37	351,084	0	0
L082	436517_7778585	436517	7778585	5.1	1.53	2,549,259	0	0
L083	433156_7778543	433156	7778543	4.5	1.16	1,710,513	0	0
L084	432963_7778537	432963	7778537	2.1	0.55	377,765	0	0
L085	435075_7778462	435075	7778462	2.2	0.51	364,821	0	0
L086	433029_7778299	433029	7778299	3.0	0.22	212,658	0	0
L087	434525_7778089	434525	7778089	2.7	0.32	282,135	0	0
L088	433896_7778079	433896	7778079	2.1	0.29	202,884	0	0
L089	432594_7778048	432594	7778048	10.1	0.96	3,142,590	0	0
L090	436221_7778003	436221	7778003	2.6	0.62	536,269	0	0
L091**	438016_7777879	438016	7777879	12.5	1.60	6,529,803	0	0
L092	436494_7777861	436494	7777861	2.3	0.24	175,938	0	0
L093	430955_7777836	430955	7777836	2.4	0.43	338,668	0	0
L094	430145_7777769	430145	7777769	187.7	2.13	130,187,395	0	0
L095	433348_7777765	433348	7777765	2.2	0.07	48,343	0	0
L096*	435329_7777654	435329	7777654	159.2	0.58	29,899,779	0	0
L097	436297_7777628	436297	7777628	3.1	0.58	577,215	0	0
L098	429410_7777559	429410	7777559	2.1	0.13	87,176	0	0
L099	430976_7777395	430976	7777395	2.3	0.09	67,099	0	0
L100	429813_7776977	429813	7776977	4.0	0.13	169,598	0	0
L101	430525_7776917	430525	7776917	10.1	0.63	2,082,203	0	0
L102	433213_7776721	433213	7776721	5.7	1.08	2,011,669	0	0
L103	428105_7776414	428105	7776414	4.6	0.20	299,042	0	0
L104	433518_7776207	433518	7776207	2.2	0.50	355,839	0	0
L105*	428573_7776012	428573	7776012	21.0	0.21	1,431,812	0	0
L106	428851_7775974	428851	7775974	2.8	0.11	105,668	0	0
L107	432509_7775922	432509	7775922	2.8	0.88	789,345	0	0
L108	428309_7775917	428309	7775917	4.6	0.09	130,765	0	0
L109	433517_7775639	433517	7775639	2.9	0.10	96,422	0	0
L110	432600_7775470	432600	7775470	6.9	0.15	326,516	0	0

Map label	Name	x utm83 (m)	y utm83 (m)	Area (acre)	Avg. depth (ft)	Volume (gal)	Volume > 5 ft (gal)	Volume > 7 ft (gal)
L111	436916_7775425	436916	7775425	3.1	0.81	824,744	0	0
L112	432105_7775396	432105	7775396	7.9	1.23	3,143,646	0	0
L113	432124_7775124	432124	7775124	2.2	0.24	171,183	0	0
L114	437180_7775117	437180	7775117	2.2	0.41	292,966	0	0
L115	429401_7775096	429401	7775096	6.6	0.54	1,150,733	0	0
L116	428462_7774996	428462	7774996	9.0	0.32	925,130	0	0
L117	431912_7774882	431912	7774882	37.4	1.06	12,868,610	0	0
L118	432617_7774793	432617	7774793	11.6	0.55	2,092,770	0	0
L119	428854_7774778	428854	7774778	2.5	0.24	192,317	0	0
L120	437541_7774511	437541	7774511	43.4	1.65	23,297,064	0	0
L121	433371_7774399	433371	7774399	2.2	0.16	112,801	0	0
L122	433780_7774244	433780	7774244	7.0	0.82	1,863,997	0	0
L123	431280_7774205	431280	7774205	7.3	1.30	3,091,076	0	0
L124	436777_7774005	436777	7774005	4.9	1.10	1,752,252	0	0
L125	436745_7773539	436745	7773539	4.9	0.54	871,239	0	0
L126	433799_7773468	433799	7773468	32.4	1.84	19,418,227	4,490	0
L127*	431189_7773394	431189	7773394	135.7	1.11	48,978,545	0	0
L128*	428552_7773249	428552	7773249	375.9	1.40	172,066,582	0	0
L129	433920_7773240	433920	7773240	2.7	0.50	442,752	0	0
L130	433166_7773199	433166	7773199	5.6	0.47	861,993	0	0
L131	436844_7773155	436844	7773155	6.1	1.28	2,542,919	0	0
L132	433258_7773151	433258	7773151	2.4	0.31	245,679	0	0
L133	432698_7773037	432698	7773037	24.4	0.78	6,217,816	0	0
L134	435376_7772791	435376	7772791	52.8	3.49	60,006,933	263,907	0
L135*	433278_7772506	433278	7772506	195.2	0.52	32,957,570	0	0
L136	431399_7772323	431399	7772323	7.5	2.12	5,208,943	0	0
L137	435639_7771996	435639	7771996	141.9	2.36	109,015,595	0	0
L138	431668_7771522	431668	7771522	2.6	0.00	264	0	0
L139	437140_7770918	437140	7770918	25.4	2.38	19,694,022	5,019	0
L140	434548_7770847	434548	7770847	6.7	0.87	1,904,151	0	0
L141	430671_7770834	430671	7770834	23.8	0.33	2,569,072	0	0
L142	436237_7770494	436237	7770494	23.1	2.48	18,633,636	48,343	0
L143	436780_7770143	436780	7770143	8.3	2.68	7,259,710	8,981	0
L144	430488_7770061	430488	7770061	56.7	2.89	53,343,987	1,320	0
L145	434142_7769348	434142	7769348	2.0	1.40	909,808	0	0
L146	437297_7769035	437297	7769035	17.0	4.13	22,905,297	1,711,042	54,155
L147	434173_7768884	434173	7768884	22.8	1.37	10,155,300	0	0
L148	436781_7768638	436781	7768638	7.8	3.45	8,787,153	44,909	0
L149*	432850_7768433	432850	7768433	44.7	1.67	24,286,388	0	0
L150	436902_7768420	436902	7768420	6.0	2.15	4,183,427	0	0

Map label	Name	x utm83 (m)	y utm83 (m)	Area (acre)	Avg. depth (ft)	Volume (gal)	Volume > 5 ft (gal)	Volume > 7 ft (gal)
L151	433814_7768323	433814	7768323	3.4	0.33	362,443	0	0
L152	433664_7768120	433664	7768120	3.6	1.10	1,289,951	0	0
L153	436155_7768061	436155	7768061	21.2	1.71	11,797,393	184,392	4,490
L154*	433223_7768011	433223	7768011	10.1	1.59	5,226,378	0	0
L155	435419_7767998	435419	7767998	3.0	3.46	3,373,740	216,621	528
L156	435487_7767782	435487	7767782	13.5	3.50	15,435,305	698,470	42,795
L157**	427589_7767622	427589	7767622	3.3	1.03	1,090,766	0	0
L158	436501_7767583	436501	7767583	8.2	2.86	7,625,853	7,396	0
L159	432828_7767288	432828	7767288	2.3	0.07	51,513	0	0
L160	435471_7766911	435471	7766911	28.9	3.77	35,478,827	2,142,434	241,453
L161	428073_7766371	428073	7766371	5.2	1.00	1,669,831	0	0
L162	435248_7766128	435248	7766128	9.9	3.80	12,293,772	597,821	22,190
L163	434805_7765738	434805	7765738	18.9	3.33	20,473,858	163,522	0
L164	427662_7765564	427662	7765564	23.2	2.60	19,619,261	78,459	0
L165	435672_7765253	435672	7765253	2.2	10.43	7,322,055	4,245,772	3,311,396
L166	434347_7764988	434347	7764988	12.1	3.29	12,966,882	101,177	0
L167	428047_7764926	428047	7764926	2.5	1.35	1,106,088	0	0
L168	434633_7764895	434633	7764895	24.5	2.23	17,755,000	78,459	1,056
L169	433724_7764586	433724	7764586	46.9	3.70	56,574,018	1,450,568	24,567
L170	427773_7764582	427773	7764582	9.0	1.22	3,563,416	0	0
L171	432852_7764200	432852	7764200	10.0	1.99	6,474,855	0	0
L172	427903_7764194	427903	7764194	22.7	0.90	6,692,797	0	0
L173	428361_7763992	428361	7763992	7.7	0.55	1,382,676	0	0
L174	433013_7763873	433013	7763873	5.9	1.57	2,988,842	0	0
L175	428571_7763421	428571	7763421	4.4	0.65	938,867	0	0
L176	433580_7763245	433580	7763245	3.4	1.26	1,380,562	0	0
L177	428075_7762911	428075	7762911	33.9	2.67	29,462,838	16,642	0
L178	433668_7762711	433668	7762711	34.3	3.38	37,792,446	98,007	1,056
L179	428142_7762241	428142	7762241	41.8	1.44	19,570,390	0	0
L180	433312_7762224	433312	7762224	69.2	2.28	51,423,721	19,284	0
L181	427721_7761965	427721	7761965	5.0	1.89	3,067,565	0	0
L182	432071_7761957	432071	7761957	180.4	2.39	140,429,344	0	0
L183	432247_7761038	432247	7761038	25.3	3.19	26,240,997	887,882	0
L184	427750_7760931	427750	7760931	5.6	0.42	770,589	0	0
L185**	427404_7760847	427404	7760847	3.7	0.24	288,475	0	0
L186	431201_7760818	431201	7760818	9.2	1.33	3,976,845	0	0
L187	431928_7760781	431928	7760781	7.3	2.43	5,754,722	130,765	0
L188	432247_7760629	432247	7760629	9.7	2.29	7,224,575	0	0
L189	432258_7760118	432258	7760118	36.0	3.19	37,427,096	61,552	0
L190	427704_7760080	427704	7760080	10.5	0.22	739,681	0	0

Map label	Name	x utm83 (m)	y utm83 (m)	Area (acre)	Avg. depth (ft)	Volume (gal)	Volume > 5 ft (gal)	Volume > 7 ft (gal)
L191	433107_7759975	433107	7759975	20.0	3.93	25,665,894	1,022,081	20,605
L192	431414_7759667	431414	7759667	2.9	0.52	486,340	0	0
L193	428267_7759499	428267	7759499	8.3	2.36	6,403,529	0	0
L194	430844_7759157	430844	7759157	12.7	1.06	4,403,218	0	0
L195	431250_7759123	431250	7759123	9.6	1.77	5,547,347	0	0
L196	430588_7758836	430588	7758836	4.5	0.46	683,941	0	0
L197	433185_7758684	433185	7758684	12.9	4.03	16,941,086	2,423,249	462,565
L198	431775_7758287	431775	7758287	3.6	0.89	1,036,875	0	0
L199	432858_7758285	432858	7758285	5.4	3.32	5,880,997	423,996	3,170
L200	430729_7758167	430729	7758167	61.1	3.71	73,945,969	872,031	0
L201	430093_7757650	430093	7757650	6.0	0.99	1,914,454	0	0
L202	432389_7757138	432389	7757138	10.0	3.22	10,506,648	113,329	0
L203	430251_7756947	430251	7756947	14.0	1.81	8,252,997	0	0
L204	432343_7756170	432343	7756170	3.0	2.65	2,550,316	236,962	19,284
L205	431872_7755982	431872	7755982	17.3	2.86	16,120,567	16,114	0
L206***	427676_7755661	427676	7755661	102.9	0.10	3,240,069	0	0
L207	430753_7755547	430753	7755547	3.7	0.93	1,124,316	0	0
L208	432222_7755464	432222	7755464	12.9	5.29	22,149,501	6,332,467	3,348,115
L209	433122_7755174	433122	7755174	2.1	0.84	582,235	0	0
L210	431630_7754501	431630	7754501	5.2	3.91	6,630,188	1,411,470	576,159
L211	427599_7754481	427599	7754481	32.3	3.09	32,478,362	3,698	0
L212	430675_7753863	430675	7753863	7.4	2.50	5,976,363	55,740	0
L213	429429_7753682	429429	7753682	2.9	0.12	116,764	0	0
L214	430786_7753473	430786	7753473	2.3	0.56	415,014	0	0
L215	428114_7753167	428114	7753167	14.2	3.27	15,089,504	163,786	0
L216	431895_7752977	431895	7752977	2.7	1.50	1,315,312	528	0
L217	428564_7752951	428564	7752951	2.7	0.82	712,736	0	0
L218	429081_7752797	429081	7752797	14.6	4.75	22,580,101	1,715,004	62,872
L219	428233_7752790	428233	7752790	6.2	1.26	2,558,769	0	0
L220	429336_7752435	429336	7752435	194.5	4.50	285,364,406	17,924,862	832,405
L221	431203_7752194	431203	7752194	4.6	2.95	4,447,071	0	0
L222	427817_7752184	427817	7752184	10.5	3.06	10,471,249	335,498	3,170
L223	431521_7752074	431521	7752074	2.8	2.94	2,677,383	264	0
L224	431448_7751752	431448	7751752	10.1	3.32	10,887,584	18,227	0
L225	431209_7751169	431209	7751169	15.2	5.10	25,319,036	3,627,345	616,313
L226	428113_7751134	428113	7751134	199.4	3.31	215,027,026	170,919	0
L227	429380_7750883	429380	7750883	5.9	1.37	2,620,850	0	0
L228	429509_7750734	429509	7750734	4.2	1.44	1,970,458	0	0
L229	428065_7750097	428065	7750097	6.6	1.31	2,823,998	0	0
L230	428433_7750065	428433	7750065	17.5	3.14	17,912,182	120,726	264

Map label	Name	x utm83 (m)	y utm83 (m)	Area (acre)	Avg. depth (ft)	Volume (gal)	Volume > 5 ft (gal)	Volume > 7 ft (gal)
L231	427836_7750030	427836	7750030	5.6	0.63	1,137,788	0	0
L232**	427233_7749524	427233	7749524	103.1	3.83	128,738,940	4,814,006	0
L233	431475_7749497	431475	7749497	95.8	3.59	112,115,125	633,220	0
L234	427845_7749321	427845	7749321	2.1	0.53	354,782	0	0
L235	427724_7749268	427724	7749268	3.1	0.27	275,267	0	0
L236*	428210_7748802	428210	7748802	141.6	1.60	73,998,275	1,849	0
L237	431318_7748449	431318	7748449	50.6	3.21	52,900,971	505,889	528
L238	432189_7748232	432189	7748232	3.7	3.16	3,797,472	33,285	0
L239	427350_7747939	427350	7747939	11.0	4.24	15,189,890	1,104,767	21,133
L240	431773_7747850	431773	7747850	10.7	3.41	11,910,722	208,167	0
L241	431164_7747793	431164	7747793	2.7	1.81	1,577,106	0	0
L242**	426867_7747681	426867	7747681	2.7	0.89	788,025	0	0
L243	427080_7747570	427080	7747570	2.5	0.16	135,784	0	0
L244	431049_7746515	431049	7746515	2.1	2.21	1,478,570	0	0
L245	430862_7745893	430862	7745893	2.0	3.25	2,116,017	6,075	0
L246*	428730_7745799	428730	7745799	384.0	3.50	437,891,243	3,423,404	0
L247	430776_7745408	430776	7745408	6.9	3.12	6,984,971	528	0
L248	427146_7745290	427146	7745290	38.8	0.52	6,513,953	0	0
L249	432120_7744998	432120	7744998	5.2	2.54	4,317,891	63,929	0
L250	432243_7744453	432243	7744453	4.5	2.49	3,647,951	74,760	0
L251	428967_7744352	428967	7744352	82.2	5.47	146,685,729	22,972,925	1,228,399
L252	432360_7743998	432360	7743998	13.0	4.22	17,898,181	2,342,941	480,793
L253	427145_7743635	427145	7743635	2.1	2.08	1,444,756	16,907	0
L254	433356_7743331	433356	7743331	5.2	3.13	5,273,665	173,032	3,698
L255	427861_7743234	427861	7743234	11.8	3.28	12,585,154	59,438	0
L256	428549_7742859	428549	7742859	3.8	1.07	1,318,482	0	0
L257	428019_7742850	428019	7742850	4.7	1.93	2,984,351	0	0
L258	428252_7742766	428252	7742766	3.9	1.56	1,968,873	0	0
L259	429698_7742669	429698	7742669	16.4	4.22	22,608,368	1,475,136	253,076
L260	431291_7742563	431291	7742563	9.6	4.12	12,927,785	1,825,428	297,193
L261	432891_7742430	432891	7742430	4.4	3.44	4,938,959	437,997	36,719
L262	428546_7742258	428546	7742258	5.8	0.81	1,525,329	0	0
L263	429951_7742198	429951	7742198	4.5	1.66	2,437,515	0	0
L264	429067_7741863	429067	7741863	22.4	3.89	28,369,695	385,691	0
L265	431449_7741634	431449	7741634	7.7	3.40	8,587,703	461,508	46,230
L266	432534_7741530	432534	7741530	8.3	4.24	11,383,435	2,066,353	731,756
L267	429708_7741526	429708	7741526	112.1	4.64	169,307,042	15,328,844	61,816
L268	434658_7741187	434658	7741187	8.9	6.02	17,459,127	7,927,537	5,504,023
L269	434671_7740970	434671	7740970	7.4	6.20	14,946,323	6,773,105	4,383,670
L270	431714_7740185	431714	7740185	8.4	4.05	11,127,188	846,935	22,982

Map label	Name	x utm83 (m)	y utm83 (m)	Area (acre)	Avg. depth (ft)	Volume (gal)	Volume > 5 ft (gal)	Volume > 7 ft (gal)
L271	429831_7740123	429831	7740123	5.0	0.79	1,275,950	0	0
L272	430186_7740091	430186	7740091	2.1	0.16	108,838	0	0
L273	432291_7740016	432291	7740016	4.7	2.24	3,402,007	65,514	0
L274	429390_7739716	429390	7739716	4.4	1.00	1,438,944	0	0
L275	429904_7739279	429904	7739279	29.2	1.07	10,172,471	0	0
L276	427498_7738847	427498	7738847	10.9	4.87	17,313,040	3,076,018	515,135
L277*	430966_7738762	430966	7738762	154.5	5.71	287,208,326	55,126,356	6,757,783
L278	433269_7738491	433269	7738491	3.3	1.25	1,365,505	0	0
L279	427449_7738438	427449	7738438	2.5	0.09	75,024	0	0
L280	430510_7737706	430510	7737706	4.2	1.97	2,709,083	0	0
L281	432844_7737199	432844	7737199	2.6	0.89	745,229	0	0
L282**	426945_7737111	426945	7737111	76.8	3.78	94,420,620	8,872,216	849,312
L283**	428541_7737099	428541	7737099	20.2	2.05	13,520,322	0	0

APPENDIX B: VOLUMETRIC COMPARISON FOR SELECTED LAKES

Name, surface area, average depth, total volume, and incremental volume of 29 lakes in the 2012 airborne survey area that included 26 in the ASRC (2012) lakes report and 3 additional lakes (17B, 25B, and 28B) surveyed by ASRC in 2013. Total volume and incremental volumes at depths greater than 5 and 7 ft from the ASRC report are shown for comparison. Complete incremental volumes at 1-ft intervals can be found in a spreadsheet in the lake volumes directory of the data volume.

ASRC Name	Name	Area (acre)	Average depth (ft)	Water volume (from lidar)			Water volume (ASRC)		
				Total (gal)	> 5 ft (gal)	> 7 ft (gal)	Total (gal)	> 5 ft (gal)	> 7 ft (gal)
Lake 2	435248_7766128	9.9	3.8	12,293,772	597,821	22,190	10,973,592	92,116	0
Lake 3	433668_7762711	34.3	3.4	37,792,446	98,007	1,056	36,266,862	0	0
Lake 4	433312_7762224	69.2	2.3	51,423,721	19,284	0	47,849,475	0	0
Lake 5	432071_7761957	180.4	2.4	140,429,344	0	0	127,015,967	0	0
Lake 6	432247_7761038	25.3	3.2	26,240,997	887,882	0	25,807,662	407,096	0
Lake 7	432258_7760118	36.0	3.2	37,427,096	61,552	0	32,006,358	9,538	0
Lake 8	433107_7759975	20.0	3.9	25,665,894	1,022,081	20,605	22,690,881	574,498	0
Lake 9	433724_7764586	46.9	3.7	56,574,018	1,450,568	24,567	58,345,202	1,138,746	4,357
Lake 10	435471_7766911	28.9	3.8	35,478,827	2,142,434	241,453	33,235,311	1,331,205	75,348
Lake 11	434805_7765738	18.9	3.3	20,473,858	163,522	0	17,393,307	0	0
Lake 12	434347_7764988	12.1	3.3	12,966,882	101,177	0	11,785,184	0	0
Lake 13	430729_7758167	61.1	3.7	73,945,969	872,031	0	68,673,564	209,358	0
Lake 14	432858_7758285	5.4	3.3	5,880,997	423,996	3,170	5,515,776	220,929	0
Lake 15	433185_7758684	12.9	4.0	16,941,086	2,423,249	462,565	15,197,033	1,540,871	183,632
Lake 16	432389_7757138	10.0	3.2	10,506,648	113,329	0	9,311,113	0	0
Lake 17	431872_7755982	17.3	2.9	16,120,567	16,114	0	15,417,312	6,443	0
Lake 18	432222_7755464	12.9	5.3	22,149,501	6,332,467	3,348,115	20,537,122	5,129,652	2,217,430
Lake 19	428113_7751134	199.4	3.3	215,027,026	170,919	0	188,608,758	0	0
Lake 20	431475_7749497	95.8	3.6	112,115,125	633,220	0	99,273,517	0	0

ASRC Name	Name	Area (acre)	Average depth (ft)	Water volume (from lidar)			Water volume (ASRC)		
				Total (gal)	> 5 ft (gal)	> 7 ft (gal)	Total (gal)	> 5 ft (gal)	> 7 ft (gal)
Lake 21	431318_7748449	50.6	3.2	52,900,971	505,889	528	46,143,209	30,750	0
Lake 22	428210_7748802	141.6	1.6	73,998,275	1,849	0			
Lake 22a	427233_7749524	103.1	3.8	128,738,940	4,814,006	0	126,276,657	1,621,174	0
Lake 23	428730_7745799	384.0	3.5	437,891,243	3,423,404	0	417,036,488	0	0
Lake 25	429336_7752435	194.5	4.5	285,364,406	17,924,862	832,405	248,111,138	5,650,263	8,488
Lake 26	437297_7769035	17.0	4.1	22,905,297	1,711,042	54,155	20,597,426	989,694	0
Lake 17B	428552_7773249	375.9	1.4	172,066,582	0	0	268,780,266	0	0
Lake 25B	433278_7772506	195.2	0.5	32,957,570	0	0	106,019,772	0	0
Lake 28B	435639_7771996	141.9	2.4	109,015,595	0	0	150,271,674	375,872	0

APPENDIX C: LIDAR-DERIVED LAKE SUMMARIES (MANUAL PROCESS)

North Slope survey area lake volumes have been generated from bathymetric lidar data following two independent approaches: semi-automatically (Appendices A and B) and interactively (this appendix). This appendix describes the interactive approach; volume summaries for 134 individual lakes can be found on the accompanying data volume. Locations of these lakes, which follow a different naming convention than those listed in Appendices A and B, are shown on figs. C1 (overview) through C13, progressing from northern to southern survey-area tiles. A description of the interactive process follows.

Data set output are classified in 5 different classes by using Lidar Suite Software (LSS). These data sets are produced from individual flight lines, and merged into each other after the calibration process. Below are the output classes:

- Class 0 – Not found (data that is not classified by the software)
- Class 4 – Land
- Class 5 – Water surface
- Class 6 – Shallow (Laser pulse returns back before reaching the bottom surface)
- Class 7 – Bottom

Class 5, 6 and 7 data sets are used to generate this report. Lake A3-b and Lake F1-a are the only lakes that ‘shallow’ class data sets are used since ‘bottom data sets are not evident to calculate metrics.

Due to the size of the data and the measurement method, larger data sets have been decimated (e.g. 1:10) and these are indicated for each individual measurement.

In general, data sets have minimal amount of data ‘noise’. Noisy data have been cleaned with different classification methods:

- Isolated points (points that far away from the cluster)
- Low points (points that sit much lower compared to the cluster)
- Air points (points that sit much higher compared to the cluster)

For measurement, metric values are used. Reports include the following measurements:

- Area size (m²)
- Fill volume (m³)
- Depth volume by 0.5 meter increments, starting by Class 5 data sets
- Depth volume is calculated until Class 7 (or Class 6) data sets are exhausted
- Total volume (m³)

Sample images are attached to lake report, and these images are based on Class 6 and 7 with height colorization. Images represent point cloud data and different colors represent depth, where blue represents the deepest areas.

Since project area is divided into 4 x 4km polygons, each lake in a specific polygon is named after the polygon name, starting by most north westerly area and moving to the southeast.

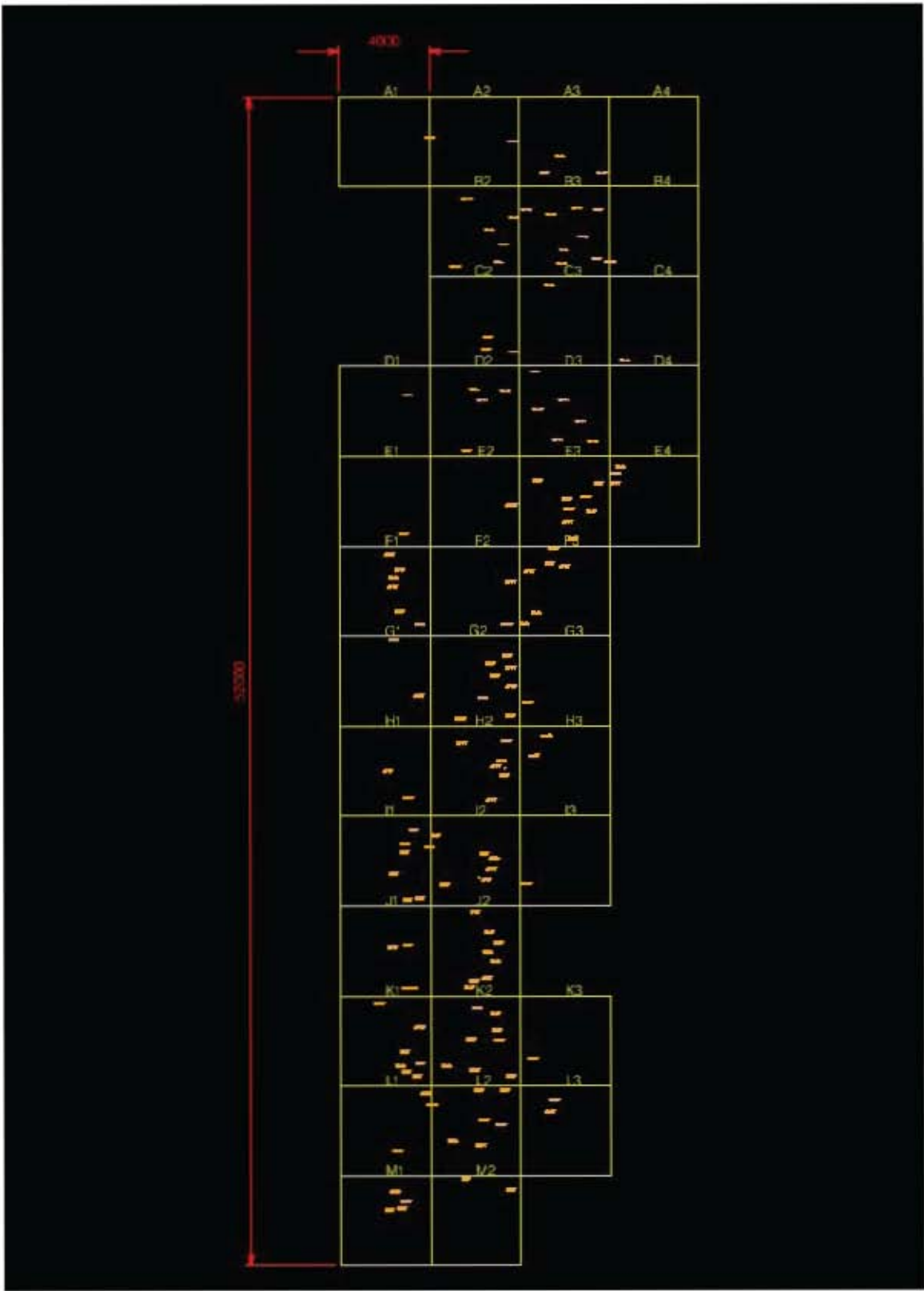


Figure C1. Overview of survey area tiles showing 137 lakes analyzed manually. Detailed lake locations are shown on fig. C2a-1. Volume statistics for individual lakes are included in a report on the data volume.

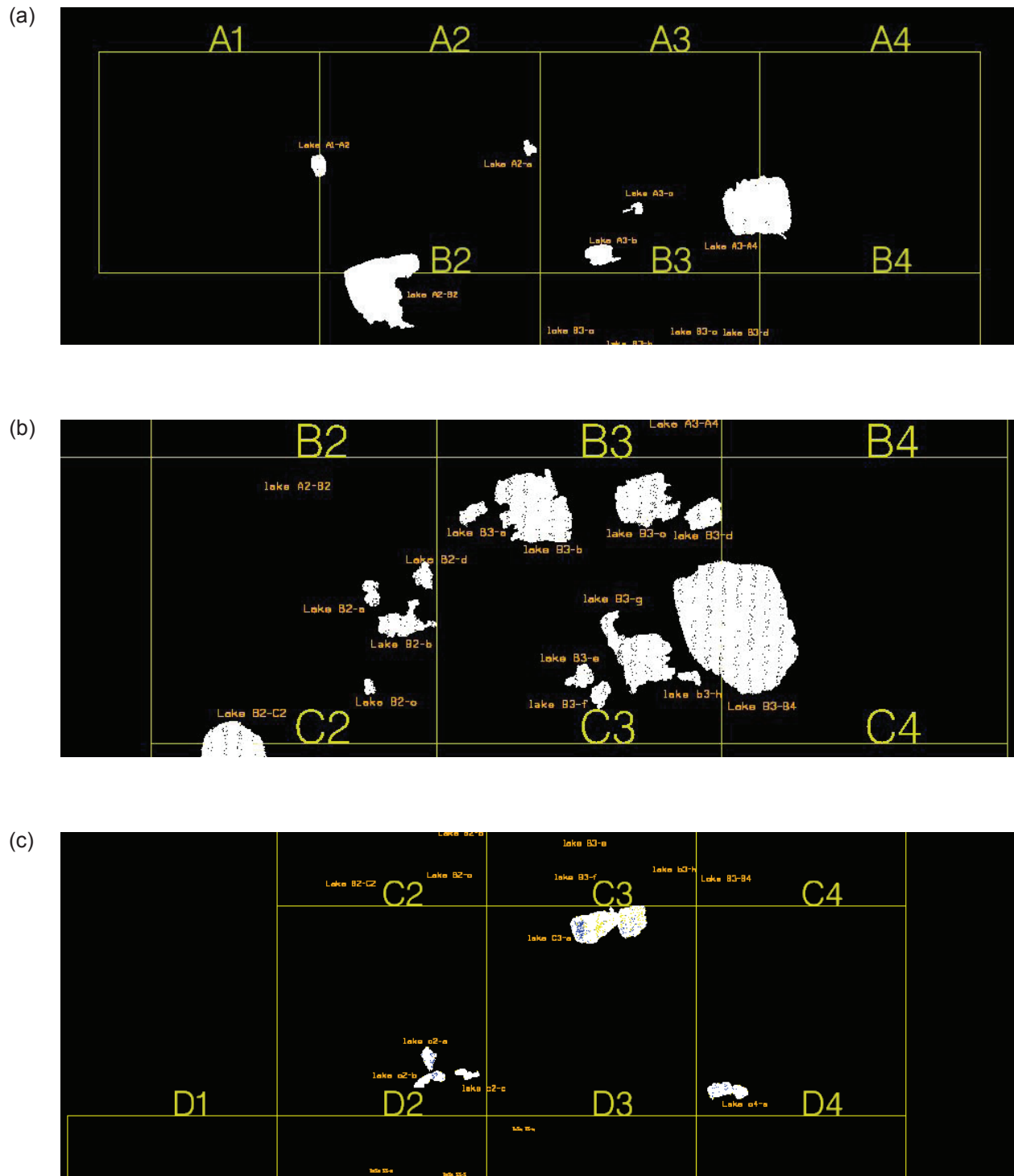


Figure C2. (a) through (l): North Slope airborne survey tiles showing individual lake locations.

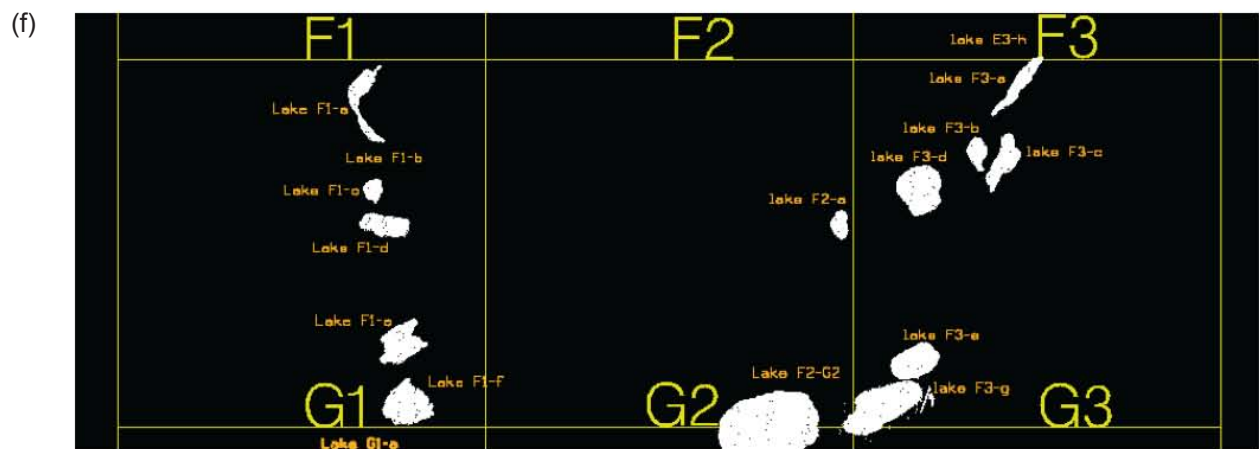
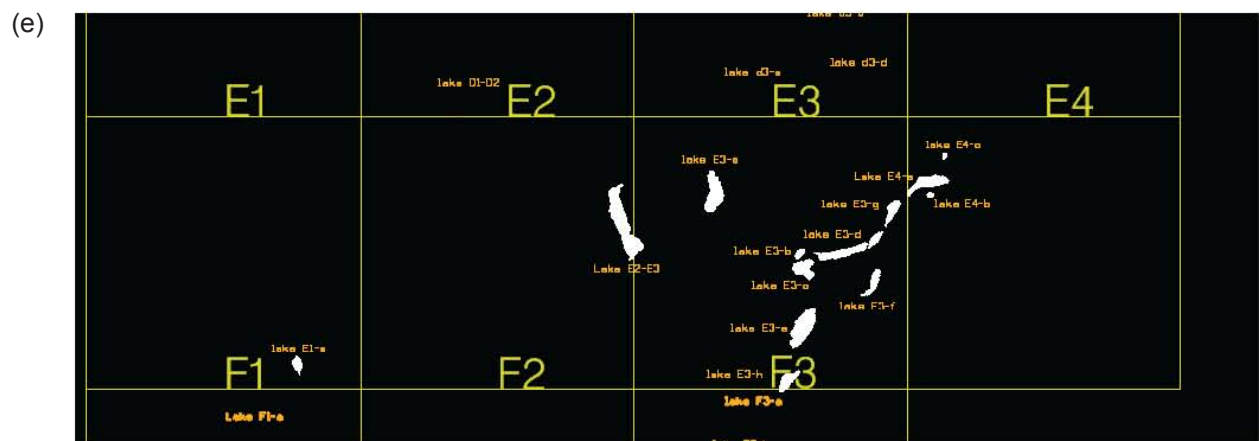
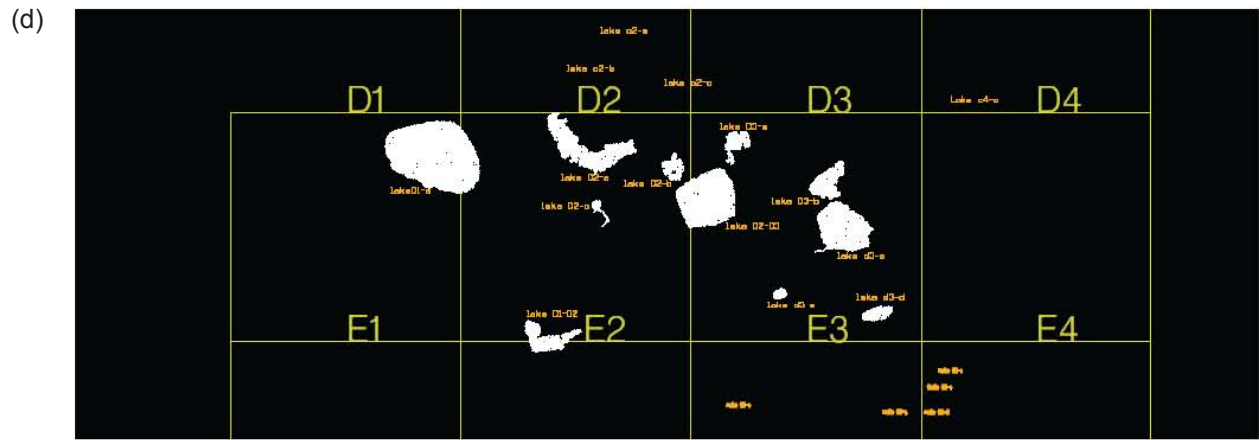


Figure C2 (continued).

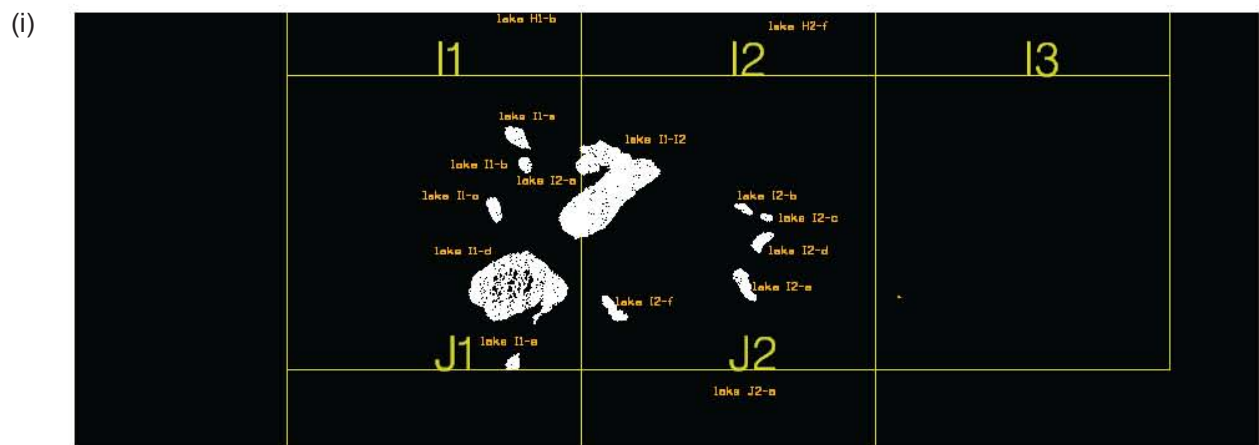
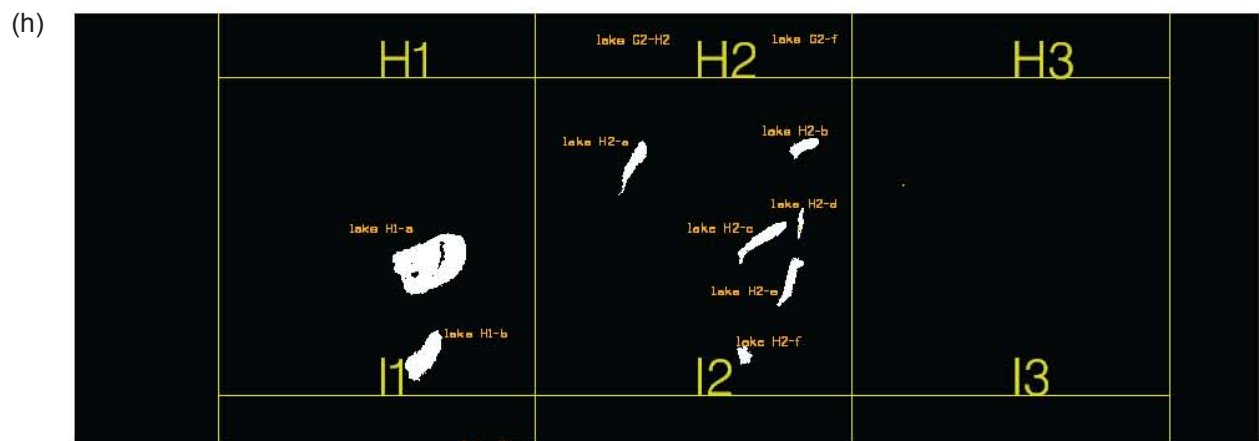
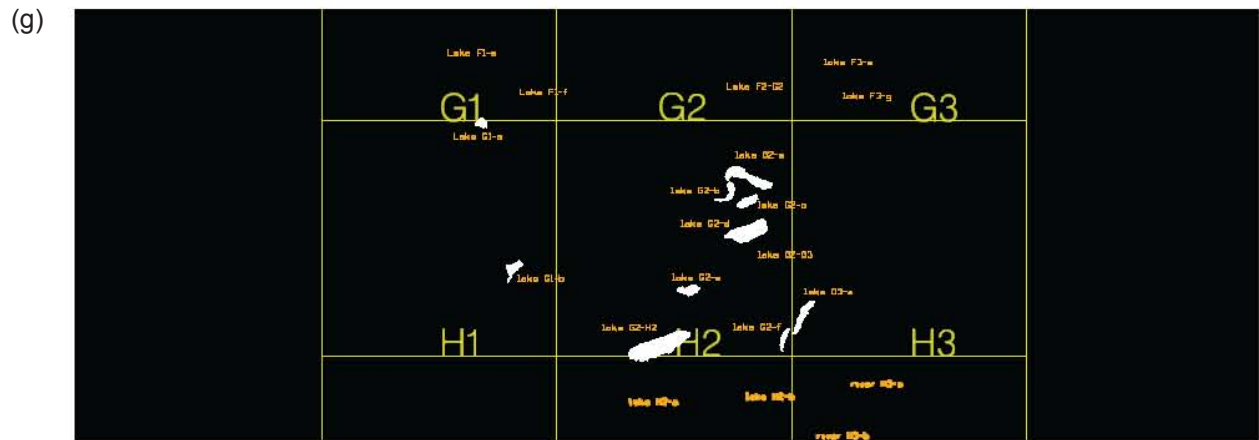


Figure C2 (continued).

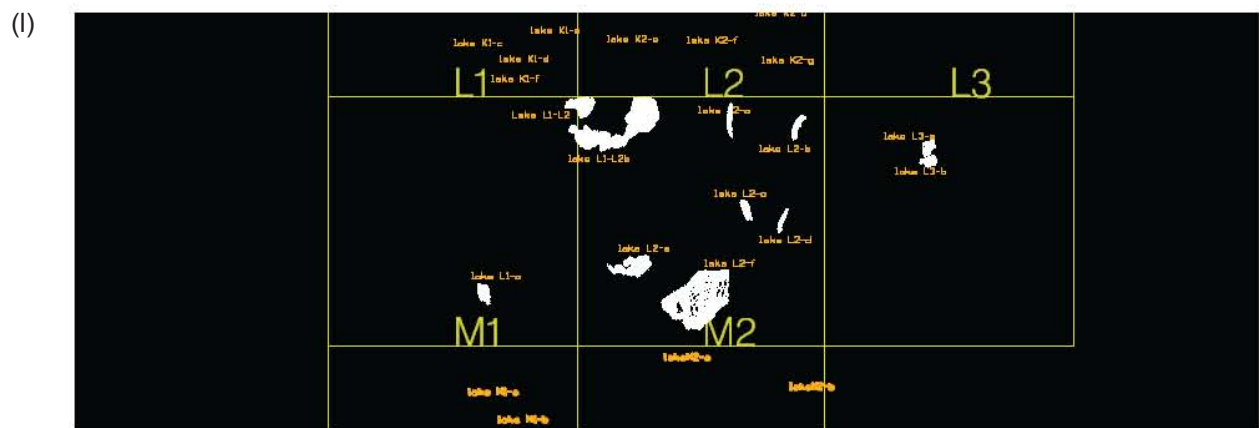
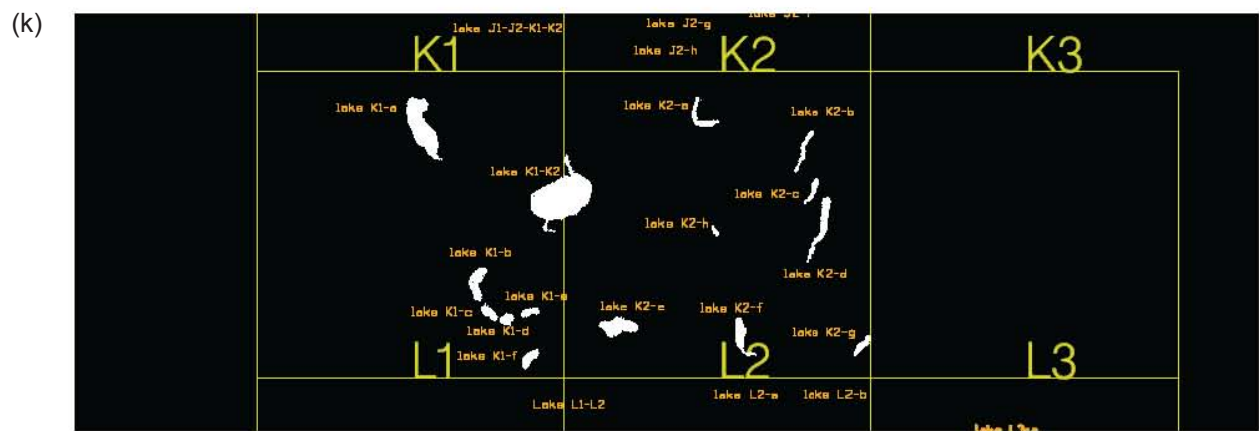
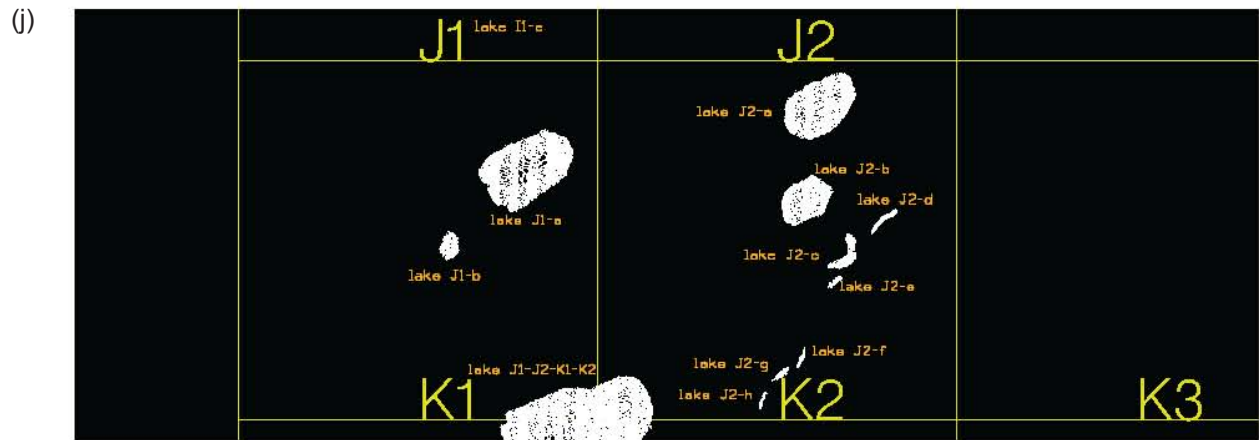


Figure C2 (continued).

(l)

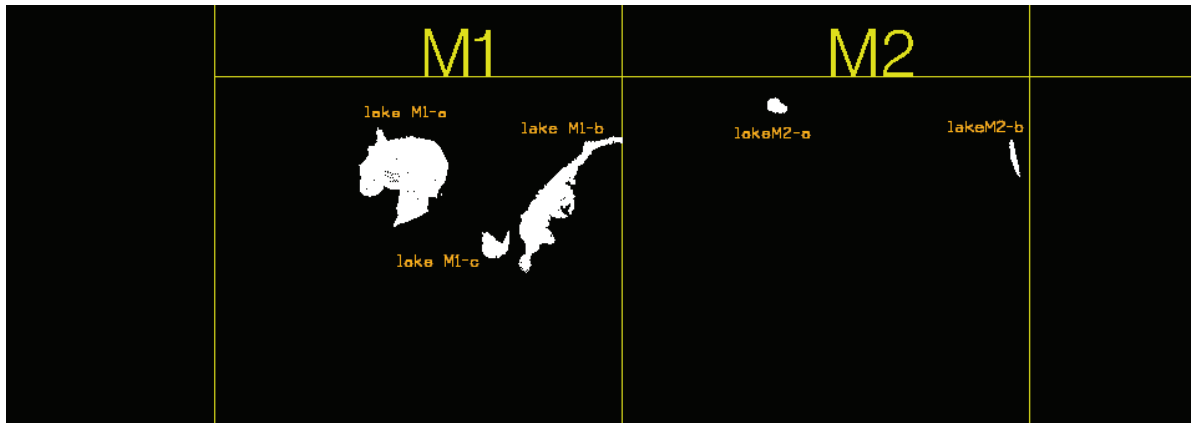


Figure C2 (continued).

Page intentionally blank

APPENDIX D: DATA VOLUME CONTENTS

The hard drive that accompanies this report contains maps, a data acquisition report, presentations, and lidar and geographic information system (ESRI ArcGIS 10.1 compatible) files from the August 2012 airborne lidar and imagery survey on the Alaska North Slope near Deadhorse conducted by the Bureau of Economic Geology, Airborne Hydrography AB, and Aspen Helicopters Inc. on behalf of Great Bear Petroleum.

All spatial data are in the UTM projection, WGS 1984 datum, zone 6 north. Elevation and coordinate units are in meters. Elevations for the digital elevation models have been converted from ellipsoid heights to geoid heights to ensure a better match with other types of topographic data that may be available. Elevations contained in raw lidar files (in las format) are given relative to the WGS 84 ellipsoid.

Because the lidar data files are very large, for convenience the survey area has been segregated into 13 lettered rows and four numbered columns of tiles measuring 4 km by 4 km. Tile A1 (row a, column 1) is at the northwest corner of the survey area. Tile M4 (row m, column 4) is at the southeast corner of the survey area. The boundaries of those tiles are shown on the maps and contained in a GIS shapefile.

A folder-by-folder description of the contents of the disk follows.

The “colorInfraredImagery” folder contains georeferenced mosaics of the color infrared imagery at 1-m resolution.

The “lakeStatistics” folder contains Excel spreadsheets presenting lake-volume statistics calculated from the semi-automated approach mentioned in appendices A and B and a pdf document (appendix C) summarizing the statistics calculated manually for 134 lakes.

The “maps” folder contains seven documents in pdf format.

gbAlaska_colorInfrared_01m.pdf: color infrared imagery mosaic of the survey area at 1-m resolution.

gbAlaska_lakeNames_beg: map of the survey area showing lake labels (Appendices A and B) used in the semi-automated determination of lake-water volumes. Labels are superimposed on water depths.

gbAlaska_mergedSurface_01m.pdf: elevation map of the survey that merges topographic and water-bottom surfaces at 1-m resolution

gbAlaska_topography_01m.pdf: elevation map of the survey area from topographic lidar data only.

gbAlaska_waterBottom_01m.pdf: water-bottom elevation over the survey area from bathymetric lidar data at 1-m resolution.

gbAlaska_waterDepth_01m.pdf: map of the survey area showing calculated water depths

gbAlaska_waterSurface_01m.pdf: water-surface elevation at 1-m resolution over the survey area from topographic lidar data.

The “presentations” folder contains Powerpoint presentations given (1) to Great Bear staff in Austin on February 4, 2013 that summarized preliminary project results, (2) at a geophysical

conference (SAGEEP) in Denver in March 2013, and (3) by Applied Research Laboratories staff to summarize the preparation of bare-earth elevation models.

The “reports” folder contains (1) a Bureau of Economic Geology report summarizing airborne data acquisition activities in August 2012, (2) a paper published in *The Leading Edge* in July 2013 about the Chiroptera system and the North Slope survey, and (3) the Final Technical Report summarizing project results summarizing project results as of 10/31/2013.

The “survey2012data” folder contains raw and GIS-compatible files related to the 2012 North Slope airborne survey. Subfolders within this folder include:

bathyLidar: processed results (point clouds) from the bathymetric lidar survey

las_ellipsoid: bathymetric lidar export files (in las format) for each tile, including water bottom and water surface returns. Elevations are relative to the WGS 1984 ellipsoid. These files have been exported at full system resolution.

gisGrids: contains grids and digital elevation models produced from the 2012 lidar survey, including:

bareEarthTiles_ARL: five GIS-compatible geotiff images of the bare-earth digital elevation model produced by Applied Research Laboratories

dems_1m_full_extents: includes area-wide grids (at 1-m resolution) of topography only, water-bottom only, merged topography and water bottom surfaces, water surface elevation determined from topographic lidar data, and water depth calculated by subtracting the water bottom elevation from the water surface elevation

ellipsoidToGeoid2012Correction: raster grid containing the distance required (in meters) to convert ellipsoid elevations to the 2012 geoid elevations determined by the National Geodetic Survey.

gisShapefiles: contains ArcGIS-compatible shapefiles

flightLines: aircraft positions recorded during the August 2012 airborne lidar survey flights

greatBearSeismic: approximate outline of the 2012 Great Bear 3D seismic survey

lidarSurveyGrid2012: outline of survey area and 4 km x 4 km tiles

topoLidar: processed results (point clouds) from the topographic lidar survey

las_ellipsoid: topographic lidar export files (in las format) for each tile. Elevations are relative to the WGS 1984 ellipsoid. These files have been decimated from the full system resolution at a 1:20 ratio.

The “wetlands” folder contains GIS-compatible files for the Bureau wetlands map.